A Study on Form-finding and Multiple Nonlinear Analyses

for Tensegrity Simulation

September, 2021

A dissertation submitted in partial fulfillment of the requirements for the degree of
Doctor of Engineering in Structural Engineering

Department of Science and Advanced Technology

Graduate School of Science and Engineering

Saga University

CHO KYI SOE

Examination Committee

—————————————

Professor Hiroyuki Obiya

(Chairman)

—————————————

Professor Katsushi Ijima

—————————————

Professor Yukihiro Ito

—————————————

Associate Professor Narumol Vongthanasunthorn

Department of Science and Advanced Technology

Graduate School of Science and Engineering

Saga University, Japan

Acknowledgement

Firstly, the author would like to express her gratitude to all the people who have been a great support in all ways to complete this dissertation. I would like to give my appreciation and greatest gratitude to my supervisor, Professor Obiya for his continuous valuable guidance, encouragement, kindness and support during the process of this dissertation. And my sincere gratitude to co-supervisors: Professor Ijima, Professor Ito and Associate Professor Narumol for giving me generous suggestions and encouragement and to technician Kawasaki and senior Dr. Nizam for the kind support and help. I am grateful to all my laboratory members, all professors from the Department of Civil Engineering, and also to the staffs and committee members of Saga University for their kind help and warm cooperation.

I would like to appreciate my family and relatives who always keep me in touch with heart and encourage me in every single case. I would like to extend my sincerity to all my teachers from my high school student hood to university hood of my home country, who fulfill all the requirements of knowledge of my life-long study. I would like to thank to all my friends and colleagues for sharing their comfort and happiness together with me.

I would like to express my special gratitude to all the members of Togami Electric Manufacturing Company for giving me a great opportunity to study in Saga University, Japan and the Japanese government for supporting me with full allowance of MEXT scholarship throughout the three years of doctoral course study. I also would like to send my regards to all the committee members of Thanlyin Technological University for their great effort for paving the great chances for me to continue the further study abroad.

I would like to thank and share all of my good deeds with all the visible and invisible supporters, giving me strength to struggle in life and saving me in my needs and providing with precious Buddhist guidance.

For the last but not the least, this post-graduate journey will not be complete without my cutie little brother, Phoe Ni and the encouragement of these three specials: Han Soe Aung, Jang Hyo Chang, Horinouchi Hikaru. I do appreciate your lighting up to my dark world and trust in me in my highs and lows. Arigatou.

「Try the best, try your best even though there is no one around keeping an eye on you」 **:)**

Table of Contents

Table of Contents

Table of Contents

Table of Contents

Chapter	Title	Page

List of Figures

List of Figures

List of Figures

List of Tables

CHAPTER 1

Introduction

1.1 Background of study

Dating back to the ancient era between 4000 and 2000 BC, the prospect of civil engineering seemed to arise in ancient Egypt and in region of Mesopotamia. Along with the Egyptians' work of pyramids, the Parthenon of the ancient Greece, the Romans' Appian Way and the Great Wall of Chin Emperor, civil engineering became a fundamental concept and came into the daily life requirements of the citizens. It was also a second earliest development in the engineering field after military engineering. It is based on the combination of physical and mathematical concepts which is in relevance with the environment. Among its many subdivisions, the construction field has greatly involved in the development of civic buildings and other infrastructures. Along with this, the civilization had improved with consequent applications of structural, water and environmental, geotechnical and transportation engineering.

As the metropolitan planning has gradually developed, many modernized infrastructures are needed to be designed and constructed in such a way that can fulfill the requirements of the specifications. In the ancient time, structures were built by not the engineers but by artisans such as carpenters, sculptors and craftsmen regardless of the theory of structure. However, time to time, it came to realize that the knowledge of structural engineering is greatly important for the stability, durability, serviceability, creativity, construction and asthenic of a structure. Therefore, it plays an important role to lead the advanced creation of building design in the modern era. Structural analysis works out the examination of various possible loading conditions and calculation of the strength and structural stability of each element and the whole system. It allows the structure design part to select the size of suitable material, composition of members and the geometric design of a structure with the adjustment of reasonable safety factor.

Nowadays, the emergence of more complex buildings and structures can be seen worldwide. Due to the advance in material science engineering, it is possible to apply the lightweight, high durable, weather resistant and ecofriendly materials while maintaining the structural stability. In the late 1940's, Kenneth Duane Snelson made an innovation to a structural system named "X piece" in which wooden structures are seemed to be floating in the air without

contacting each other but can remain in the balance by a set of cable members (figure1.1). Around 1950's, Buckminster Fuller initiated the term "tensegrity" which came from a combination of tension and integrity. Among the work of structures based on tensegrity theory, Snelson's Needle Tower is one of the most popular instances which was built in 1968 (figure 1.2). Later on, the Kurilpa Bridge was constructed in 2009 which is the largest tensegrity based hybrid bridge in the world (figure 1.3). Since the tensegrity structure is extremely lightweight, aesthetic, deployable and robust, it withdraws the attention of many researchers from various fields. In 2003, R. Motro modified the definition of the formers that a tensegrity system is a stable self-equilibrium state in which compression members are discontinuous while tension members are connected each other. Numerous researches have been done in structural, architectural, mathematical, biological, robotic and aerospace. Many valuable findings and statements have revealed the nature of tensegrity systems throughout the intense studies in recent decades. However, a lot of investigation from various aspects are still needed due to its mysteriousness in unique morphology.
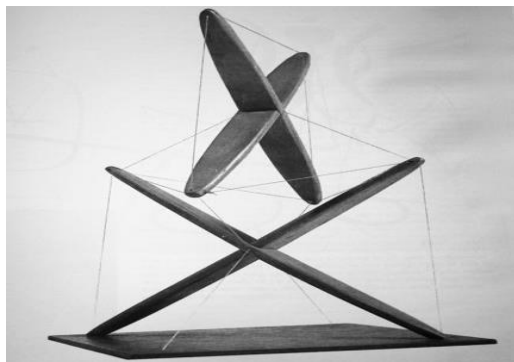
Figure 1.1 Kenneth Snelson's X-piece
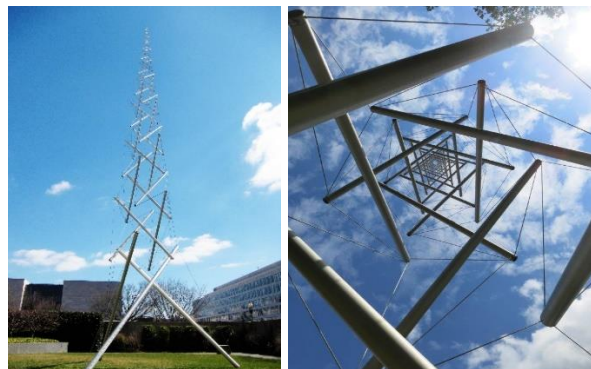
Figure 1.2 Snelson's needle tower

Figure 1.3 Kurilpa bridge

1.2 Involvement of tensegrity and its application

Tensegrity is composed of two types of structure members: the discontinuous compression members (referring to strut or bar) and continuous tension members (referring to string or cable). These members are connected by pin joints which are considered to be frictionless, making the self-supporting structural system. The structure can be stabilized by the introduction of pre-stress in tensile members and maintained in self-equilibrium condition without the external loading. The whole weight of the tensegrity can be neglected if the pre-stress is large enough compared to the self-weight of the composed members. Tensegrity possesses a unique morphology that can undergo various configurations under the strong geometrical nonlinearity. This unique characteristic attracts the interest of many researchers over the last few decades, and leads to an extensive range of their innovative applications in various fields such as in architectural and structural designs, smart systems, biomechanics and robotics and biology.

Tensegrity is effectively used in architectural and structural designs since its development. Landolf et al. designed the tensegrity modules for the pedestrian bridges and evaluated the structural performance by three types of ring module [1]. Skelton et al. optimized the topology of tensegrity bridge by the minimum mass design, considering the parametric methodology and multiscale complexity [2]. Nizar et al. further made extension for the dynamic analysis for the tensegrity-based footbridge [3]. And later, Nicolas et al. designed deployment system for a mid-span connection under the active control methodology. They proposed a symmetric tensegrity footbridge structure in which two bridge halves are controlled to meet at the mid-span and designed for nearly full-scale deployment.

Recently, the concept of tensegrity is applied in composite structures such as meta-materials and construction of sustainable buildings and renewable energy production structures. Cimmino et al. made an innovation for the composite solar facade and wind generators in which the opening and closing processes of the tensegrity solar screens are controlled by extending or restraining of the cable lengths [4]. Amendola et al. suggested the tensegrity prisms as composite bi-materials. These kinds of prisms are manipulated as the building cores of nonlinear periodic lattices and acoustic meta-materials [5]. Fraternali et al. suggested a tensegrity approach for the reinforcement of masonry domes and vaults by using fiber-reinforced composite materials [6]. Ma

et al. designed the meta-tensegrity in which the strut of the tensegrity prism is introduced by the metal rubber to support the energy absorption with the mechanical and dynamic properties [7].

Meta-material based tensegrity prisms and lattices also become a common practice for conducting wave transmission under the nonlinear dynamic responses. The structures based on tensegrity prisms exhibit the geometrical nonlinear performance where stiffening may gradually switch to softening, featuring large displacement through the pre-stress variables [8] [9]. Fraternali et al. applied the tensegrity prisms as a medium to transport the energy through solitary waves and examined the speed and form of wave propagation under the symmetric axial loading [10]. Julian and Raj developed a three-dimensional tensegrity lattices from the truncated octahedron unit cells and investigated the mechanical response of pre-stressed configurations under various loading conditions [11]. Fabbrocino and Carpentieri constructed structural lattices based on meta-material tensegrity units and studied the wave dynamics response subjected to the impulsive compression loading [12].

Since the space exploration paved the way for the requirement of developing ultra-light weight space structures, tensegrity came to serve to fulfill the demand due to its multi-functionality and adaptability. Yang and Sultan [13] established tensegrity-membrane system for the space structure and investigated the static and dynamic behaviors when it is in deployment situation. Fazli and Abedian [14] developed a design methodology based on the finite element analysis for the deployable mesh antennas with a model of hexagonal prismatic tensegrity structure, and it is aimed to provide the potential utilization in the micro-satellites.

Tensegrity units are also fascinating to design as the minimal mass structures since tensegrity networks can achieve the strength with little mass [15]. Skelton et al. stated that T-bar and D-bar systems have low mass requirement than a continuous single bar system to support the compression loading [16]. Chen and Skelton presented a unified approach to reduce the thickness of structural bars for both solid and hollow types, considering yielding and buckling constraints of each structural member [15]. The introduction of the minimal mass design is also found in tensegrity cantilever structures [17] and tensegrity-based lattices, which are also known as T-bar structures. The mass of the tensegrity lattices can be minimized either by optimizing the pre-stress distribution or members' cross-sectional area of the structure, where the latter needs less mass for load-bearing [18].

The application of tensegrity theory is gradually increased not only in the fields of structure and architecture, but also in the biology and medical science. The term, bio-tensegrity refers to the integration of tensegrity with the biological process and makes it possible to understand the hierarchical organization of human body and the behavior of body changes when the mechanical forces applied during the manipulative treatment. Scarr [19]made some publications about the consideration of the body organism system from a view point of tensegrity structure. Siemsen and Dittrich [20] studied the distribution of forces in the human body and made an explanation through the finite elements theory and tensegrity model. The demonstration of tensegrity principles utilized in the osteopathic medical practice can be observed in the recent review of Swanson [21]. David et. al [22] proposed the practice of tensegrity in manual therapy and investigated the usefulness of tensegrity concept in decision-making process for the practitioners.

Although tensegrity is a relatively new development in structural work, it quickly gains the popularity in recent years. The usefulness of tensegrity in various fields attracts the researcher to explore the deeper insight of its behavioral study from every viewpoint of structural analysis. Therefore, tensegrity is selected as my research model in this study. Many literatures related to tensegrity were studied, however, many aspects of tensegrity structural analyses still remain untouched which motivates the author to explore the further new findings of tensegrity structures in this dissertation.

1.3 Scope and aim

Since the introduction of the concept of tensegrity, many researchers have been trying to find out the characteristic of tensegrity and its response in various analyses such as load-displacement, form-finding, folding and deployment, static and dynamic, by approaching in numerous ways with different methods. For instance, force density method (FDM) is one of the popular methods for analyzing tensegrity structures since FDM is able to obtain a solution using a linear stiffness equation. However, the determination of feasible sets of force density by the non-linear analysis equation is required before solving the linear stiffness. Furthermore, the application of commercial software is not actively cost-effective for all-in-one package analysis. Therefore, it is necessary to find out an alternative method which is consistent and simple but effective and reliable that can fulfill the requirement in conducting structural analyses of tensegrity structures.

Meanwhile, our research team has adopted the tangent stiffness method which can be widely used in various types of structures. Obiya [23], Ijima [24] and their fellows intensively conducted numerous researches and proved the accuracy and versatility of tangent stiffness method [25]. This includes a wide range from the equilibrium analysis of plane frame structures [26], mesh optimization problem [27] of membrane structures, snapping phenomena of inflated dome structure [28] to the contact analysis of beam elements and consideration of shear deformation on the convergability with large displacement [29]. Furthermore, the tangent stiffness method is actively applied in tensegrity structures from the shape analysis to bifurcation path problems [30]. Dynamic studies have also been approached by the tangent stiffness method to some inelastic structures [31], but still remain a lot to treat in tensegrity structures. This initiates me to start a dynamic involvement in tensegrity structures while maintaining the concept of tangent stiffness method as a backbone of analytical procedures.

The main purpose of this research is to develop the algorithm in which the proposed tensegrity model can undergo a series of structural analyses, valid for both static and dynamic. In the algorithm, the purpose of each analysis is achieved by introducing the corresponding element force equation that describes the element behavior in the element stiffness component of tangent stiffness matrixes. In this study, the form-finding process is approached by integrating the high and low level of stiffness that defines the shape formation of tensegrity structure. At the same time, the mechanical behavior of hyper-elastic material is examined using the rubber structure which will later be adopted in developing tensegrity with real elements. In consequence, the proposed model will go through the folding analysis in which the structural members will perfectly overlapped under the given compulsory displacement. After this, the flatted tensegrity will be taken back to its original equilibrium configuration under the applied external force. Moreover, the process of deployment will be accompanied by the dynamic analysis in which the implicit time integration method is approached by Newmark $\beta = 1/4$. Finally, the complete algorithm to analyze tensegrity model is accomplished by the novel tangent stiffness method.

1.4 Structure of dissertation

This thesis is composed of six chapters, and the brief outline is as follow. Chapter 1 introduces the general background of tensegrity, the involvement of its application, the purpose of research and the outline of the dissertation. Chapter 2 defines the fundamental concept and formula

derivation of geometrical nonlinear analysis and the tangent stiffness method. The relations between the compatibility equation, element edge force equation, equilibrium equation and the tangent stiffness equation are explained in a flow and the iteration algorithm is illustrated step by step procedure. The derivation of the tangent stiffness matrix based on the principal of total potential energy conservation is also demonstrated consequently.

Chapter 3 presents the form-finding analysis of tensegrity structures, the discussion of the measure potential and the power function to approach the form-finding framework. The influence of each coefficient in the element force equation on finding the stably self-equilibrated solutions is examined and the idea of the multiple non-stressed length is introduced in order to investigate a wider diversity of equilibrium configurations of a proposed model.

Chapter 4 discusses the mechanical behavior of the hyper-elastic material by defining the Ogden model with an integration of least square function. The net structures composed of the hyper-elastic elements without compression are assumed for conducting the large deformation and large displacement analyses. The relaxation process is also performed where the sagging behavior is occurred in the compression deformation and the hardening behavior is achieved under the higher tension. A rational computational procedure is proposed to switch between the modified Newton-Raphson method and the iteration of strict tangent stiffness equation, followed by the examination of the efficient switching level for the proposed model.

Chapter 5 combines the concept of form-finding of tensegrity and the behavior of the hyper-elastic elements from the previous studies. After the establishment of tensegrity model with real structural elements, folding process is carried out by applying the appropriate compulsory displacement. The deployment of folded tensegrity will be explained by the dynamic analysis. The fundamental concept of Newmark β in the time integration method is presented and the dynamic behavior during deploying will be examined by the case study of time increment, the number of segment nodes and the stiffness of material. A brief algorithm for both static and dynamic analyses is demonstrated to give a better understanding of calculation processes.

Chapter 6 concludes all the results obtained from the proposed tensegrity model and discusses the findings from the current work. The collection from this dissertation is aimed to give a basic guideline to conduct other related researches in a more efficient way and provide a reference for future studies.

Chapter 1 : Introduction

- Background of tensegrity and its application
- Scope and aim
- Outline of dissertation

Chapter 2 : Tangent Stiffness Method in Geometrical Nonlinear Analysis

- Geometrical nonlinear analysis and formula derivation
- Iteration algorithm of TSM

Chapter 3 : Form-finding of Tensegrity: Integration of Real and Virtual Element

- Form-finding process proposed by the power function of the measure potential and the investigation of the influence of each coefficient
- Introduction of the multiple non-stressed lengths for finding a wider diversity of equilibrium configurations

Chapter 4 : Large Deformation and Large Displacement Analysis of Hyper-Elastic Elements

- Realization of the mechanical behavior and relaxation process of hyper-elastic material by interpolation function of Ogden model
- Investigation of the efficient switching level of tangent in the iteration process by modified Newton-Raphson method

Chapter 5 : Static Folding and Dynamic Deployment

- Characterization of tensegrity with real stiffness after determining the stably self-equilibrated configuration
- Simulation of folding process by the designated compulsory displacement
- Deployment process accompanied by the dynamic analysis using Newmark $\beta = 1/4$ method

Chapter 6 : Discussion and Conclusion

Figure 1.4 Outline of dissertation

References

[1] R. Landolf, N. Ali, R. Motro and I.Smith, "Designing tensegrity modules for pedestrian bridges," *Engineering Structures,* vol. 32, no. 4, pp. 1158-1167, April 2010.

[2] R. Skelton, F. Fraternali, G. Carpentieri and A. Micheletti, "Minimum mass design of tensegrity bridges with parametric architecture and multiscale complexity," *Mechanics Research Communications,* vol. 58, pp. 124-132, June 2014.

[3] N. Ali, R. Landolf, A. Alberto, P. Albi and I. Smith, "Design optimization and dynamic analysis of a tensegrity-based footbridge," *Engineering Structures,* vol. 32, no. 11, pp. 3650-3659, 2010.

[4] M. Cimmino, R. Miranda, E. Sicignano, A.Ferreira, R. Skelton and F. Fraternali, "Composite solar façades and wind generators with tensegrity architecture," *Composites Part B: Engineering,* vol. 115, pp. 275-281, 15 April 2017.

[5] A. Amendola, E. Nava, R. Goodall, I.Todd, R.E.Skelton and F.Fraternali, "On the additive manufacturing, post-tensioning and testing of bi-material tensegrity structures," *Composite Structures,* vol. 131, pp. 66-71, 1 November 2015.

[6] F. Fraternali, G. Carpentieri, M. Modano, F. Fabbrocino and R. Skelton, "A tensegrity approach to the optimal reinforcement of masonry domes and vaults through fiber-reinforced composite materials," *Composite Structures,* vol. 134, pp. 247-254, 15 December 2015.

[7] Y. Ma, Q. Zhang, Y. Dobah, F. Scarpa, F.Fraternali, R. Skelton, D. Zhang and J. Honga, "Meta-tensegrity: Design of a tensegrity prism with metal rubber," *Composite Structures,* vol. 206, pp. 644-657, 15 December 2018.

[8] A. Amendola, G. Carpentieri, M. Oliveira, R. Skelton and F. Fraternali, "Experimental investigation of the softening–stiffening response of tensegrity prisms under compressive loading," *Composite Structures,* vol. 117, pp. 234-243, 2014.

[9] F. Fraternali, G. Carpentieri and A. Amendola, "On the mechanical modeling of the extreme softening/stiffening response of axially loaded tensegrity prisms," *Journal of the Mechanics and Physics of Solids,* vol. 74, pp. 136-157, 2015.

[10] F. Fraternali, L. Senatore and C. Daraio, "Solitary waves on tensegrity lattices," *Journal of the Mechanics and Physics of Solids,* vol. 60, no. 6, pp. 1137-1144, 2012.

[11] R. Julian and K. Raj , "Mechanical response of 3-dimensional tensegrity lattices," *Composites Part B: Engineering,* vol. 115, pp. 30-42, 15 April 2017.

[12] F. Fabbrocino and G. Carpentieri, "Three-dimensional modeling of the wave dynamics of tensegrity lattices," *Composite Structures,* vol. 173, pp. 9-16, 2017.

[13] Shu Yang and Cornel Sultan, "Modeling of tensegrity-membrane systems," *International Journal of Solids and Structures,* vol. 82, no. 15, pp. 125-143, March 2016.

[14] N. Fazli and A. Abedian, "Design of tensegrity structures for supporting deployable mesh antennas," *Scientia Iranica,* vol. 18, no. 5, pp. 1078-1087, October 2011.

[15] M. Chen and R. Skelton, "A general approach to minimal mass tensegrity," *Composite Structures,* vol. 248, p. 112454, 2020.

[16] R. Skelton and M. Oliveria, "Tensegrity systems," *Springer,* vol. 1, 2009.

[17] S. Ma , M. Chen and R. Skelton, "Design of a new tensegrity cantilever structure," *Composite Structures,* vol. 243, pp. 112-188, 2020.

[18] R. Goyal, R. Skelton and E. Hernandez, "Design of minimal mass load-bearing tensegrity lattices," *Mechanics Research Communications,* vol. 103, p. 103477, 2020.

[19] G. Scarr, "Simple geometry in complex organisms," *Journal of Bodywork and Movement Therapies,* vol. 14, pp. 424-444, 2010.

[20] C. Siemsen and H. Dittrich, "Force distribution in human body using the example of weight lifters_tensegrity as a model of explanation," *International Journal of Osteopathic Medicine,* vol. 10, pp. 14-18, 2009.

[21] R. Swanson, "Biotensegrity: a unifying theory of biological architecture with applications to osteopathic practice, education, and research-areview and analysis," *The Journal of the American Osteopathic Association,* vol. 113, pp. 34-52, 2013.

[22] J. David, S. Hohenschurz, E. Jorge and P. Oliver, "Tensegrity and manual therapy practice:a qualitative study," *International Journal of the American Osteopathic Association,* vol. 113, pp. 34-52, September 2016.

[23] H. Obiya, K. Ijima, N. Kawasaki and S. Iguchi, "Form and Structural Analysis of High-Rise Pneumatic Structures," in *Proc. of the mt. Conf. on Computational and Experimental Engineering and Sciences (ICCEES 04)*, 2004.

[24] K.Ijima, H. Obiya, M. Kishimura and Y. Ostrikov, "A composite element of springs and rigid bars and its applicaiton to nonlinear analysis," in *APCOM'07-EPMESC XI*, 2007.

[25] H. Obiya, "A study on accuracy and versatile of the tangent stiffness method by seperation of element stiffness from geometrical stiffness (In Japanese)," in *Saga University*, Japan, 1998.

[26] H. Obiya, S. Goto, K. Ijima and K. Koga, "Equilibrium analysis of plane structures by the tangent stiffness method," *International Colloquium Stability of Steel Structures,* vol. 2, pp. 305-312, 1995.

[27] T. Kawakami, H. Obiya, C.K. Soe, M.Nizam and K. Ijima, "Mesh optimization based on a process of geometrical nonlinear analysis," in *IOP Conf. Series: Earth and Environmental Science*, May 2018.

[28] S. Yamada, K. Ijima, H. Obiya and M. Nizam, "An orthotropic membrane model for the large deformation analysis and snapping phenomena of the dome inflated," in *MATEC Web of Conference*, 2016.

[29] A. Yamasaki, H. Obiya, K. Ijima and M. Nizam, "A numerical case study on contact analysis with large displacement," in *MATEC Web of Conference*, 2016.

[30] H. Obiya, Z.M. Nizam, K. Ijima, N. Kawasaki and A. Matsuo, "A study on equilibrium shape of tensegrity structures with virtual stiffness through some numerical experiments," *Journal of Applied Mechanics JSCE,* vol. 15, pp. 45-56, 2012.

[31] M. Miyahara, K. Ijima, H. Obiya and M. Nizam, "An accurate algorithm of numerical integration for computing seismic responses of inelastic structures," *International Journal of Integrated Engineering, Special Issue 2018: Civil and Environmental Engineering,* vol. 10, no. 2, pp. 82-86, May 2018.

CHAPTER 2

Tangent Stiffness Method in Geometrical Nonlinear Analysis

2.1 Introduction

In case of the small displacement of a structure, the direct linear analysis is enough for solving the structural problems. When the structure suffers high loading or deforms in a large amount, the geometrical nonlinearity is required to be taken into account in the structural analysis for more accurate and reliable solutions. When the geometrically nonlinear analysis is executed, two different factors are obviously distinguished, one is caused by the rigid body displacement of elements and the other is by the element's own deformation. It is possible to evaluate the exact response for the former one by using the tangent geometrical stiffness derived by the element edge forces. On the other hand, the later one should be assumed based on the material and/or the geometrical property of the element. These mechanical behaviors can be prescribed by the tangent stiffness method which is effective in solving the geometrical nonlinearity problems and valid for a wide range of structures. In this chapter, the concept of tangent stiffness method will be presented with the relation to the geometrical nonlinear analysis.

2.2 Fundamental concept of geometrical nonlinear analysis
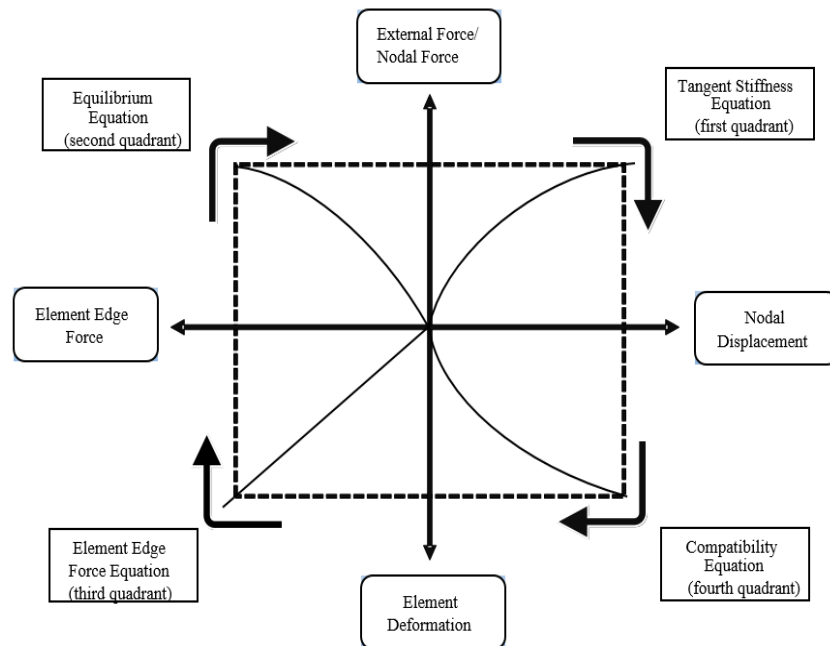
Figure 2.1 Relation between mechanical and geometrical values in case of finite displacement

Figure 2.1 shows the relation between the mechanical and geometrical values using in the structural calculations in case of finite displacement. The calculation process will be executed in the clockwise direction. The first quadrant represents the tangent stiffness equation for one member, and the fourth quadrant shows the relation of the compatibility equation between the displacement of nodes in the global coordinate system and the deformation of the element in the local coordinate system. In the third quadrant, the element's behavior can be prescribed by the element edge force equation to obtain the element force vector. The equilibrium equation in the fourth quadrant adjusts the balance between the element forces and the nodal force. And the system will be iterated until the structure keeps its stability in the equilibrium state.

☐ **Compatibility equation**
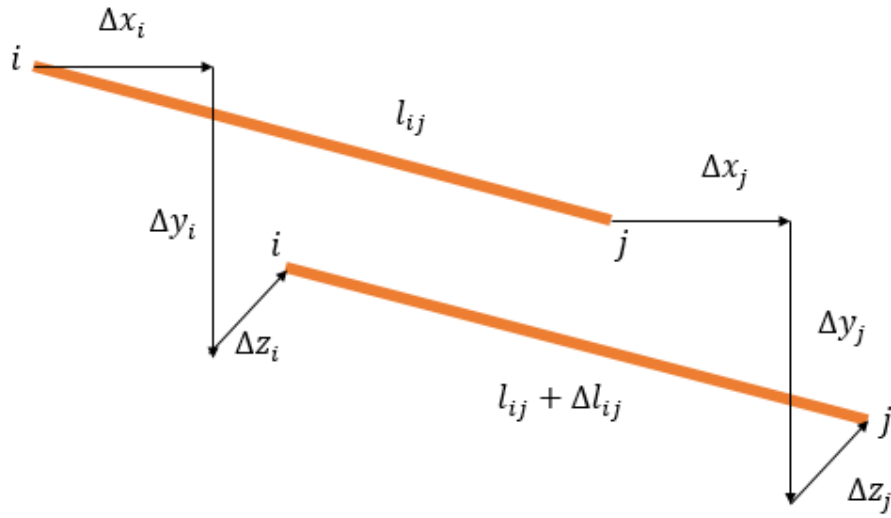
Figure 2.2 Relationship between the elongation of element and nodal displacement at both ends

Let α, β and γ be the components of cosine vector of the member, while l_0 is the initial non-stressed length, l is the current length and Δl is the increment of the length of ij member.

Also, let x_i, y_i, z_i be the horizontal and vertical positions of node i whereas x_j, y_j, z_j are those of node j, and $\Delta x_{ij}, \Delta y_{ij}, \Delta z_{ij}$ are the respective displacements of node i and node j.

By Pythagoras Theorem, the formulation of current length of ij member is as follow.

$$(l + \Delta l_{ij})^2 = (x_{ij} + \Delta x_{ij})^2 + (y_{ij} + \Delta y_{ij})^2 + (z_{ij} + \Delta z_{ij})^2 \tag{2.1}$$

In case of small displacement, the compatibility equation can be derived linearly as shown in equation (2.2) while neglecting the second order term of displacement.

$$\Delta l_{ij} = [-\alpha, -\beta, -\gamma, \alpha, \beta, \gamma] \begin{bmatrix} \delta x_i \\ \delta y_i \\ \delta z_i \\ \delta x_j \\ \delta y_j \\ \delta z_j \end{bmatrix} \tag{2.2}$$

However, in case of large displacement, the amount of the second order term will be involved to some extent comparing with the member size and should be taken into account for the exact description.

$$\Delta l_{ij} = \sqrt{(x_{ij} + \Delta x_{ij})^2 + (y_{ij} + \Delta y_{ij})^2 + (z_{ij} + \Delta z_{ij})^2} - l_{0ij} \tag{2.3}$$

Therefore, equation (2.3) represents the nonlinear compatibility by means of the curve representation in the fourth quadrant.

☐ **Element edge force equation**

Figure 2.3 Relationship between the axial force and the elongation

In the element edge force formula for the axial force member, the rigidity relationship between the axial force and the elongation is described when the statically indeterminate and stable support condition is applied in the member as shown in figure 2.3.

$$N_{ij} = \frac{EA}{l_{0ij}} \Delta l_{ij} \tag{2.4}$$

In equation (2.4), the element deformation is proportionated to the element forces linearly due to the stiffness relation of $\frac{EA}{l_{0ij}}$, in which the non-stressed length l_{0ij} will remain the same and the Young's Modules E and the cross sectional area A of the member can be assumed as constant

under the elastic condition. Therefore, the element edge force equation can be expressed by a linear function and consequently the third quadrant can be described by a linear straight line.

☐ **Equilibrium equation**
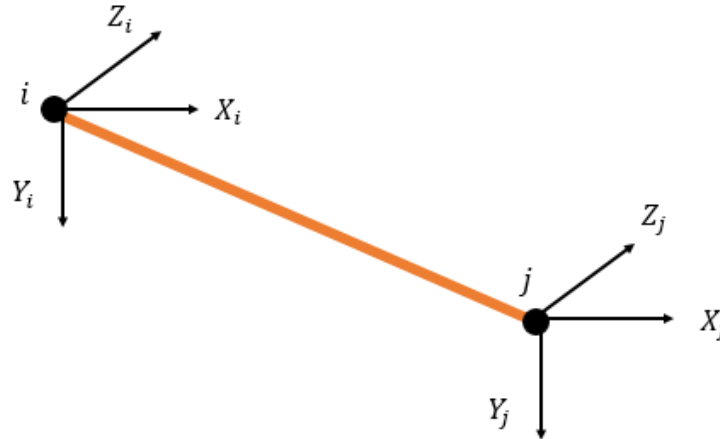
Figure 2.4 Nodal forces at the both ends of one member
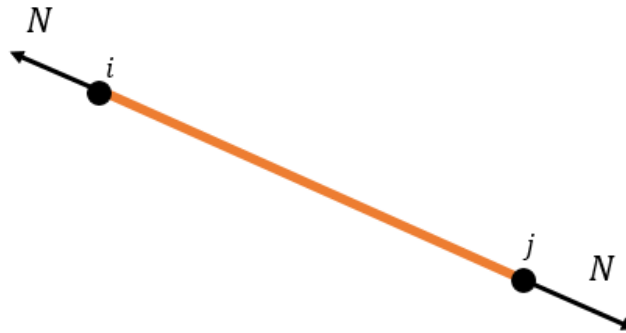
Figure 2.5 Member force at both ends of one member

If a common coordinate system is set with the horizontal direction as x axis, the vertical downward direction as y axis, and the inner direction as z axis, we can express the nodal forces in three directions acting on the nodes at both ends of one member as shown in figure 2.4. In addition, the member force N is given to a rod as in figure 2.5 and the components of translational nodal force can be described by the terms of cosine vectors of the axial force as below.

$$X_i = -\alpha N \ , \qquad Y_i = -\beta N \ , \qquad Z_i = -\gamma N \tag{2.5}$$

$$X_j = \alpha N \ , \qquad Y_j = \beta N \ , \qquad Z_j = \gamma N \tag{2.6}$$

And nodal forces can be expressed in matrix form as shown in equation (2.7).

$$
\begin{bmatrix} X_i \\ Y_i \\ Z_i \\ X_j \\ Y_j \\ Z_j \end{bmatrix} = \begin{bmatrix} -\alpha \\ -\beta \\ -\gamma \\ \alpha \\ \beta \\ \gamma \end{bmatrix} N
\tag{2.7}
$$

The cosine vectors of the equilibrium equation (2.7) will be updated to the post deformation in each iteration, therefore the second quadrant will be the nonlinear curve.

☐ **Total stiffness equation for one member**

Consequently, the total stiffness equation (2.8) is the combination of the equation (2.3), (2.4) and (2.7), therefore, the first quadrant can be expressed by the curve relation in the geometrical nonlinear analysis as

$$
\begin{bmatrix} X_i \\ Y_i \\ Z_i \\ X_j \\ Y_j \\ Z_j \end{bmatrix} = \frac{EA}{l_{oij}} \begin{bmatrix} \alpha^2 & \alpha\beta & \alpha\gamma & -\alpha^2 & -\alpha\beta & -\alpha\gamma \\ \alpha\beta & \beta^2 & \beta\gamma & -\alpha\beta & -\beta^2 & -\beta\gamma \\ \alpha\gamma & \beta\gamma & \gamma^2 & -\alpha\gamma & -\beta\gamma & -\gamma^2 \\ -\alpha^2 & -\alpha\beta & -\alpha\gamma & \alpha^2 & \alpha\beta & \alpha\gamma \\ -\alpha\beta & -\beta^2 & -\beta\gamma & \alpha\beta & \beta^2 & \beta\gamma \\ -\alpha\gamma & -\beta\gamma & -\gamma^2 & \alpha\gamma & \beta\gamma & \gamma^2 \end{bmatrix} \begin{bmatrix} \delta x_i \\ \delta y_i \\ \delta z_i \\ \delta x_j \\ \delta y_j \\ \delta z_j \end{bmatrix}
\tag{2.8}
$$

2.3 Basic concept of tangent stiffness method

The geometrical nonlinearity of finite element method in a structure means the nonlinearity caused by the rigid body displacement of each element divided into finite elements, and it can be separately considered from the element deformation caused by the displacement between the nodes connecting each component. In the performance of geometrical nonlinear analysis, it is necessary to evaluate the two geometrical nonlinearities strictly. The effect of element deformation can be mitigated by making the larger element division of the finite element structure, whereas the effect of rigid body displacement cannot be mitigated since the effect becomes distinct corresponding to the increase in the number of nodes. In another words, the necessity of considering the nonlinearity in the rigid body displacement should be strictly prescribed in the large deformation range when the nodal displacement becomes larger. In the tangent rigidity, the structure is divided into finite

elements in which only the rigid body displacement is constrained in each finite element, providing the stable and statically indeterminate support condition. Moreover, the element deformation in the unconstrained direction of the support condition shows the behavior of each independent element, and this is called the element deformation vector. Therefore, the relation between the element deformation vector **h** and the element edge force vector **T** can be expressed as in equation (2.9) where **k** refers to the stiffness matrix.

$$\mathbf{T} = \mathbf{kh} \tag{2.9}$$

In addition, the equilibrium equation is the relation between the nodal force vector **B** in the reference coordinate system (global coordinate system) and the element edge force vector **T** in the element coordinate system (local coordinate system), balanced by the equilibrium matrix **J**.

$$\mathbf{B} = \mathbf{JT} \tag{2.10}$$

And the tangent stiffness equation can be easily formulated by the first-order differentiation of the equilibrium equation.

$$\boldsymbol{\delta}\mathbf{B} = \boldsymbol{\delta}\mathbf{J}.\,\mathbf{T} + \mathbf{J}.\,\boldsymbol{\delta}\mathbf{T} \tag{2.11}$$

Furthermore, since the first and second terms on the right side of equation (2.11) can be exactly expressed as a linear function of the incremental displacement $\boldsymbol{\delta}\mathbf{d}$ in the global coordinate system, equation (2.11) can be rewritten as in equation (2.12).

$$\boldsymbol{\delta}\mathbf{B} = (\mathbf{K_0} + \mathbf{K_G})\boldsymbol{\delta}\mathbf{d} \tag{2.12}$$

Therefore, the expression between the nodal force vector and the increment of the nodal displacement from the previous state can be easily derived by the tangent stiffness equation. By using the tangent geometrical stiffness matrix, it is possible to express the strict tangent stiffness that perfectly matches the element behavior specified in the element edge force equation.

Here, $\mathbf{K_G}$ is the tangent geometrical stiffness related to the expression of the equilibrium equation. Since the element coordinate system defined here can be changed in position in accordance with the rigid body displacement, the nonlinearity caused by the displacement of rigid body is strictly evaluated in the geometrical stiffness matrix.

And $\mathbf{K_0}$ is the element stiffness related to the nonlinearity of the element edge force equation which is an expression between the element deformation vector and the element edge force vector. This evaluates the nonlinearity caused by the peculiarity of the element stiffness and provides the element behavior in the element coordinate.

In this way, if the geometrical nonlinearity can be strictly evaluated, the element stiffness can be completely separated from the tangent geometrical stiffness in the tangent stiffness method. This superior characteristic of tangent stiffness method allows the designer to select any type of structure member as long as the rigid body displacement is strictly constrained in the whole structural system.

2.4 Derivation of tangent geometric stiffness from the viewpoint of energy theory

The tangent geometric stiffness can be expressed by using the principle of total potential energy conservation which can be derived from the element edge force vector of the previously known condition.

Figure 2.6 shows the conceptual diagram of energy against the mechanical quantities related to the nodal displacement, element deformation, element forces and the nodal forces which are the major components in the tangent stiffness method. The shaded area in the first quadrant indicates the loss in potential energy due to the displacement of the loading point. The shaded area in the third quadrant shows the strain energy obtained from the deformation and the edge forces in the element coordinate system.

In addition, the part surrounded by the inner rectangle represents the known mechanical quantities of the preceding equilibrium state. Let U be the strain energy and V be the loss in potential energy due to external force, then the total potential energy Π in the prior equilibrium state can be described as follow.

$$\Pi = U - V \tag{2.13}$$

Similarly, the part surrounded by the outer rectangle expresses the equilibrium condition of the post-deformation after the load variation during the incremental process. Therefore, the total potential energy Π' in the post-deformation can be expressed as below.

$$\Pi' = U' - V' = \Pi + \Delta\Pi \tag{2.14}$$

$$\Pi' = \Pi + (\Delta U + U^{\#}) - (\Delta V + V^{\#} + V_c^{\#}) \tag{2.15}$$
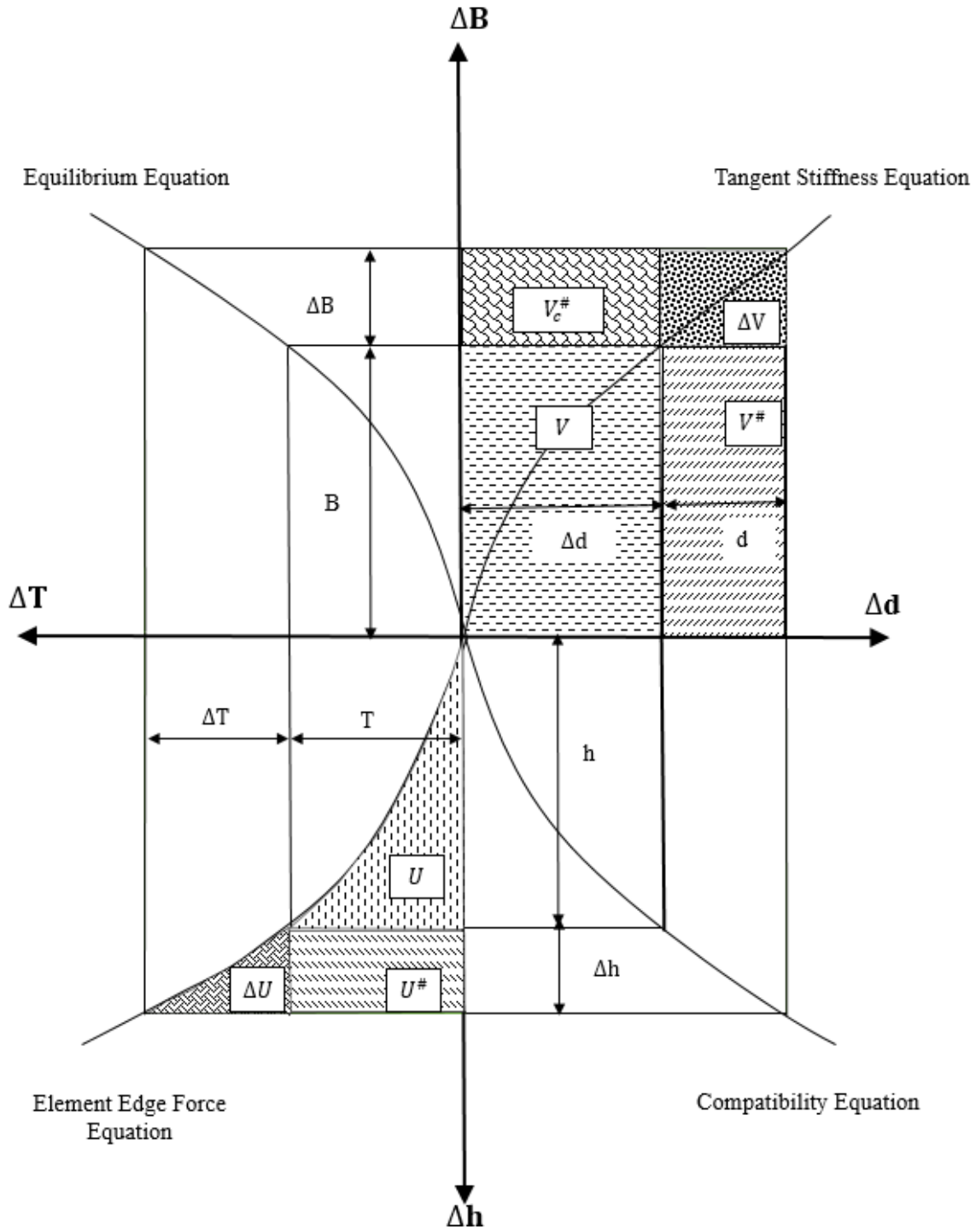
18

Figure 2.6 The conceptual diagram of energy against the mechanical quantities

However, the equilibrium condition is maintained both in pre and post deformation according to the energy conservation, therefore, the total potential energy for both conditions is

$$\frac{\partial \Pi}{\partial \Delta \mathbf{d}} = 0 \tag{2.16}$$

$$\frac{\partial \Pi'}{\partial \Delta \mathbf{d}} = 0 \tag{2.17}$$

From the equation (2.15) to (2.17), we can rewrite the equation (2.18) as follow.

$$\frac{\partial \Pi}{\partial \Delta \mathbf{d}} = \frac{\partial}{\partial \Delta \mathbf{d}} \{ (\Delta U + U^{\#}) - (\Delta V + V^{\#} + V_c^{\#}) \} = 0 \tag{2.18}$$

Here, $U^{\#}$ is strain energy stored by the element edge forces of the preceding state with respect to the element deformation.

$$U^{\#} = \Delta \mathbf{h}^{\mathrm{T}} \mathbf{T} \tag{2.19}$$

And the derivative of $U^{\#}$ by the incremental displacement $\Delta \mathbf{d}$ is

$$\frac{\partial U^{\#}}{\partial \Delta \mathbf{d}} = \frac{\partial \Delta \mathbf{h}^{\mathrm{T}}}{\partial \Delta \mathbf{d}} \mathbf{T} \tag{2.20}$$

Moreover, ΔU is the increment of the strain energy.

$$\Delta U = \int_0^{\Delta \mathbf{h}} \Delta \mathbf{T}^{\mathrm{T}} \mathbf{d} \Delta \mathbf{h} \tag{2.21}$$

If ΔU is differentiate by the incremental displacement $\Delta \mathbf{d}$,

$$\frac{\partial \Delta U}{\partial \Delta \mathbf{d}} = \frac{\partial}{\partial \Delta \mathbf{d}} \int_0^{\Delta \mathbf{h}} \Delta \mathbf{T}^{\mathrm{T}} \mathbf{d} \Delta \mathbf{h} = \frac{\partial \Delta \mathbf{h}^{\mathrm{T}}}{\partial \Delta \mathbf{d}} \cdot \frac{\partial}{\partial \Delta \mathbf{h}} \int_0^{\Delta \mathbf{h}} \Delta \mathbf{T} \mathbf{d} \Delta \mathbf{h} = \frac{\partial \Delta \mathbf{h}^{\mathrm{T}}}{\partial \Delta \mathbf{d}} \Delta \mathbf{T} \tag{2.22}$$

On the other hand, ΔV, $V^{\#}$ and $V_c^{\#}$ indicate the loss in potential energy due to the displacement of the loading point, thus the equation for each component can be written as

$$\Delta V = \Delta \mathbf{d}^{\mathrm{T}} \Delta \mathbf{B} \tag{2.23}$$

$$V^{\#} = \Delta \mathbf{d}^{\mathrm{T}} \mathbf{B} \tag{2.24}$$

$$V_c^{\#} = \mathbf{d}^{\mathrm{T}} \Delta \mathbf{B} \tag{2.25}$$

And differentiation of each component by the incremental displacement $\Delta\mathbf{d}$ can be described as follow.

$$\frac{\partial\Delta V}{\partial\Delta\mathbf{d}} = \frac{\partial\Delta\mathbf{d}^{\mathrm{T}}}{\partial\Delta\mathbf{d}}\Delta\mathbf{B} = \Delta\mathbf{B} \tag{2.26}$$

$$\frac{\partial\Delta V^{\#}}{\partial\Delta\mathbf{d}} = \frac{\partial\Delta\mathbf{d}^{\mathrm{T}}}{\partial\Delta\mathbf{d}}\mathbf{B} = \mathbf{B} \tag{2.27}$$

$$\frac{\partial\Delta V_c^{\#}}{\partial\Delta\mathbf{d}} = \frac{\partial}{\partial\Delta\mathbf{d}}(\mathbf{d}^{\mathrm{T}}\Delta\mathbf{B}) = 0 \tag{2.28}$$

From equation (2.19) to (2.28), equation (2.18) can be rewritten as in equation (2.29).

$$\frac{\partial\Delta\mathbf{h}^{\mathrm{T}}}{\partial\Delta\mathbf{d}}(\mathbf{T} + \Delta\mathbf{T}) = \mathbf{T} + \Delta\mathbf{T} \tag{2.29}$$

It is possible to achieve the equilibrium equation between the element edge force vector and the nodal force vector of the post-deformation condition. By comparing the equation (2.10) with equation (2.29), the equilibrium matrix can be concluded as.

$$\mathbf{J} + \Delta\mathbf{J} = \frac{\partial\Delta\mathbf{h}^{\mathrm{T}}}{\partial\Delta\mathbf{d}} \tag{2.30}$$

On the other hand, referring to the equation (2.11) and (2.12), we can express the equation (2.31) as below.

$$\delta\mathbf{J}\mathbf{T} = \mathbf{K_G}\delta\mathbf{d} \tag{2.31}$$

And converted to the term of tangent geometric stiffness matrix, we will have,

$$\mathbf{K_G} = \frac{\partial(\delta\mathbf{J}\mathbf{T})^{\mathrm{T}}}{\partial\Delta\mathbf{d}} = \left(\frac{\Delta\mathbf{J}\mathbf{T}}{\partial\Delta\mathbf{d}}\right)^{\mathrm{T}}_{\Delta\mathbf{d}\to 0} \tag{2.32}$$

Here, from the equation (2.30),

$$\frac{\partial\Delta\mathbf{J}}{\partial\Delta\mathbf{d}} = \frac{\partial}{\partial\Delta\mathbf{d}}\left(\frac{\partial\Delta\mathbf{h}^{\mathrm{T}}}{\partial\Delta\mathbf{d}}\right) \tag{2.33}$$

Therefore, the geometric stiffness matrix can be expressed as follow.

$$\mathbf{K_G} = \frac{\partial}{\partial\Delta\mathbf{d}}\left(\frac{\partial\Delta\mathbf{h}^{\mathrm{T}}\mathbf{T}}{\partial\Delta\mathbf{d}}\right)^{\mathrm{T}}\Bigg|_{\Delta\mathbf{d}\to 0} \tag{2.34}$$

2.5 Iteration procedure of TSM in geometrical nonlinear analysis

A brief procedure for developing the iterated algorithm is shown in figure 2.7 Starting from the information of the applied external force on the designated nodes, the calculation process will be iterated clock-wisely in the order of (1^*), (2), (3) and (4). However, the physical values and the cosine vectors at the primary state of pre-deformation are required to be known before starting the iteration process. The iteration process will be illustrated in color in which the solid line represents the tangent of the nonlinear curve in the first quadrant while the dotted line expresses the looping algorithm in each step. Besides, the notation of $\delta \mathbf{d}$ indicates the increment of displacement from the previous state (i.e. the solution of the nth iterative step). Meanwhile, the notation of $\Delta \mathbf{d}$ refers to the total amount of displacement from the primary state (i.e. the sum of the solutions of the tangent stiffness equations from 1st to n^{th} steps).

The process will initiate from the original tangent point of 0, and the green tangent is drawn at the given value of the external force, then the displacement is calculated by solving the tangent stiffness equation. In the first step, the total displacement $\Delta \mathbf{d_1}$ will be the same as the first increment $\delta \mathbf{d_1}$. From the information of the nodal displacement $\delta \mathbf{d_1}$, the compatibility equation gives the element deformation, from which the element forces can be executed by applying the element force equation consequently. The equilibrium equation gives the nodal force $\Delta \mathbf{B_1}$ which is not balanced against the given amount of the external force.

The unbalanced force $\delta \mathbf{B_1}$ is calculated and the tangent point of 1 is reset as the primary state. The orange tangent is drawn according to $\delta \mathbf{B_1}$ and then acted to the tangent stiffness equation, producing $\delta \mathbf{d_2}$. The new displacement $\Delta \mathbf{d_2}$ is then achieved by adding the $\delta \mathbf{d_2}$ to the previous $\Delta \mathbf{d_1}$. The corresponding mechanical values are then computed in the same process and the difference between the obtained nodal force and the load given ($\delta \mathbf{B_2}$) decreases subsequently. Similarly, the calculation for the third step shown in the blue lines will be the same and the algorithm will be repeated until the unbalanced force converges to zero at the nth step as shown in the yellow lines. Finally, the analysis achieves the equilibrium state and produces the converged solution after adjusting the unbalanced force in each step during the iteration process. Therefore, the iteration process in the tangent stiffness method can be expressed as follow.

$$\Delta \mathbf{d_{n+1}} = \Delta \mathbf{d_n} + \mathbf{K_{Tn}^{-1}} \cdot (\mathbf{B_0} + \Delta \mathbf{B} - \mathbf{J_n T_n}) \tag{2.35}$$

ΔB

Equilibrium
Equation

Tangent Stiffness
Equation

Given External Force

(4)

(1*)

δB_2

δB_1

ΔB_2 ΔB_1

1

ΔT ←—————————————————————→ Δd

0

δd_1 δd_2

(3)

(2)

Element Edge Force
Equation

Compatibility
Equation

Δh
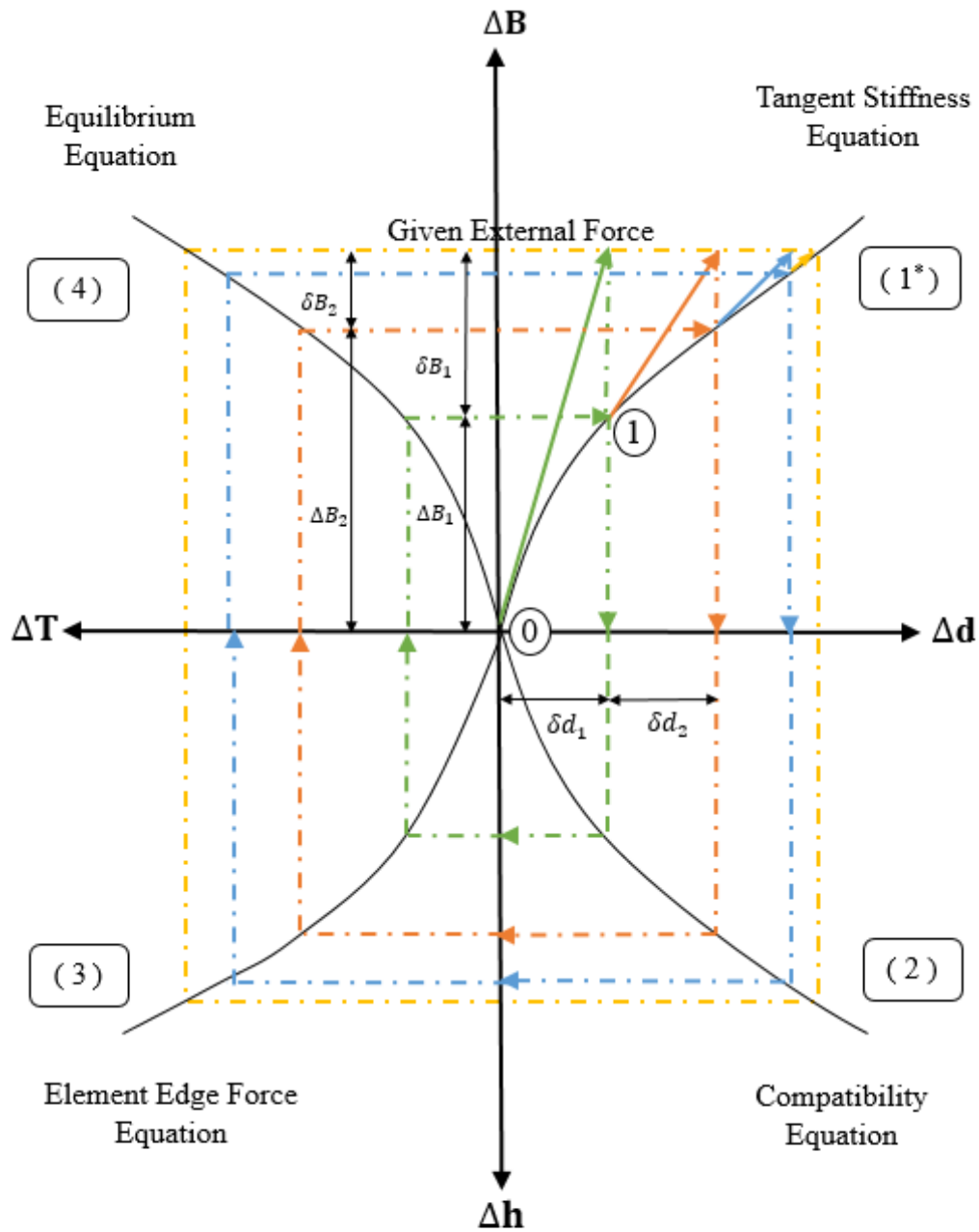
- ΔB = External/Nodal Force   ▪ Δh = Element Deformation

- Δd = Nodal Displacement   ▪ ΔT = Element Edge Force

Figure 2.7 Iteration process of tangent stiffness method

23

2.6. Algorithm of tangent stiffness method

In the nonlinear algorithm, the calculation procedure based on the tangent stiffness method is carried out iteratively. Firstly, the required input data is given for setting up the initial configuration of the proposed structure. This includes the number of nodes and numbers of members in a structure, the nodal positions and connectivity of the members to the nodes, the element properties, the applied nodal forces and the support conditions. After establishing the information for the primary unbalanced structure, the maximum band width and size of the total stiffness matrix are determined based on the number of nodes.

Next, the main algorithm is initiated with a series of structural equations. The element deformation is found out by the application of strict compatibility equation which is a relation between the nodal displacements and element deformation vector. From the information of element elongation or reduction, the element edge forces can be calculated by element edge force equation which defines the element behavior based on the material stiffness of elements. Then, the nodal force vector can be obtained from the equilibrium equations which adjusts the balance between the element edge forces and the nodal forces at each coordinate point. From this, the resulted nodal forces will give the information of unbalanced force which can be determined from the difference between the obtained and applied nodal forces. If the maximum unbalanced force is found to be beyond the boundaries of allowable limitation, the iteration of the algorithm is started to make the convergence of the unbalanced force.

The total tangent stiffness matrix is established by the combination of tangent element stiffness and tangent geometrical stiffness. Each stiffness matrix will be superimposed to develop the total stiffness for the whole structure. The iteration process will be rapidly directed to be convergent due to the strict compatibility of tangent stiffness method. The simultaneous mathematical equations will be solved by the Gauss elimination method from which the displacement of each node can be obtained. The resulted incremental displacement will be applied to the previous coordinates of each node. After renewing the nodal positions, the algorithm will be repeated until the judgement of convergence of resulted unbalanced nodal forces is satisfied. When the convergent results meet with the required limitations of accuracy, the iteration procedure is terminated and the solutions will be obtained. The whole algorithm of the tangent stiffness method is demonstrated in figure 2.8.
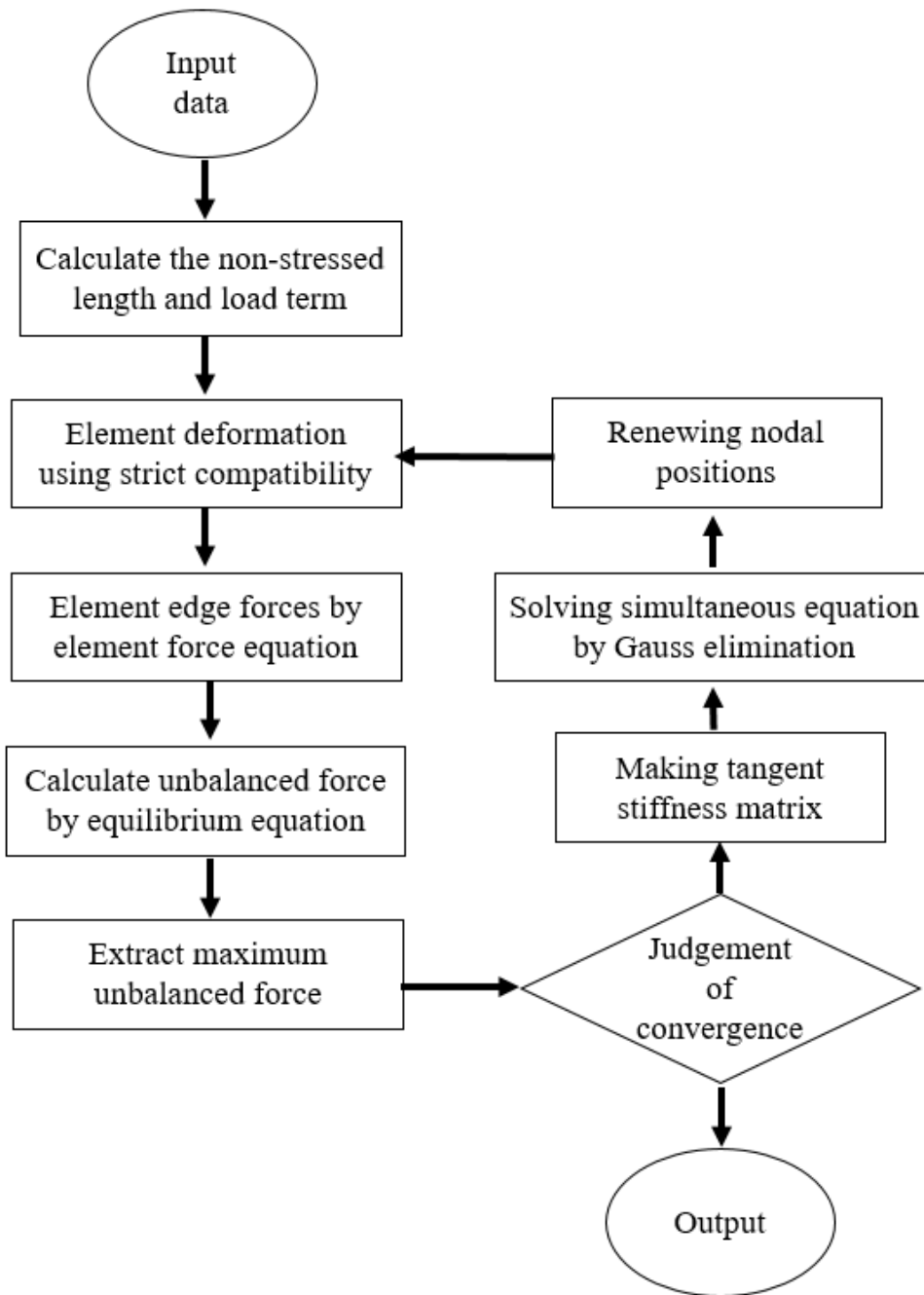
Figure 2.8 Flow chart of tangent stiffness method

2.7 Summary of chapter 2

In this chapter, the detail derivation of the tangent stiffness method is discussed. The concept of geometrical nonlinear analysis is proposed and the formulations used for tangent stiffness method are prepared with their application in plane truss element. The iteration process of tangent stiffness method is explained step by step, showing the working process of equations in each part of iterated algorithm.

From this methodology, it is found out that the nonlinear process can be conducted in much simpler approach with the linear tangent of the nonlinear iteration curve with which the complicated calculation of nonlinearity can be avoid and the reliable solutions can be obtained due to the strict rigid compatibility of structural elements in this proposed tangent stiffness method. The application of tangent stiffness method in the form-finding analysis of tensegrity structures will be discussed in the following chapter.

List of Symbols

Symbol		Description
x	:	Nodal coordinate in horizontal direction
y	:	Nodal coordinate in vertical direction
z	:	Nodal coordinate in inner direction
l_0	:	Non-stressed length
Δl	:	Increment of length
α	:	Cosine vector component in horizontal direction
β	:	Cosine vector component in vertical direction
γ	:	Cosine vector component in inner direction
N_{ij}	:	Axial force of member ij
E	:	Young's modulus
A	:	Cross-sectional area
X	:	Nodal force in x direction
Y	:	Nodal force in y direction
Z	:	Nodal force in z direction
T	:	Element edge force vector
k	:	Stiffness matrix
h	:	Element deformation vector
d	:	Nodal displacement vector
B	:	External force vector
J	:	Equilibrium matrix
$\mathbf{K_0}$	:	Element stiffness matrix
$\mathbf{K_G}$	:	Tangent geometrical stiffness matrix
U	:	Strain energy
V	:	Loss in potential energy
Π	:	Total potential energy

CHAPTER 3

Form-finding of Tensegrity: Integration of Real and Virtual Element

3.1 Introduction

Tensegrity processes a unique geometrical morphology which is composed of disconnected compression members in a connected network of tension members. It can be stabilized in a self-equilibrium state and can achieve deformation in a large scale. Therefore, finding its equilibrium shape is one of the key points for designing tensegrity structures, which is known as form-finding analysis. In this study, the form-finding process is presented from the viewpoint of geometrically nonlinear analysis. Since the tensegrity structure can largely deform in its self-equilibrium state, the geometrical nonlinearity must be considered in the large deformational structures.

In this study, the tangent stiffness method is applied to conduct the form-finding analysis since it is quite effective in the geometrical nonlinear analysis due to its strict rigid body displacement of elements. Since the tangent stiffness method allows us to define the element behavior freely, the author proposes a unique approach to characterize the tensegrity structure having both real and virtual elements. The introduction of element's measure potential makes it possible to explore the formation of equilibrium configuration by using this integrated structural behavior. In this chapter, each component in the proposed measure potential is examined in detail and their influence on the out coming equilibrium solutions is discussed with calculation examples. Furthermore, the concept of multiple non-stressed length is introduced for seeking a wider diversity of equilibrium formation in the shape analysis of tensegrity.

3.2 Methods applied in the form-finding of tensegrity

The existing form-finding methods can be widely divided into two approaches: analytical and numerical approaches. In general, the analytical approaches are assigned for the explicit expression of highly symmetric structures such as tensegrity prisms and truncated regular polyhedral tensegrities [1]. Meanwhile, the numerical form-finding produces the discrete feasible solutions case by case [2], giving a functional approach to more complicated types of structures including irregular tensegrities [3]. In the former literatures, the regular truncated polyhedral tensegrities are investigated either by analytical or numerical approach. Tsuura et al. [4] conducted the equilibrium and stability analysis numerically for the tetrahedral, hexahedral and octahedral

28

structures. However, the numerical approaches may lead to the complicated comprehension of self-equilibrium and stability properties of the structures [5]. As a result, the analytical approaches are enable to process in a compact form more efficiently as long as the structures are highly maintained in their symmetric geometry [2].

3.2.1 Analytical approach

The analytical procedures are an efficient tool in implementing the mechanical behavior of tensegrity structures where the shape analysis is mainly considered by the proper degree of symmetrical condition. Zhang et al. proposed an analytical approach to drive the block-diagonalization force density matrices with a combination of group representation theory which simplifies the symmetric problems [6] for prismatic tensegrity [7] [8] and star-shaped tensegrity [9] where both systems resemble the dihedral symmetry. Later, they made an extension to apply in the tensegrity structures with tetrahedral symmetry [10]. Recently, Zhang and his fellows derived a unified solution analytically for the Z-based truncated regular polyhedral (TRP) [11] and rhombic tensegrities [12]. The properties of self-equilibrium and super stability are significantly achieved under the analytical conditions. Murakami and Nishimura investigated the static and dynamic characterization [13] of truncated dodecahedral and icosahedral tensegrities and Zhang et al. [5] modified the force density matrix in the symmetry-adapted form to establish the stability of the self-equilibrated truncated hexahedral and octahedral tensegrity modules, satisfying the non-degeneracy condition of the structure.

In the above analytical approaches, structural equilibrium or force density matrix is mainly involved to establish the self-equilibrium conditions. Koohestani and Guest [14] introduced a new approach to form-finding of tensegrity in both analytical and numerical ways by combining the equilibrium equations and geometrical compatibility equations with a specification of Cartesian components of the element length of the structure. Koohestani developed a simplified analytical form-finding method with an introduction of Faddeev-LeVerrieer algorithm which provides the required explicit conditions of the self-stressed states [2]. Recently, Zhang et al. [15] attempted to construct a large scale tensegrity structure by an innovative assembly scheme in which the truncated polyhedral cells are specified as main blocks and prismatic elementary cells are used as a bridge-connection. The analytical results are helpful to understand the self-equilibrium and stability properties of tensegrities, however, most of the analytical methods are only feasible for

highly symmetric structures of small or medium scale due to the need of symbolic mathematical operations used in these form-finding methods.

3.2.2 Numerical Approach

The form-finding of the tensegrity structures are achieved by the numerical approach in a broader version. Numerical procedures let the researchers deal with more diverse calculation methods to treat the various compositions of complex tensegrity structures. Estrada et al. proposed a numerical form-finding procedure for statically indeterminate tensegrity structures with the iteration processes by using rank constraints on the stress and rigidity matrices [16]. Zhang et al. presented a new approach to design the geometry of the tensegrity directly by specifying the axial forces of the element and nodal coordinates as variables [17]. Zhang et al. established a stiffness matrix-based form-finding method for both regular and irregular tensegrities where the stably self-equilibrated configurations can be rapidly determined from the initial arbitrary stage [18]. Inspired by Monte Carlo method [19], Li et al. modified the form finding scheme, employing a stochastic algorithm to determine the equilibrium solutions with minimum potential energy for large scale and irregular tensegrity models [20]. Yuan et al. adopted Levenberg-Marquardt based form-finding method in which nonlinear equilibrium equations are converted to nonlinear least-squares problems. Dealing with singularity of the stiffness matrix, the L-M method can treat both regular and irregular tensegrities under external loading [21]. Micheletti and Williams conducted form-finding analysis based on a marching procedure with the characterization of rank-deficiency manifold for a large system. However, it is only feasible for a small portion of non-regular tensegrities [22]. The followings are some of the popular methods applied in the structural analyses by the numerical approach.

☐ **Dynamic relaxation method**

One of the popular methods used in tracing the change in motion and movement of the structural elements is dynamic relaxation method [23] which has been effectively used in the cable structures [24] and in truss and frame structures [25] and tensegrity structures [26]. DR method transforms the static problem into a pseudo-dynamic process and controls the structural equilibrium by integrating fictitious inertia and damping terms in dynamic equations [26]. Dynamic relaxation traces the motion of each node of a structure until the structure comes to rest in static equilibrium. Ali et al. [27] applied a modified dynamic relaxation algorithm to analyze

the form-finding of the clustered tensegrity structures with continuous cables and compared the results with tangent stiffness method. Baudriller et al. modeled the complex tensegrity based on the cell cytoskeleton concept to generate the non-regular structures with higher diversity using dynamic relaxation method [28].

☐ **Finite element method**

As a powerful tool for structural analysis, the finite element formulations have been effectively used in sliding cable elements of suspension systems [29] [30], tensioned fabric structures [31] and recently, also in numerical form-finding problems of tensegrity structures. Pagitz and Tur [32] proposed a two-step algorithm which minimizes of the total potential energy and realizes the symmetry transformation matrixes. This approach enables to seek the statically determinate or kinematic tensegrity configurations in a quicker convergence with a few iterations. By integrating the finite element method and mathematical programming, Klinka et al. developed an energy optimization based form-finding method for the tensegrities without supported constraints [33].

☐ **Nonlinear programming method**

The non-linear programming method [34] is a general method for pin-jointed structures which can be applied in the tensegrity form-finding. Burkhardt [35] presented non-linear programming approach in the form-finding and folding analysis of the prismatic tensegrity structures by using the fictitious elastic material properties for cables and minimizing the difference between squared sums of member length. Using affine transformation of equilibrium shape, folding analysis is simulated by using constrained optimization with small non-stressed length of cables. This method can make the use of general purpose in software, and various geometrical configurations of a structure can be obtained from the same topological condition. However, it will be time consuming and not feasible for a large and irregular tensegrity when the number of elements and constraint equations increases [36].

☐ **Force density method**

Recently, force density method gains its popularity in conducting the numerical analyses in various structures including the tensegrity. Force density method, first proposed by Linkwitz [37] and Schek [38], is based on the concept of the ratio between the internal force and associated

element length, which is known as force density. Force density based approaches are actively applied to structures with tensional members where the lengths of the members are not specified in the initial stage [38]. In the form-finding process of tensegrity by introducing the concept of element force density, the nonlinear equations are linearized and the self-equilibrium condition is determined if the force density matrix can satisfy the rank deficiency condition [39]. However, the force density method cannot directly control over the variation of element length and geometric parameters of the structure [16], [40].

☐ **Modified force density method**

There are already some researchers who modified the original force density method applied to cable net structures [41], cable-membrane structures [42] and tensegrity structures. Masic et al. extended the force density method in an algebraic approach with the involvement of shape constraints to the symmetric tensegrity structures [43]. Miki and Kawaguchi developed an extended force density method based on the energy function and solved the optimization problems of cable nets and tension structures [44]. Lee and Lee modified the force density method with an integration of genetic algorithm to determine the self-equilibrium and stability properties of tensegrity structures with arbitrary strut and cable members [45]. The force density method is extended as an advanced version in the form finding problem of tensegrity structures where the eigenvalue analysis and single value decomposition are performed iteratively for the feasible sets of force densities and nodal coordinates that satisfy the minimum requirement of rank deficiencies of the force density and equilibrium matrices with respect to the nodal coordinates [46] [47].

☐ **Genetic algorithm**

Recently, the genetic algorithm becomes popular to assign in the form-finding problem of tensegrity structures since it enables to solve the self-equilibrium state with least design variables [48]. Lee et al. [49] introduced a double-loop genetic algorithm that realize a fully automatic group selection for the form-finding process and Koohestani [50] also applied the genetic algorithm as an optimization technique but the proposed models are limited to the regular tensegrity structures. Xu and Luo [51] introduced binary-coded genetic algorithm and used the consideration of constrained optimization problem in the form-finding process of non-regular tensegrity. Gan et al. integrated the node-based genetic algorithm encoding scheme in the form-finding procedure for irregular tensegrity structures [52].

☐ **Optimization algorithm**

In addition, numerous approaches based on optimization algorithms [53] have been suggested by many researchers to solve the problem. Modified evolutional algorithm has been widely used in constrained [54], unconstrained [55] and continuous [56] optimization problems. Do et al. combined the modified differential evolution algorithm with force density method to evaluate optimal solutions of two and three dimensional tensegrity structures with a reduced the computational cost [57]. Paul et al. [58] proposed an evolutionary algorithm based on direct encoding to evolve the connectivity pattern and parameter values of tensegrity structures with maximal volume. Rieffel et al. [59] investigated the automated optimization for huge and complex irregular tensegrities. Their evolutional algorithm involves a generative representation approach based on a map L-system. Cai and Feng established an optimization-based form finding method with gradient descent algorithm to obtain the force density by minimizing an objective function that satisfies the non-degeneracy condition [60]. Researchers optimized the form-finding problem by many approaches such as matrix iteration approach [61], simulated annealing algorithm [62], ant colony algorithm [63] to reinforce the better performance of form-finding framework.

3.2.3 TSM in tensegrity form-finding

The tangent stiffness method has a good practice in the design of frame or membrane structures. Besides, it can be applied as a great tool in solving the form-finding problems of tensegrity structures. With the introduction of virtual stiffness, Obiya et al. [95] implemented tangent stiffness method in the equilibrium shape analysis of tensegrity. The virtual potential functions having parameters of element measurement are presented for the form-finding process, and its differential functions as the element force equations prescribing the element behaviour. Abe et al. studied the multi-bifurcation paths using the tangent stiffness method [65]. Matsuo et al. [66] applied the truss elements and axial force lines elements for the tensegrity tower and Nizam et al. [67] presented the path-finding procedure for the virtual tensegrity structure using the same axial line elements. In their studies, the self-equilibrated solutions are obtained by tracing the equilibrium path on the load-displacement curve with the examination of gravitational influence. However, the equilibrium solutions are formed unsymmetrically in the bifurcation paths. Therefore, a modified method will be proposed in this study that will explain the element behaviour either in terms of real or virtual structural elements, leading to a unique approach in form-finding analysis.

3.3 Development of stiffness equation for strut member with truss behavior

When deriving the tangent stiffness equation in the analysis of three-dimensional truss structure, the tangent stiffness matrix can be easily obtained by the first derivative of the equilibrium equation.

Firstly, let us define the nodal force vector of equation (3.1) and the equilibrium matrix of equation (3.2) as follow.

$$\mathbf{B_{ij}} = \left[-x_i, -y_i, -z_i, x_j, y_j, z_j\right]^{\mathrm{T}} \tag{3.1}$$

$$\mathbf{J_{ij}} = \left[-\alpha_{ij}, -\beta_{ij}, -\gamma_{ij}, \alpha_{ij}, \beta_{ij}, \gamma_{ij}\right]^{\mathrm{T}} \tag{3.2}$$

And if the axial force is subjected on the *ij* member of the truss element, then the equilibrium equation can be written as,

$$\mathbf{B_{ij}} = \mathbf{J_{ij}} N_{ij} \tag{3.3}$$

By differentiating equation (3.3) on both sides,

$$\delta \mathbf{B_{ij}} = \delta \mathbf{J_{ij}} N_{ij} + \mathbf{J_{ij}} \delta N_{ij} \tag{3.4}$$

Since it can be expressed as a linear form of the small increment δx_{ij}, the differential expression of $\delta \mathbf{J_{ij}}$ and δN_{ij} will be expanded in detail as follow. The original form of element edge force vector is linear function, therefore, δN_{ij} can be described by using Young's modulus E, cross-sectional area A, and non-stressed length l_0 as below.

$$\delta N_{ij} = \frac{EA}{l_{oij}} \delta l_{ij} \tag{3.5}$$

By differentiating the Pythagoras Theorem in equation (3.6), equation (3.7) will be obtained.

$$l_{ij}{}^2 = x_{ij}{}^2 + y_{ij}{}^2 + z_{ij}{}^2 \tag{3.6}$$

$$2l_{ij}.\,\delta l_{ij} = 2x_{ij}.\,\delta x_{ij} + 2y_{ij}.\,\delta y_{ij} + 2z_{ij}.\,\delta z_{ij} \tag{3.7}$$

When the both sides of equation (3.7) is divided by $2l_{ij}$, and applying the cosine vector between *i* and *j* nodes as,

$$\delta x_{ij} = \delta x_j - \delta x_i, \qquad \delta y_{ij} = \delta y_j - \delta y_i, \qquad \delta z_{ij} = \delta z_j - \delta z_i \qquad (3.8)$$

$$\delta l_{ij} = \left[-\alpha_{ij}, -\beta_{ij}, -\gamma_{ij}, \alpha_{ij}, \beta_{ij}, \gamma_{ij} \right] \begin{bmatrix} \delta x_i \\ \delta y_i \\ \delta z_i \\ \delta x_j \\ \delta y_j \\ \delta z_j \end{bmatrix} = \mathbf{J}_{ij}^{\mathbf{T}} \, \delta \bar{\mathbf{x}}_{ij} \qquad (3.9)$$

Then, combining from equation (3.5) to equation (3.9) and substituting in the right side of equation (3.4), $\mathbf{J}_{ij} \delta N_{ij}$ can be derived as follow.

$$\mathbf{J}_{ij} \delta N_{ij} = \frac{EA}{l_{oij}} \mathbf{J}_{ij} \mathbf{J}_{ij}^{\mathbf{T}} \, \delta \bar{\mathbf{x}}_{ij} = \frac{EA}{l_{oij}} \begin{bmatrix} \alpha^2 & \alpha\beta & \alpha\gamma & -\alpha^2 & -\alpha\beta & -\alpha\gamma \\ \alpha\beta & \beta^2 & \beta\gamma & -\alpha\beta & -\beta^2 & -\beta\gamma \\ \alpha\gamma & \beta\gamma & \gamma^2 & -\alpha\gamma & -\beta\gamma & -\gamma^2 \\ -\alpha^2 & -\alpha\beta & -\alpha\gamma & \alpha^2 & \alpha\beta & \alpha\gamma \\ -\alpha\beta & -\beta^2 & -\beta\gamma & \alpha\beta & \beta^2 & \beta\gamma \\ -\alpha\gamma & -\beta\gamma & -\gamma^2 & \alpha\gamma & \beta\gamma & \gamma^2 \end{bmatrix}_{ij} \delta \bar{\mathbf{x}}_{ij} \qquad (3.10)$$

On the other hand, the rest part of equation (3.4) will be derived as following. Since $\boldsymbol{\delta J_{ij}}$ is the variation of the equilibrium equation composed of consine vector, the differential calculus of cosine vector α, β and γ will be calculated.

$$\delta \alpha_{ij} = \frac{x_j - x_i}{l_{ij}}, \qquad \delta \beta_{ij} = \frac{y_j - y_i}{l_{ij}} \quad , \qquad \delta \gamma_{ij} = \frac{z_j - z_i}{l_{ij}} \qquad (3.11)$$

And their differential forms are,

$$\delta \alpha_{ij} = \frac{1}{l_{ij}} \left[-(1 - \alpha^2), \alpha\beta, \alpha\gamma, (1 - \alpha^2), -\alpha\beta, -\alpha\gamma \right]_{ij} \begin{bmatrix} \delta x_i \\ \delta y_i \\ \delta z_i \\ \delta x_j \\ \delta y_j \\ \delta z_j \end{bmatrix} \qquad (3.12)$$

$$\delta \beta_{ij} = \frac{1}{l_{ij}} \left[\alpha\beta, -(1 - \beta^2), \beta\gamma, -\alpha\beta, (1 - \beta^2), -\beta\gamma \right]_{ij} \begin{bmatrix} \delta x_i \\ \delta y_i \\ \delta z_i \\ \delta x_j \\ \delta y_j \\ \delta z_j \end{bmatrix} \qquad (3.13)$$

$$\delta\gamma_{ij} = \frac{1}{l_{ij}}[\,\alpha\gamma, \beta\gamma, -(1-\gamma^2), -\alpha\gamma, -\beta\gamma, -(1-\gamma^2)]_{ij}\begin{bmatrix}\delta x_i \\ \delta y_i \\ \delta z_i \\ \delta x_j \\ \delta y_j \\ \delta z_j\end{bmatrix} \qquad (3.14)$$

Therefore, the formulation of $\delta\mathbf{J_{ij}}N_{ij}$ can be expressed as below.

$$\delta\mathbf{J_{ij}}N_{ij} = \frac{N_{ij}}{l_{ij}}\begin{bmatrix} (1-\alpha^2) & -\alpha\beta & -\alpha\gamma & -(1-\alpha^2) & \alpha\beta & \alpha\gamma \\ -\alpha\beta & (1-\beta^2) & -\beta\gamma & \alpha\beta & -(1-\beta^2) & \beta\gamma \\ -\alpha\gamma & -\beta\gamma & (1-\gamma^2) & \alpha\gamma & \beta\gamma & -(1-\gamma^2) \\ -(1-\alpha^2) & \alpha\beta & \alpha\gamma & (1-\alpha^2) & -\alpha\beta & -\alpha\gamma \\ \alpha\beta & -(1-\beta^2) & \beta\gamma & -\alpha\beta & (1-\beta^2) & -\beta\gamma \\ \alpha\gamma & \beta\gamma & -(1-\gamma^2) & -\alpha\gamma & -\beta\gamma & (1-\gamma^2) \end{bmatrix}_{ij}$$

$$(3.15)$$

Simple expressions for equation (3.10) and equation (3.15) are as follow,

$$\mathbf{k_0} = \frac{EA}{l_{oij}}\begin{bmatrix} \alpha^2 & \alpha\beta & \alpha\gamma \\ \alpha\beta & \beta^2 & \beta\gamma \\ \alpha\gamma & \beta\gamma & \gamma^2 \end{bmatrix}_{ij} \qquad (3.16)$$

$$\mathbf{k_G} = \frac{N_{ij}}{l_{oij}}\begin{bmatrix} (1-\alpha^2) & -\alpha\beta & -\alpha\gamma \\ -\alpha\beta & (1-\beta^2) & -\beta\gamma \\ -\alpha\gamma & -\beta\gamma & (1-\gamma^2) \end{bmatrix}_{ij} \qquad (3.17)$$

By combining equation (3.16) and equation (3.17) and substitute into equation (3.4), the tangent stiffness equation of one element can be expressed as

$$\begin{bmatrix}\delta X_i \\ \delta Y_i \\ \delta Z_i \\ \delta X_j \\ \delta Y_j \\ \delta Z_j\end{bmatrix} = \left\{\begin{bmatrix}\mathbf{k_0} & \mathbf{k_0} \\ \mathbf{k_0} & \mathbf{k_0}\end{bmatrix} + \begin{bmatrix}\mathbf{k_G} & \mathbf{k_G} \\ \mathbf{k_G} & \mathbf{k_G}\end{bmatrix}\right\}\begin{bmatrix}\delta x_i \\ \delta y_i \\ \delta z_i \\ \delta x_j \\ \delta y_j \\ \delta z_j\end{bmatrix} \qquad (3.18)$$

When equation (3.18) is rewritten into a simpler form, the tangent stiffness equation for one truss element is

$$\delta\mathbf{B_{ij}} = (\mathbf{K_0} + \mathbf{K_G})\,\delta\mathbf{d_{ij}} \qquad (3.19)$$

in which $\delta \mathbf{d_{ij}}$ refers to the nodal displacement vector of ij member. $\mathbf{K_0}$ is the tangent element stiffness caused by the relation between the increment of element edge forces and $\mathbf{K_G}$ is the tangent geometrical stiffness associated with changing of cosine vectors. Therefore, $\mathbf{K_G}$ provides the rigid body rotations and displacements. Since the geometrical stiffness matrix is derived strictly for any type of structure, only the element stiffness matrix is required to make adjustment in each analysis.

3.4 Defining element measurement's potential for cable member

Tensegrity having components of stiffer elements (strut) and softer elements (cable) can be prescribed as a group of axial line elements in which the consideration for end moment can be neglected. The shape formation of tensegrity is mainly governed by the structural type of the composed members (element behavior) and the member forces bearing the stiffness. The measure potential proportionate to $(n+1)^{th}$ power of element length is an active approach for the form-finding of tensegrities. The line elements with the measure potential have axial forces proportionate to n^{th} power of its length and it is called "n^{th} power axial force line element".

$$P = c(l - l_0)^{n+1} \tag{3.20}$$

When n is equal to 1, it gives the stiffness equation in a linear function and the process of computation becomes quite similar to the force density method. In this paper, the strut of proposed tensegrity is defined by the linear function of $n=1$, making it similar to the truss behavior. On the other hand, the element behavior in the element force equation can be designated freely by taking the advantage of tangent stiffness method. Therefore, this enables the cable members to have the multiplier "n" with any amount of magnitude. Moreover, the proposed measure potential is composed of the power function of the length difference, in which the non-stressed length can have a single or multiple functions depending on the purpose of analyses.

3.5 Element force equation for power function

In the form-finding process by the tangent stiffness method, the axial force line elements can be defined as the "virtual" potential functions having the parameters of element measurement and its differential functions as the element force equations prescribing the element behavior as in equation (3.21).

$$N = \frac{dP}{dl} \tag{3.21}$$

in which N is axial force and l is the length of elements. Therefore, the element force equation for the power function will be obtained as follow.

$$N = (n+1)c(l - l_0)^n = C\,(l - l_0)^n \tag{3.22}$$

in which C is the coefficient of stiffness, l_0 is the non-stressed length, and n is the multiplier respectively. In case of equation (3.22), the element stiffness matrix is prepared as below.

$$\mathbf{K_0} = nC(l - l_0)^n \begin{bmatrix} \mathbf{JJ^T} & -\mathbf{JJ^T} \\ -\mathbf{JJ^T} & \mathbf{JJ^T} \end{bmatrix} \tag{3.23}$$

3.6 Proposed tensegrity model for numerical analyses

Since the aim of this study is to establish a series of analyses in one algorithm, the same tensegrity model will be treated in the whole procedure. The connectivity of each member and the constraint condition are demonstrated in the bird's eye view, plan view and side view as in figure 3.1. This double-layered pentagonal tensegrity is in the state of primary unbalanced condition. In each layer, it consists of 5 stiffer elements (referring to struts) which are connected by 15 softer elements (referring to cables). The extra 10 cables serve as a connecting medium between the base and top layers to form double-standing tensegrity model. The struts are illustrated in blue color whereas the cables are in red color. One black base point is fixed supported in all directions, one pink base point is fixed in two directions and the yellow base points are given fixed in the vertical direction. All the other upper layer points and the layer connecting joints are given as free points illustrated in green color.
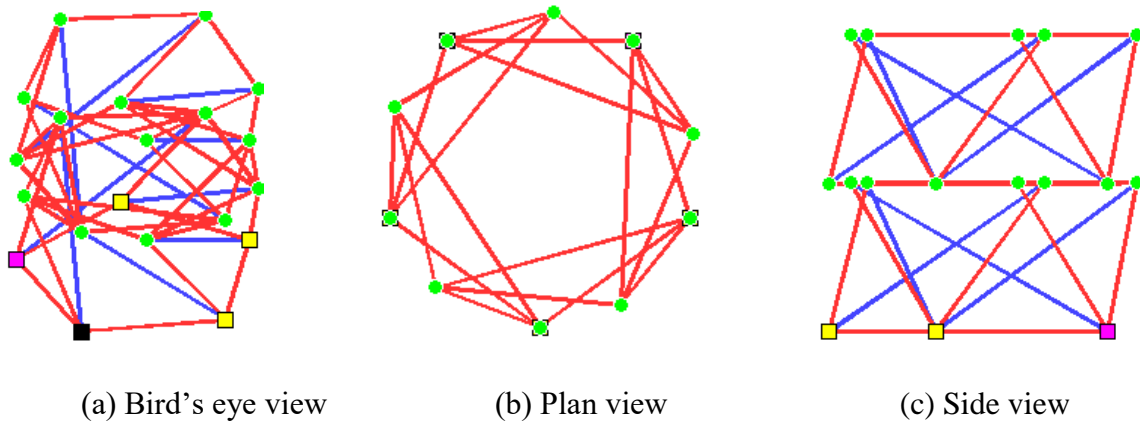

(a) Bird's eye view   (b) Plan view   (c) Side view

Figure 3.1 Connectivity and support condition of primary unbalanced configuration

3.7 Evaluation of coefficients in power function

3.7.1 Setting the coefficients for each element

Taking the advantage of the tangent stiffness method, it is possible to set the element behavior freely, even real or virtual. Therefore, referring to equation (3.22), the stiffer element is designated as the truss behavior with constant stiffness ($C_s = 2 \times 10^9$ and $n_s = 1$). For the softer element, three kinds of virtual coefficients are proposed. In each analysis, the setting is made with respect to the coefficient of stiffness C_c at five different values of (1, 10 100, 1000, 10000), the multiplier n_c (setting from 1 to 10) and for the non-stressed length ratio, it is defined in term of ratio $R = l_{0c}/l_{0s}$ (cable/strut) in the range of (0 to 1) with 5% increment. The assignment of coefficient values is summarized as below.

Table 3.1 Assignment of designated values for each coefficient of element force equation

Element force equation	$N = C\,(l - l_0)^n$	
Related coefficients	**For stiffer elements (strut)**	**For softer elements (cable)**
C	$C_s = EA/l_0$ ($EA{=}2{\times}\,10^9$)	$C_c = 1, 10, 100, 1000, 10000$
n	$n_s = 1$	$n_c = 1$ to 10
l_0	$l_{0s} = 7.0$	$R = l_{0c}/l_{0s}$ (cable/strut) in range of (0 to 1) with 5% increment

3.7.2 Influence of each coefficient in the form-finding

From the above setting of each coefficient, total 562 converged equilibrium solutions are obtained out of 1050 trials with wide diversity of shape formation. The coefficient of stiffness C_c results out 69% of the total trials as equilibrium solutions as shown in figure 3.2 in which the variation of stiffness amount within the designated range has only slight difference in finding the

equilibrium configurations since the softer element's stiffness is much lower than compared to that of stiffer element. Meanwhile, the application of the multiplier n_c accounts for 53% in finding equilibrium solutions. As shown in figure 3.3, the multiplier n_c with odd number has a typical tendency to capture more equilibrium solutions than with even number.
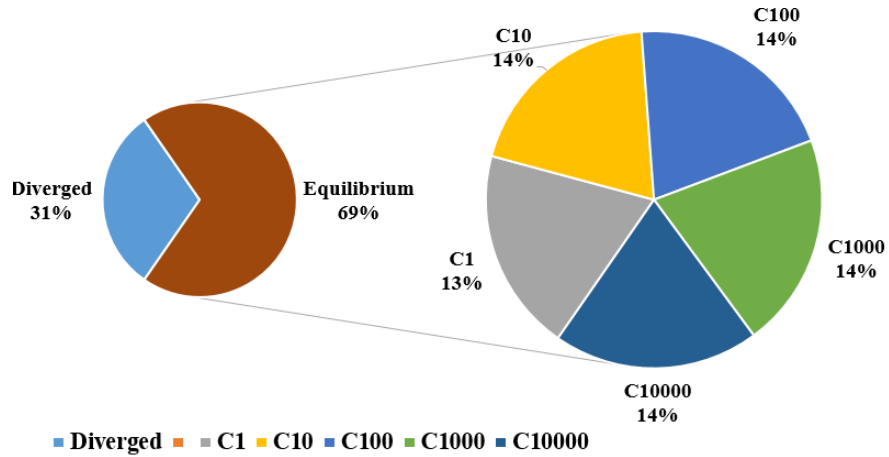
Figure 3.2 Influence of coefficient of stiffness C_c
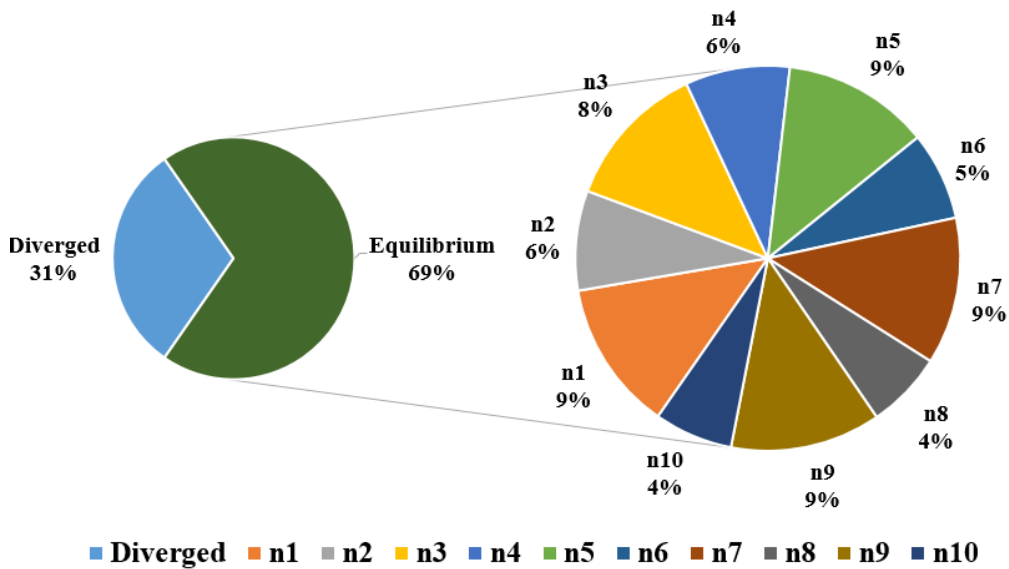
Figure 3.3 Influence of coefficient of multiplier n_c

Moreover, the influence of the odd and even multipliers can be seen significantly in figure 3.4. The vertical axis of the graph shows the possibility of obtaining equilibrium solutions where 50 trials are conducted in each non-stressed length ratio R of the horizontal axis, against the variation of stiffness coefficient C_c and the multiplier n_c.

40
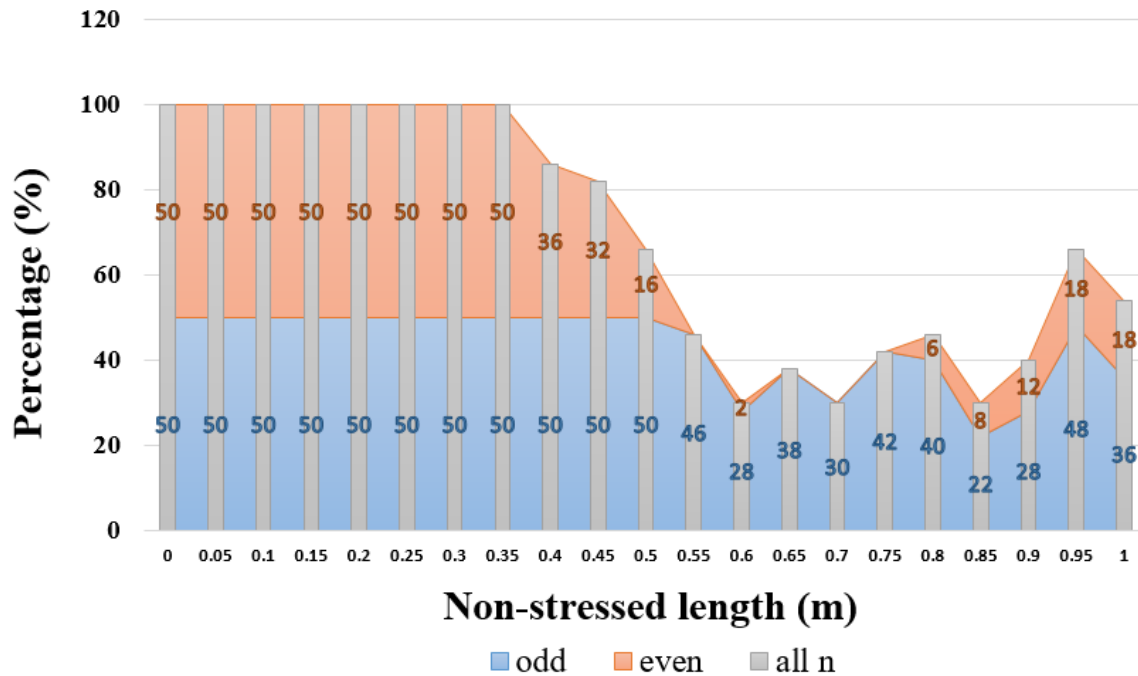
Figure 3.4 Influence of non-stressed length ratio R against C_c and n_c

The column graph represents the possibility to obtain the equilibrium solutions by means of all the multiplier n_c (1~10). The blue shaded area illustrates the percentage occupied by the odd number multiplier whereas the orange shaded area demonstrates the even number multiplier. From the graph, it can be seen that higher possibility to collect the equilibrium solutions can be expected in the lower non-stressed length ratio, either for the even or odd number of the multiplier. On the other hand, the possibility is getting decreased in the higher non-stressed length ratio in which the odd number multiplier accounts for much higher percentage than the even number multiplier. In this way, the possibility to explore the various shape formation of tensegrity can be maximized according to the different setting of each coefficient.

3.8 Development of finding wider diversity of equilibrium solutions

3.8.1 Element force equation for multiple non-stressed length

Actually, any type of the measure potential or the element force equation can be freely defined, if the relation between terms in equation (3.21) is approved. In this section, the element force equation (3.24), whose potential has multiple stoppage points, is examined in order to develop the diversity of equilibrium solutions. Moreover, equation (3.25) is the differential of equation (3.24) which will be applied in the corresponding tangent stiffness matrix.

41

$$N = C \, (l - l_{01})(l - l_{02}) \ldots \ldots (l - l_{0n}) \tag{3.24}$$

$$\delta N = \left(\sum_{i=1}^{n} \frac{1}{l - l_{0i}} \right) N . \delta l \tag{3.25}$$

in which l_{0n} is the non-stressed length of elements conducting the stoppage points of the potential. In case of equation (3.24), the element stiffness matrix is described as below.

$$\mathbf{K_0} = \left(\sum_{i=1}^{n} \frac{N}{l - l_{0i}} \right) \begin{bmatrix} \mathbf{JJ^T} & -\mathbf{JJ^T} \\ -\mathbf{JJ^T} & \mathbf{JJ^T} \end{bmatrix} \tag{3.26}$$

3.8.2 Setting the coefficient for each element

The application of the measure potential and the virtual stiffness allows the author to set a free choice of each coefficient. For this section, the coefficients for stiffer elements in equation (3.22) are applied same as before ($C_s = 2 \times 10^9$, $n_s = 1$, $l_{0s} = 7.0$). Therefore, the stiffer elements behave as the boundary condition for the element length. On the other hand, based on the experience of coefficient variation of softer element in the previous section, this time the coefficients of softer elements are adopted as ($C_c = 1000$, $n_c = 3$), and the equilibrium shapes are examined with the change of non-stressed length l_{0c}.

● Stiffer Element ● Vertical Softer Element ● Horizontal Softer Element ● Layer Connecting Softer Element
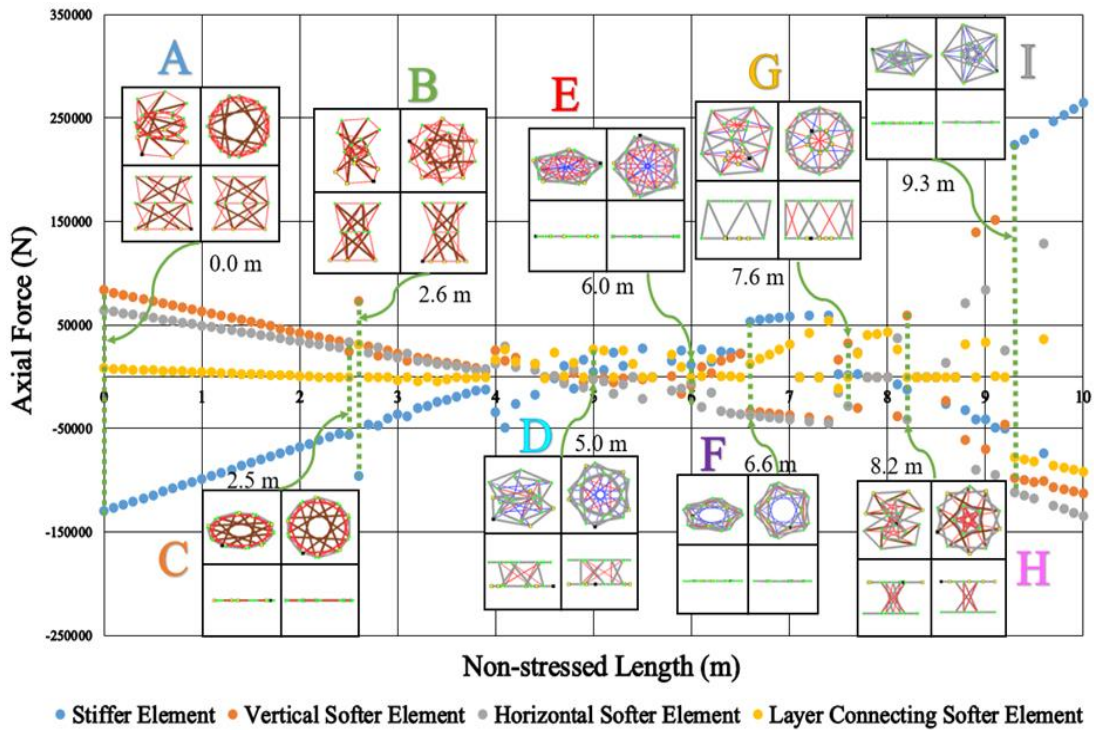
Figure 3.5 Result of one-time analysis of a two-layered pentagonal tensegrity

Figure 3.5 shows the relation between the non-stressed length and the axial force of the equilibrium solutions resulted from one-time analysis from the origin of the primary unbalanced configuration. The shape of each solution is resembled by a set of each dot in four color series of axial force. Axial force of the stiffer element is represented by blue color whereas orange and grey color indicate ones of the vertical and horizontal softer elements and yellow color for one of the connections between layers. The graph in figure 3.5 shows the discrete solutions obtained by the one-time analysis when one of the non-stressed lengths in equation (3.24) is let to move between the range of 0~10 m with 0.1 m of interval while the other ones are fixed at 0.1 m and 0.3 m respectively. The total 90 of converged equilibrium solutions are achieved out of 100 trials with the wide diversity of shape formation.

3.8.3 Total potential energy of each equilibrium solution

Let U be the strain energy for the stiffer element (strut), V is the axial line potential for the softer element (cable) and W is the loss in potential of the external force. Then the total potential energy Π can be defined as below.
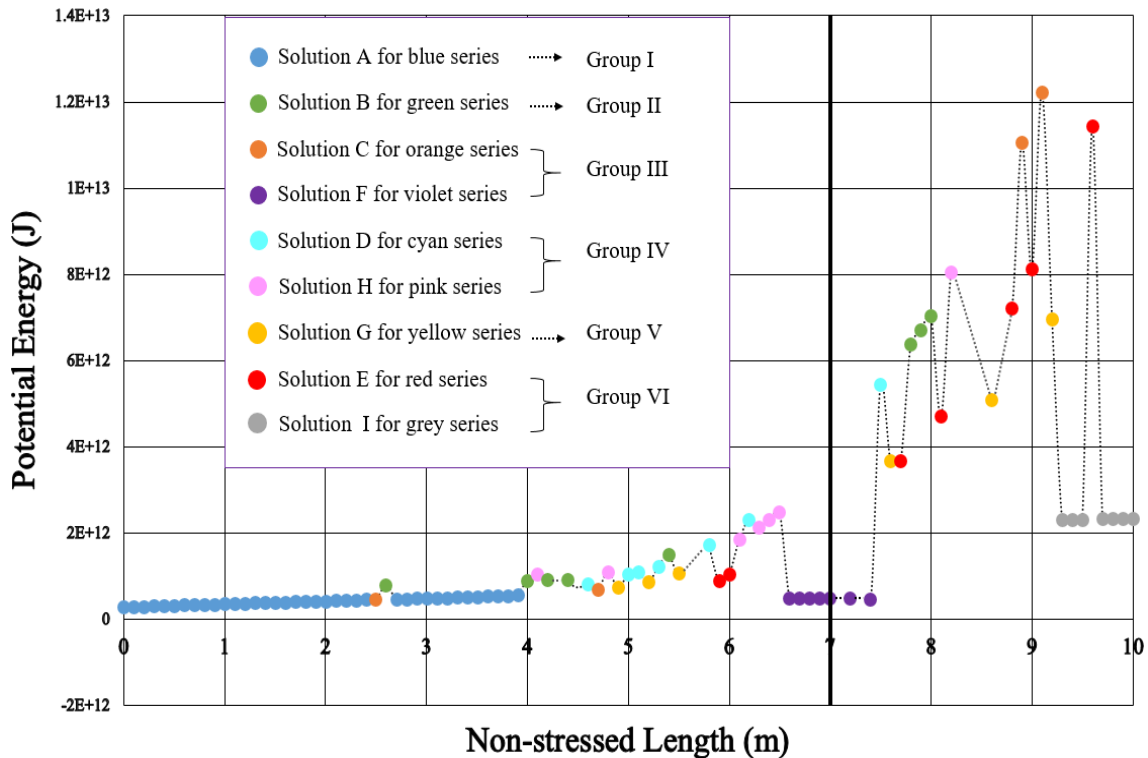
$$\Pi=U+V-W \tag{3.27}$$

Figure 3.6 Potential energy for one-time analysis

Meanwhile, total potential energy of discrete solutions of one-time analysis is checked in figure 3.6 in order to categorize their similarity. Total 9 series can be expected and each series is denoted by a distinct color and represented by example solutions (A~I). By following the similarity of each color series, it can be organized into total 6 groups in which some color series are found to be related and corresponding to each other. The thick line at 7 m indicates the non-stressed length of softer element become equal to that of the stiffer element. Each solution in each group is picked up and reset as the primary form to conduct the incremental analysis where the non-stressed length of softer element is continuously increased or decreased in order to follow the path of each discrete solution.

3.8.4 Result of multiple non-stressed length setting
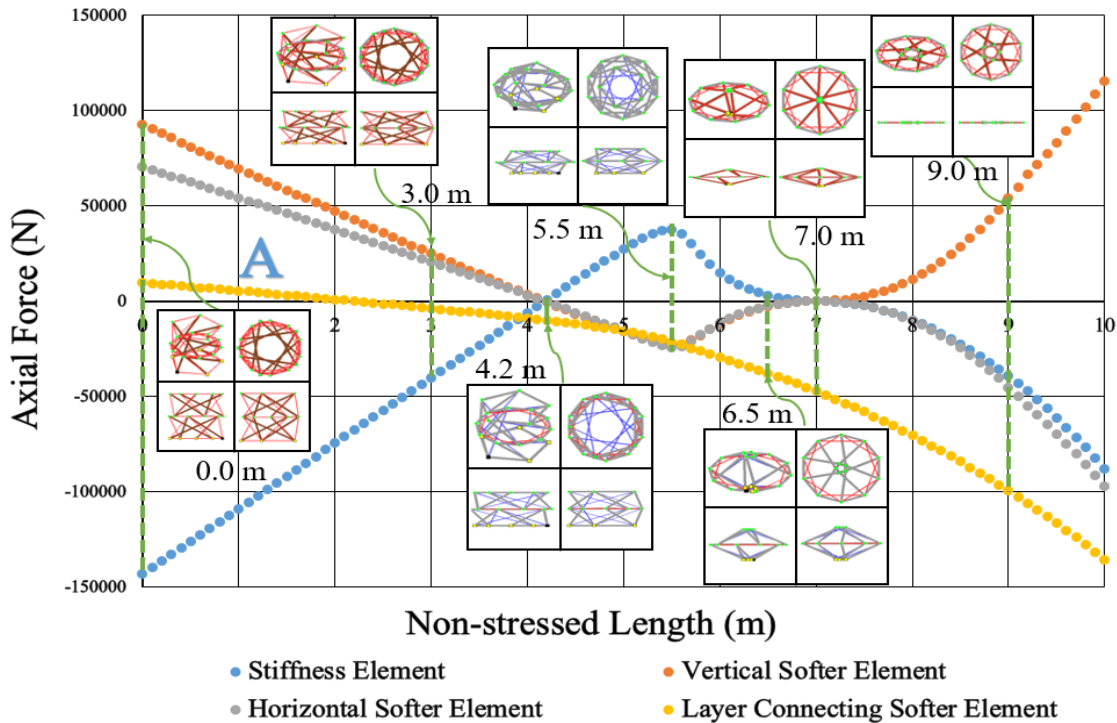
Figure 3.7 Incremental analysis for Group I

Figure 3.7 shows the pattern for Group I in which solution A gives the continuous path of equilibrium solutions where the proposed tensegrity is smoothly and perfectly folded along with the gradual increment of softer non-stressed length. Most of the discrete solutions of blue series from figure 3.5 fall into this pattern, forming the strongest path. Figure 3.8 shows the solution B of Group II in which the three dimensional solution suffers a large amount of difference in axial

force after the critical point of 4.7 m where the axial force of layer connecting softer element is much larger compared to that of vertical and horizontal softer elements. The small amount of axial forces is zoomed-in and attached in figure 3.8.
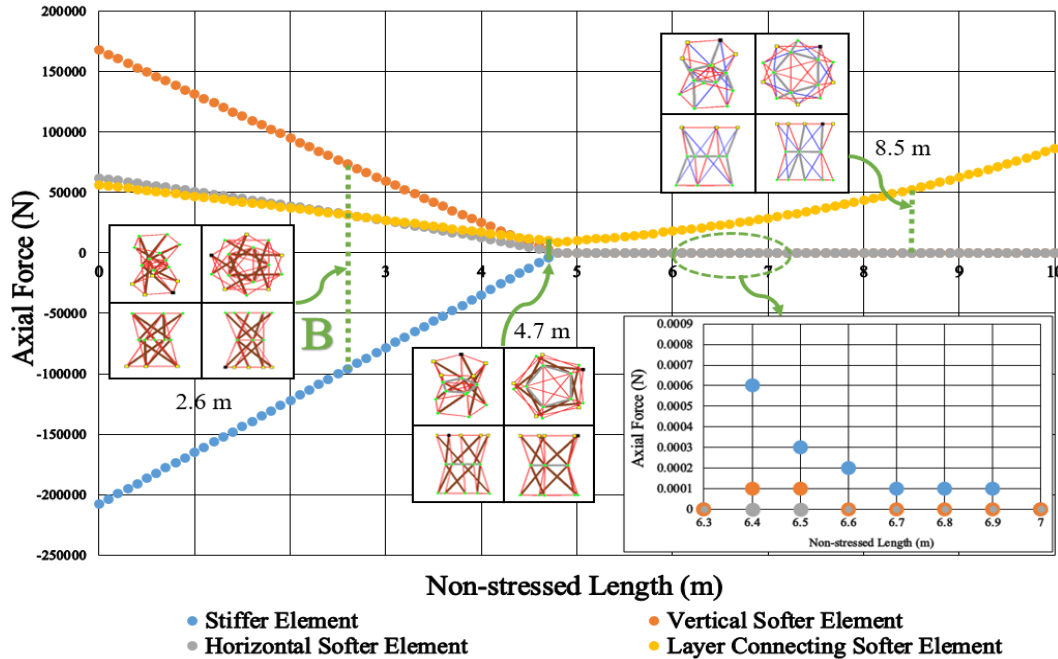
Figure 3.8 Incremental analysis for Group II
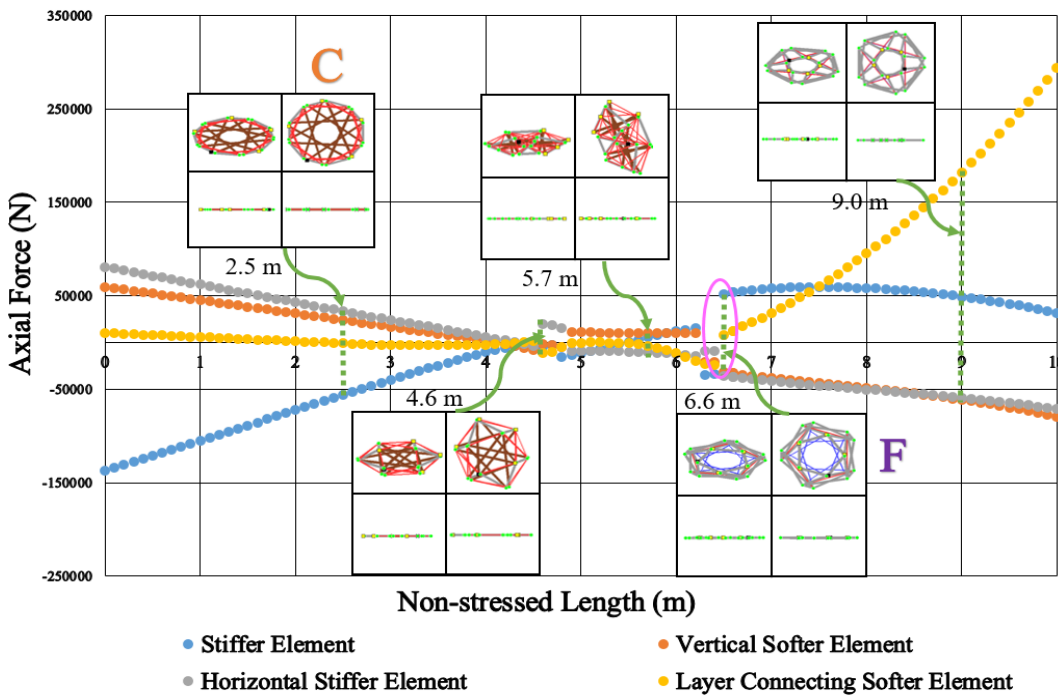
Figure 3.9 Incremental analysis for Group III

The pattern drawn in figure 3.9 belongs to Group III where the two dimensional solution C of orange series and solution F of violet series are associated with each other after the snap through at 6.6 m. Similarly, solution D and solution H are formed in the same Group IV in which cyan series is found to be sandwiched between two snap through points at 4.1 m and 7.7 m of pink series as shown in figure 3.10.
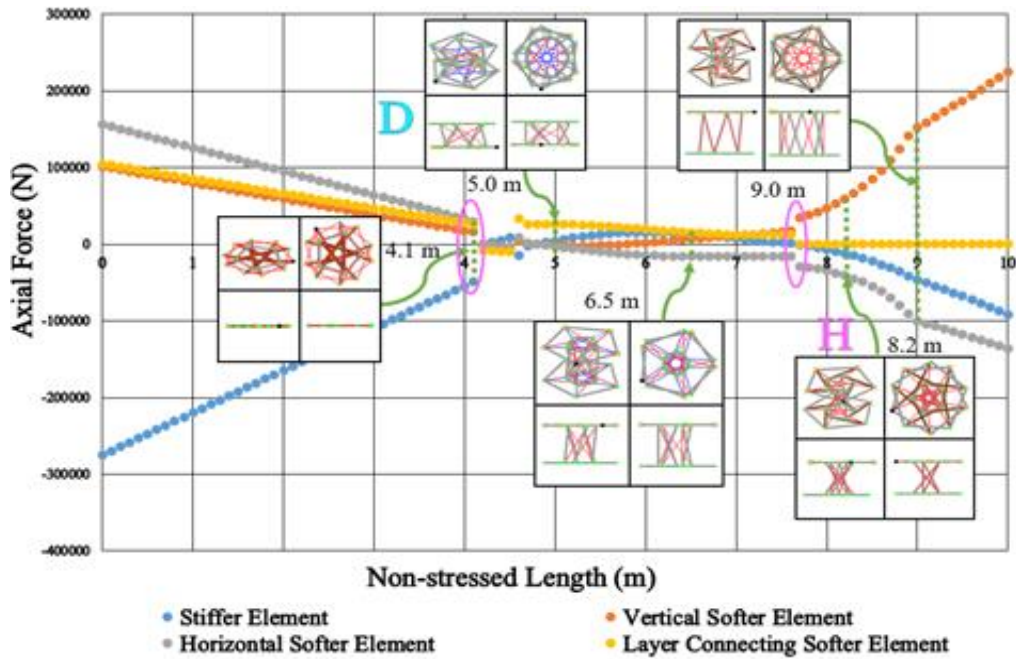
Figure 3.10 Incremental analysis for Group IV
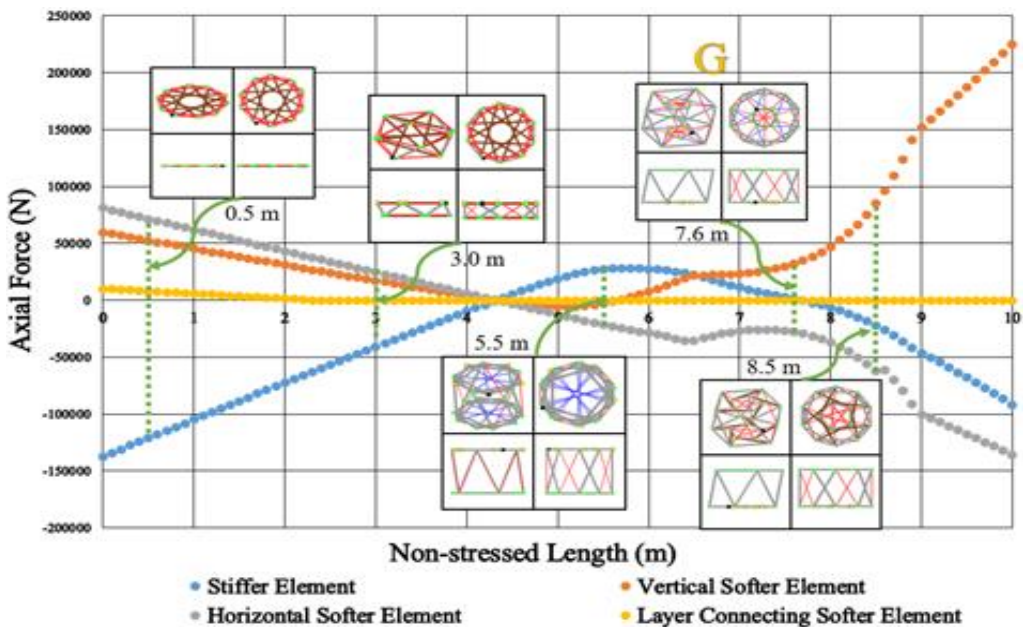
Figure 3.11 Incremental analysis for Group V

Group V in figure 3.11 indicates the consecutive pattern of solution G that deployed steadily along with the gradual increment of softer non-stressed length. The two dimensional equilibrium solution E of pink series is corresponding to Group VI where the path is deviated at 7.5 m, forming the solution I of grey series as depicted in figure 3.12.
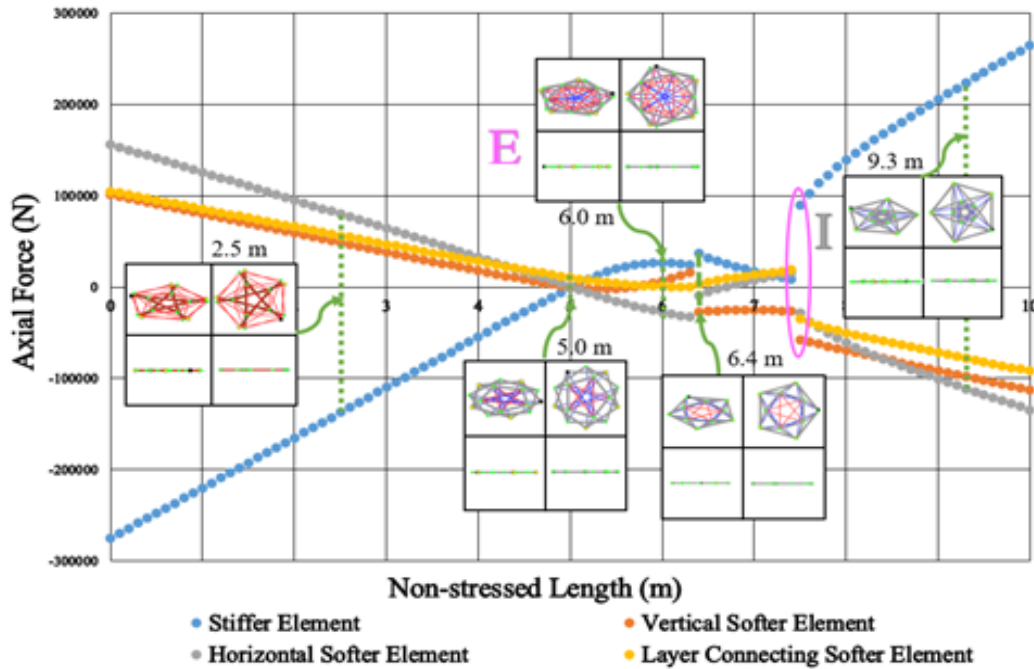
Figure 3.12 Incremental analysis for Group VI

Figure 3.13 illustrates that various types of three dimensional equilibrium solutions can be expected from one-time analysis by the combination of different multiple non-stressed lengths even for the same initial primary unbalanced configuration. By using the method of controlling the non-stressed length, the number of equilibrium solutions obtained is 3 times more than by the method which seeks the self-equilibrium solutions in the points with zero external forces on path finding process. Therefore, the application of multiple non-stressed length can expect the higher possibility of obtaining equilibrium solutions in the shape analysis of tensegrity. Moreover, the grey color in each illustration refers to the cable members carrying the compression force. In the general sense of tensegrity definition, the compression members are constructed in separation where only the tensional cables can be connected to each other in order to maintain the stability. However, in the proposed method of shape analysis, many types of equilibrium configurations are successfully achieved where both the compression and tension members are allowed to come in connection while following the rules of stably self-equilibrium condition.

$l_{01} = 0.5\ m$ $l_{02} = 3.5\ m$ $l_{03} = 4.8\ m$	$l_{01} = 2.0\ m$ $l_{02} = 6.0\ m$ $l_{03} = 4.8\ m$	$l_{01} = 2.5\ m$ $l_{02} = 5.0\ m$ $l_{03} = 2.9\ m$	$l_{01} = 4.0\ m$ $l_{02} = 6.0\ m$ $l_{03} = 9.0\ m$
$l_{01} = 0.5\ m$ $l_{02} = 0.5\ m$ $l_{03} = 5.9\ m$	$l_{01} = 1.5\ m$ $l_{02} = 1.0\ m$ $l_{03} = 3.5\ m$	$l_{01} = 2.5\ m$ $l_{02} = 5.0\ m$ $l_{03} = 2.7\ m$	$l_{01} = 4.0\ m$ $l_{02} = 6.0\ m$ $l_{03} = 5.1\ m$
$l_{01} = 3.0\ m$ $l_{02} = 8.0\ m$ $l_{03} = 3.5\ m$	$l_{01} = 4.5\ m$ $l_{02} = 8.5\ m$ $l_{03} = 4.4\ m$	$l_{01} = 4.0\ m$ $l_{02} = 7.0\ m$ $l_{03} = 8.0\ m$	$l_{01} = 6.9\ m$ $l_{02} = 6.9\ m$ $l_{03} = 7.1\ m$
$l_{01} = 1.0\ m$ $l_{02} = 3.0\ m$ $l_{03} = 5.5\ m$	$l_{01} = 2.5\ m$ $l_{02} = 5.5\ m$ $l_{03} = 3.1\ m$	$l_{01} = 4.5\ m$ $l_{02} = 6.0\ m$ $l_{03} = 9.7\ m$	$l_{01} = 0.2\ m$ $l_{02} = 0.4\ m$ $l_{03} = 9.0\ m$

Figure 3.13 Results of one-time analysis with multiple setting of non-stressed length
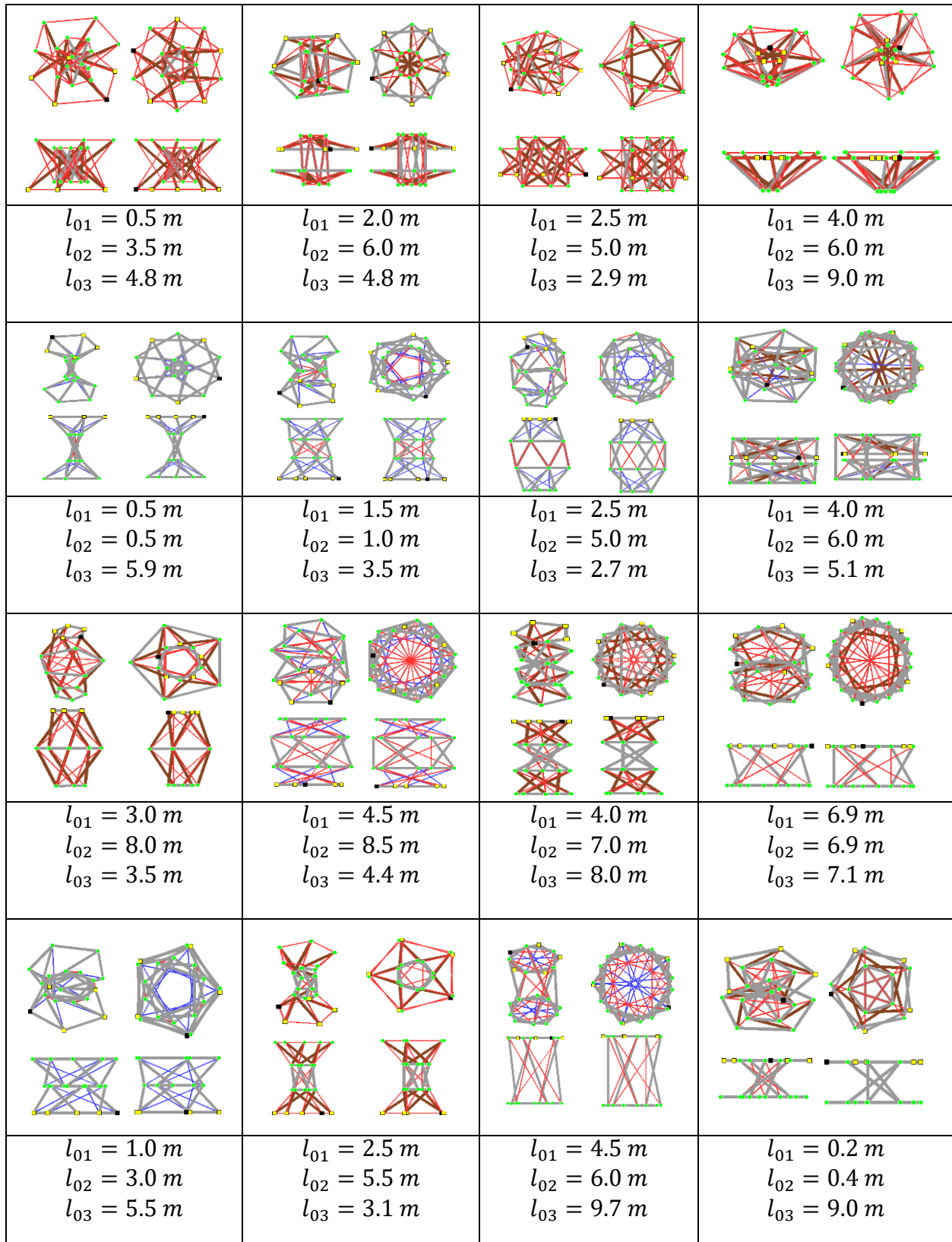
3.9 Summary of chapter 3

Since a large deformation is associated with tensegrity, the geometrical nonlinearity should be considered in the form-finding of tensegrity structures. Therefore, the tangent stiffness method is adopted to solve the nonlinear problems that allows us to define many types of element force equation. The measure potential of the power function gives a wide option to define the virtual coefficients freely. Among them, variation of the coefficient of stiffness shows no big effect while the multiplier with odd number has more influence to find out the equilibrium solutions. On the other hand, the non-stressed length ratio seems to be a complex factor in the shape analysis. From the numerous solutions, it is found that the possibility to obtain the equilibrium solutions can be increased by defining and selecting the appropriate combination of coefficients.

Moreover, it is a great advantage to apply the multiple non-stressed lengths to describe a wide range of element behavior while the rigid body displacement is strongly restricted by the geometric stiffness. In this study, the concept of diversity is highlighted for the versatile application in tensegrity structures. The proposed tensegrity model is simple but unique which will be in accordance with the fundamental concepts of tensegrity structures. All in all, this analysis is able to find out numerous equilibrium solutions even under the same connectivity from which the equilibrium paths can be traced, leading to a wider diversity of form-finding procedure of tensegrity structures.

List of Symbols

Symbol		Description
B	:	External force vector
J	:	Equilibrium matrix
N_{ij}	:	Axial force of member ij
E	:	Young's modulus
A	:	Cross-sectional area
α	:	Cosine vector component in horizontal direction
β	:	Cosine vector component in vertical direction
γ	:	Cosine vector component in inner direction
x	:	Nodal coordinate in horizontal direction
y	:	Nodal coordinate in vertical direction
z	:	Nodal coordinate in inner direction
d	:	Nodal displacement vector
$\mathbf{K_0}$	:	Element stiffness matrix
$\mathbf{K_G}$	:	Tangent geometrical stiffness matrix
P	:	Element's measure potential
R	:	Ratio of non-stressed length
C_s	:	Coefficient of stiffness for strut
C_c	:	Coefficient of stiffness for cable
n_s	:	Multiplier for strut
n_c	:	Multiplier for cable
l_{0s}	:	Non-stressed length for strut
l_{0c}	:	Non-stressed length for cable
U	:	Strain energy for strut
V	:	Axial line potential for cable
W	:	Loss in potential due to external force
Π	:	Total potential energy

References

[1] L. Zhang, Y. Li , Y. Cao and X. Feng, "Stiffness matrix based form-finding method of tensegrity structures," *Engineering Structures,* vol. 58, pp. 36-48, 2014.

[2] K. Koohestani, "On the analytical form-finding of tensegrities," *Composite Structures,* vol. 166, pp. 114-119, 2017.

[3] L. Zhang, S. Zhu, S. Li and G. Xu, "Analytical form-finding of tensegrities using determinant of force-density matrix," *Composite Structures,* vol. 189, pp. 87-98, 2018.

[4] F. Tsuura, J. Zhang and M. Ohsaki, "Self-equilibrium and Stability of Tensegrity Structures with Polyhedral Symmetries," *Proceedings of International Association for Shell and Spatial Structures,* 2010.

[5] J. Zhang, M.Ohsaki and F.Tsuura, "Self-equilibrium and super-stability of truncated regular hexahedral and octahedral tensegrity structures," *International Journal of Solids and Structures,* vol. 161, pp. 182-192, 2019.

[6] R. Kangwai, S. Guest and S. Pellegrino, "An introduction to the analysis of symmetric structures," *Computers & Structures,* vol. 71, no. 6, pp. 671-688, 1999.

[7] J. Zhang, S. Guest and M.Ohsaki, "Symmetric prismatic tensegrity structures. Part II: Symmetry-adapted formulations," *International Journal of Solids and Structures,* vol. 46, no. 1, pp. 15-30, 2009.

[8] J. Zhang, S. Guest and M.Ohsaki, "Symmetric prismatic tensegrity structures: Part I. Configuration and stability," *International Journal of Solids and Structures,* vol. 46, no. 1, pp. 1-14, 2009.

[9] J. Zhang, S. Guest, R.Connelly and M.Ohsaki, "Dihedral 'Star' tensegrity structures," *International Journal of Solids and Structures,* vol. 47, no. 1, pp. 1-9, 2010.

[10] J. Zhang and M.Ohsaki, "Self-equilibrium and stability of regular truncated tetrahedral tensegrity structures," *Journal of the Mechanics and Physics of Solids,* vol. 60, no. 10, pp. 1757-1770, 2012.

[11] L. Zhang, Y. Li, Y. Cao, X. Feng and H. Gao, "Self-equilibrium and super-stability of truncated regular polyhedral tensegrity structures: a unified analytical solution," *Journal of mathematical, physical and engineering sciences,* July 2012.

[12] L. Zhang, Y. Li, Y. Cao and X. Feng, "A unified solution for self-equilibrium and super-stability of rhombic truncated regular polyhedral tensegrities," *International Journal of Solids and Structures,* vol. 50, no. 1, pp. 234-245, 2013.

[13] H. Murakami and Y. Nishimura, "Static and dynamic characterization of regular truncated icosahedral and dodecahedral tensegrity modules," *International Journal of Solids and Structures,* vol. 38, no. 50-51, pp. 9359-9381, December 2001.

[14] K. Koohestani and S. Guest, "A new approach to the analytical and numerical form-finding of tensegrity structures," *International Journal of Solids and Structures,* vol. 50, no. 19, pp. 2995-3007, 2013.

[15] L. Zhang, S. Li, S. Zhua, B. Zhang and G. Xu, "Automatically assembled large-scale tensegrities by truncated regular polyhedral and prismatic elementary cells," *Composite Structures,* vol. 184, pp. 30-40, 2018.

[16] G. Estrada, H. Bungartz and C. Mohrdieck, "Numerical form-finding of tensegrity structures," *International Journal of Solids and Structures,* vol. 43, no. 22-23, pp. 6855-6868, 2006.

[17] J. Zhang, M. Ohsaki and Y. Kanno, "A direct approach to design of geometry and forces of tensegrity systems," *International Journal of Solids and Structures,* vol. 43, no. 7-8, pp. 2260-2278, 2006.

[18] L. Zhang, Y. Li, Y. Cao and X. Feng, "Stiffness matrix based form-finding method of tensegrity structures," *Engineering Structures,* vol. 58, pp. 36-48, 2014.

[19] N. Metropolis and S. Ulam, "The Monte Carlo Method," *Journal of the American Statistical Association,* pp. 335-341, 1949.

[20] Y. Li, X. Feng, Y. Cao and H. Gao, "A Monte Carlo form-finding method for large scale regular and irregular tensegrity structures," *International Journal of Solids and Structures,* vol. 47, no. 14-15, pp. 1888-1898, 2010.

[21] X. Yuan, S. Ma and S. Jiang, "Form-finding of tensegrity structures based on the Levenberg–Marquardt method," *Computers & Structures,* vol. 192, pp. 171-180, 2017.

[22] A. Micheletti and W. Williams, "A marching procedure for form-finding of tensegrity structures," *Journal of Mechanics of Materials and Structures,* vol. 2, pp. 857-882, 2007.

[23] A. Day, "An introduction to dynamic relaxation," *The Engineer,* vol. 219, pp. 218-221, 1965.

[24] M. Hüttner, J. Máca and P. Fajman, "The efficiency of dynamic relaxation methods in static analysis of cable structures," *Advances in Engineering Software,* vol. 89, pp. 28-35, 2015.

[25] M. Pajand, S. Sarafrazi and H. Rezaiee, "Efficiency of dynamic relaxation methods in nonlinear analysis of truss and frame structures," *Computers & Structures,* Vols. 112-113, pp. 295-310, 2012.

[26] L. Zhang, B. Maurin and R. Motro, "Form-finding of nonregular tensegrity systems," *Journal of Structural Engineering ASCE,* vol. 132, pp. 1435-1440, 2006.

[27] N. Ali, R. Landolf and I. Smith, "Analysis of clustered tensegrity structures using a modified dynamic relaxation algorithm," *International Journal of Solids and Structures,* vol. 48, no. 5, pp. 637-647, 2011.

[28] H. Baudriller, B. Maurin, P. Cañadas, P. Montcourrier, A. Parmeggiani and N. Bettache, "Form-finding of complex tensegrity structures: application to cell cytoskeleton modelling," *Comptes Rendus Mécanique,* vol. 334, no. 11, pp. 662-668, 2006.

[29] M. Aufaure, "A finite element of cable passing through a pulley," *Computers & Structures,* vol. 46, no. 5, pp. 807-812, 1993.

[30] B. Zhou, M. Accorsi and J. Leonard, "Finite element formulation for modeling sliding cable elements," *Computers & Structures,* vol. 82, no. 2-3, pp. 271-280, 2004.

[31] J. Pargana, D. Smith and B. Izzuddin, "Fully integrated design and analysis of tensioned fabric structures: finite elements and case studies," *Engineering Structures,* vol. 32, no. 4, pp. 1054-1068, 2010.

[32] M. Pagitz and J. Tur, "Finite element based form-finding algorithm for tensegrity structures," *International Journal of Solids and Structures,* vol. 46, no. 17, pp. 3235-3240, 2009.

[33] K. Klinka, V. Arcaro and D. Gasparini, "Form finding of tensegrity structures using finite elements and mathematical programming," *Journal of Mechanics of Materials and Structures,* vol. 7, no. 10, pp. 899-907, 2012.

[34] S. Pellegrino and C. Calladine, "Matrix analysis of statically and kinematically indeterminate frameworks," *International Journal of Solids and Structures,* vol. 22, no. 4, pp. 409-428, 1986.

[35] R. Burkhardt, "The applicaiton of nonlinear programming to the design and validation of tensegrity structures with special attention to skew prisms," *Journal of the International Association for Shell and Spatial Structures,* vol. 47, pp. 3-15, 2006.

[36] S. Juan and J. Tur, "Tensegrity frameworks: static analysis review," *Mechanism and Machine Theory,* vol. 43, no. 7, pp. 859-881, 2008.

[37] K. Linkwitz, "Form-finding by the "direct approach" and pertinent strategies for the conceptual design of prestressed and hanging structures," *International Journal of Space Structures,* vol. 14, no. 2, pp. 73-87, 1999.

[38] H. Schek, "The force density method for form finding and computation of general networks," *Computer Methods in Applied Mechanics and Engineering,* vol. 3, no. 1, pp. 115-134, 1974.

[39] R. Motro, S. Najari and P. Jouanna, "Static and dynamic analysis of tensegrity systems," in *Proceedings of the ASCE International Symposium*, NewYork, 1986.

[40] A. Tibert and S. Pellegrino, "Review of form-finding methods for tensegrity structures," *International Journal of Space Structures,* 2003.

[41] G. Nasr and S. Mourad, "An extended force density method for form finding of constrained cable nets," *Case Studies in Structural Engineering,* vol. 3, pp. 19-32, 2015.

[42] Y. Gu, J. Du, D. Yang , Y. Zhang and S. Zhang, "Form-finding design of electrostatically controlled deployable membrane antenna based on an extended force density method," *Acta Astronautica,* vol. 152, pp. 757-767, 2018.

[43] M. Masic, R. Skelton and P. Gill, "Algebraic tensegrity form-finding," *International Journal of Solids and Structures,* vol. 42, no. 16-17, pp. 4833-4858, 2005.

[44] M. Miki and K. Kawaguchi, "Extended Force Density Method for Form-Finding of Tension Structures," *Journal of IASS,* vol. 51, pp. 291-303, 2010.

[45] S. Lee and J. Lee, "Form-finding of tensegrity structures with arbitrary strut and cable members," *International Journal of Mechanical Sciences,* vol. 85, pp. 55-62, 2014.

[46] J. Zhang and M.Ohsaki, "Adaptive force density method for form-finding problem of tensegrity structures," *International Journal of Solids and Structures,* vol. 43, no. 18-19, pp. 5658-5673, 2006.

[47] H. Tran and J. Lee, "Advanced form-finding of tensegrity structures," *Computers & Structures,* vol. 88, no. 3-4, pp. 237-246, 2010.

[48] M.Yamamoto, B. Gan, K. Fujita and J. Kurokawa, "A genetic algorithm based form-finding for tensegrity structures," *Procedia Engineering,* vol. 14, pp. 2949-2956, 2011.

[49] S. Lee, B. Gan and J. Lee, "A fully automatic group selection for form-finding process of truncated tetrahedral tensegrity structures via a double-loop genetic algorithm," *Composites Part B: Engineering,* vol. 106, pp. 308-315, 2016.

[50] K. Koohestani, "Form-finding of tensegrity structures via genetic algorithm," *International Journal of Solids and Structures,* vol. 49, no. 5, pp. 739-747, 2012.

[51] X. Xu and Y. Luo, "Form-finding of nonregular tensegrities using a genetic algorithm," *Mechanics Research Communications,* vol. 37, no. 1, pp. 85-91, 2010.

[52] B. Gan, J. Zhang, D. Nguyen and E. Nouchi, "Node-based genetic form-finding of irregular tensegrity structures," *Computers & Structures,* vol. 159, pp. 61-73, 2015.

[53] M. Masic, R. Skelton and P. Gill, "Optimization of tensegrity structures," *International Journal of Solids and Structures,* vol. 43, pp. 4687-4703, 2006.

[54] D. Zou, H. Liu , L. Gao and S. Li, "A novel modified differential evolution algorithm for constrained optimization problems," *Computers & Mathematics with Applications,* vol. 61, no. 6, pp. 1608-1623, 2011.

[55] Dexuan Zou, Jianhua Wu, Liqun Gao, Steven Li, "A modified differential evolution algorithm for unconstrained optimization problems," *Neurocomputing ,* vol. 120, pp. 469-481, November 2013.

[56] W. Yi, Y. Zhou, L. Gao, X. Li and J. Mou, "An improved adaptive differential evolution algorithm for continuous optimization," *Expert Systems with Applications,* vol. 44, pp. 1-12, 2016.

[57] D. Do, S. Lee and J. Lee, "A modified differential evolution algorithm for tensegrity structures," *Composite Structures,* vol. 158, pp. 11-19, 2016.

[58] C. Paul, H. Lipson and F. Cuevas, "Evolutionary form-finding of tensegrity structures," in *Conference on Genetic and Evolutionary Computation*, NewYork, USA, 2005.

[59] J. Rieffel, F. Cuevas and H. Lipson, "Automated discovery and optimization of large irregular tensegrity structures," *Computers & Structures,* vol. 87, no. 5-6, pp. 368-379, 2009.

[60] J. Cai and J. Feng, "Form-finding of tensegrity structures using an optimization method," *Engineering Structures,* vol. 104, pp. 126-132, 2015.

[61] J. Lu, N. Li and G. Shu, "Form-finding analysis of irregular tensegrity structures by matrix iteration," *Advanced Steel Construction,* vol. 11, no. 4, pp. 507-516, 2015.

[62] X. Xu and Y. Luo, "Force Finding of Tensegrity Systems Using Simulated Annealing Algorithm," *Journal of Structural Engineering,* vol. 136, no. 8, pp. 1027-1031, August 2010.

[63] Y. Chen, J. Feng and Y. Wu, "Novel Form-Finding of Tensegrity Structures Using Ant Colony Systems," *Journal of Mechanisms and Robotics,* vol. 4, no. 3, pp. 1283-1289, 2012.

[64] H. Obiya, S. Goto, K. Ijima and K. Koga, "Equilibrium analysis of plane structures by the tangent stiffness method," *International Colloquium Stability of Steel Structures,* vol. 2, pp. 305-312, 1995.

[65] K. Abe, H. Obiya and K. Ijima, "A Study on Multi-bifurcation Equilibrium Paths using the Tangent Stiffness Method," in *APCOM'07-EPMESC XI*, 2007.

[66] A. Matsuo, H. Obiya, K. Ijima and M. Zakaria, "Form-finding of extensive tensegrity using truss elements and axial force lines," in *Int. Conf. on Textie Compsites and Inflatable Structures, Structural Membrane 2011*, October 2011.

[67] Z. Nizam, A. Matsuo, H. Obiya and K. Ijima, "Path Finding of Virtual Structure Composed Of Axial Force Line Elements," in *Proceedings of IASS-APCS*, May 2012.

CHAPTER 4

Large Deformation and Large Displacement Analysis of Hyper-elastic Elements

4.1 Introduction

In the previous chapter, the author studied the form-finding analysis of tensegrity which is one of the fundamental but important key steps in exploring the mechanical behavior of tensegrity structures. In the form-finding analysis, many self-equilibrated configurations were successfully obtained from the proposed element force equations and discovered the influence of related coefficients on finding the equilibrium solutions. Taking the advantage of the tangent stiffness method, the elements defined in the element force formulations were freely designated either by the real or virtual element. Therefore, the virtual elements were adopted for cables in the proposed tensegrity structure although the struts were assigned as truss element. Therefore, the equilibrium solution determined from the shape analysis will need to be substituted by the real elements for both strut and cable members before moving on the upcoming analyzes.

Since tensegrity itself has strong nonlinearity and can deform in a large scale compared to the other structures, the material to be applied in the cable members should be in high compatibility with the large deformation process. Therefore, hyper-elastic material will be adopted in this study and its properties will need to be figured out before substituting in the cable members of the equilibrated tensegrity solution. In this chapter, the mechanical behavior of hyper-elastic elements will be presented in detail using the constitutive model and the derivation of appropriate element force equation for the hyper-elastic model will be proposed.

In order to explore the actual response of the hyper-elastic material to a full extent, the experimental model proposed in numerical example will be the net structure composed of rubber-like hyper-elastic material. The large deformation and large displacement analysis of the net structure will be conducted with and without the treatment of relaxation process. The material values applied in the large deformation analysis are derived from the theoretical and the experimental data. In order to improve the structural performance of iteration algorithm, the modified Newton Raphson method comes in the combination with strict tangent stiffness method. The proposed algorithm will explain the iterative phenomenon of nonlinear analysis and describe the nature of mechanical behavior of hyper-elastic elements.

4.2 Hyper-elastic materials in geometrical nonlinear analysis

Hyper-elastic materials are the special class of materials that can response elastically even if they undergo the large deformation under the large loading condition [1]. They possess the high elastic properties and show a nonlinear material behavior. Exhibiting a highly nonlinear stress-strain relation, they exhibit large elastic (recoverable) deformation, stretching in the range of 100 to over 500% and can retain the original shape when the applied loading is removed. One of the significant characteristics of hyper-elastic materials is that they are nearly incompressible where the overall volume remains almost constant although their configuration can be altered in a different way. Many polymers such as elastomers, rubbers and other similar soft flexible materials show the hyper-elastic behavior. Among them, rubber is one of the commonly used materials due to its practical applicability in the nonlinear analysis of hyper-elastic models.

Hyper-elastic materials have broadened its applicability in many aspects, from structural fields to biomedical engineering. Han et al. investigated the mechanical behavior of porous D-L lactide and non-hydroxyapatite biological scaffold material with four compressible hyper-elastic models under the various stress conditions [2]. Saccomandi et al. applied the generalized Mooney-Rivlin model to fit the experimental data of strain energy function in describing the mechanical behavior of brain tissue as hyper-elastic material [3]. Ramezani et al. [4] introduced the concept of hyper-elasticity in the micropolar continuum theory. They generalized the constitutive equations for the Neo-Hookean and Mooney-Rivlin models using the representation theory [5] also with updated Lagrangian finite element formulation. Damanpack et al. tested hyper-elastic beam model under bi-axial normal and shear loading, adopting Mooney-Rivlin strain energy function [6].

There are also a wide range of literatures about nonlinear elastic deformations [7]. Rivlin examined the homogenous deformation for the isotropic materials [8] and carried out their stability analysis under dead loading [9] whereas Ogden checked the stability for the asymmetric deformation and bifurcation process in finite elasticity [10]. Lazopoulos and Bakoginni extended and classified the singularities of homogeneous deformation for any hyper-elastic material, being constrained and/or anisotropic type given under the conservative quasi-static loading [11].

Nowadays, rubber-like materials have gained the popularity in applied industry for their energy absorption and high deformability. Gudsoorkar and Bindu simulated tire rubber deformation by the pure shear using four hyper-elastic models, stating that Yeoh and Arruda-

Boycee models are in stable alignment with their experimental results [12]. Suraj et al. used Mooney-Rivlin model for the hyper-elastic material in inflating circular membrane with periphery boundary condition, and made experiment on the consequences of material model change at different principal stretches in the inflation process [13].

Hyper-viscoelastic models are also used to describe the mechanical behavior of rubber-like materials and soft tissues where their viscoelasticity prescribes the rate-dependent response of materials. Zheng presented new numerical stress solutions for the combination of Ogden-Roxburgh pseudo-elastic model [5] and Prony linear viscoelastic model [14] to predict the stress response and minimize the error difference between the predicted and the measured ones. Peng et al. adopted Mooney –Rivlin model for the derivation and simulation of corneal hyper-elastic material [15] whereas Maedeh et al. identified the material parameters using Neo-Hookean model under dynamic loading [16]. Li and Lua presented hyper-viscoelastic modelling for polyurea using the Ogden material [17] whereas Bai et al. combined the three-parameter Mooney-Rivlin and Ogden models. This implementation produces more accuracy to describe the mechanical behavior of polyurea under uniaxial compressive loading [18].

Even in recent years, many researchers have tried to analyze the structure consisting of hyper-elastic material as the geometrically nonlinear problems. This is why quite higher techniques are required to conduct the large displacement and large deformation simultaneously. For example, Lin et al. [19] have carried out a contact analysis between a rigid sphere object and soft hyper-elastic slab with comparison of several constitutive models. Saavedra Flores et al. [20] applied the simple Ogden model with one term to a buckling problem of carbon nanotubes. Bodaghi et al. [21] have compared the numerical results with the experimental data of the model made by 3D printer. Damanpack et al. [22] examined the similar experiment for the lattice structure and unit cells deformation, in which Mooney-Rivlin model and nonlinear Green-Lagrange are used for the hyper-elastic constitutive equation and the geometrical nonlinear procedure respectively. Moreover, Yamada [23] proposed a kind of weak formulation to solve the large deformational problem with incompressible hyper-elasticity and applied it to examples with solid elements. Tomioka et al. [24] analyzed the large deformation of flexible membrane with experiment and Kido et al. [25] presented the method to replace the membrane structures by flexible cable elements and conducted large deformation analysis. Therefore, it is necessary to examine the mechanical behavior of the flexible elements and their efficiency which will be discussed in next section.

4.3. Hyper-elastic models

The hyper-elastic models are of constitutive equations that can be defined using stress-strain relationship derived from the strain energy density function [26]. Up to now, many models have been proposed to characterize the mechanical properties of hyper-elastic material. Among them, Mooney-Rivlin, Neo-Hookean, Arruda-Boyce and Ogden models are the most common ones that describe the nonlinear behavior of hyper-elastic material.

4.3.1 Mooney-Rivlin model

The model was first introduced by Melvin Mooney in 1940 and Ronald Rivlin proposed the expression in terms of invariants in 1948. The form of strain-energy potential for a two-parameter Mooney-Rivlin model is

$$W = C_1(\bar{I}_1 - 3) + C_2(\bar{I}_2 - 3) \tag{4.1}$$

where C_1 and C_2 are empirically determined material constants, while $\bar{I}_1$ and $\bar{I}_2$ are the first and second invariant of $\bar{B}$.

$$\bar{B} = (det\, B)^{-1/3}\, B \tag{4.2}$$

where B is the left Cauchy-Green deformation tensor.

$$\bar{I}_1 = J^{-2/3}\, I_1 \qquad , \qquad \bar{I}_2 = J^{-4/3}\, I_2 \tag{4.3}$$

$$I_1 = \lambda_1^2 + \lambda_2^2 + \lambda_3^2 \qquad , \qquad I_2 = \lambda_1^2 \cdot \lambda_2^2 + \lambda_2^2 \cdot \lambda_3^2 + \lambda_3^2 \cdot \lambda_1^2 \tag{4.4}$$

If the material is assumed as incompressible, $J = 1$.

This model is based on the level order as in two parameters, three parameters, five parameters and nine parameters. However, the higher the order, the more complex the stress-strain relation, and this makes the model require more sophisticated computation steps, experimental data and the parameter fitting. The Mooney-Rivilin model is widely used to describe the precise mechanical behavior of rubber material, especially in the small to medium strain definition. Later, the application of Mooney-Rivilin model can also be found in the explanation of incompressible biological tissue. However, the model losses its efficiency when the deformation exceeds 150% or the parameter becomes higher order, and it is not suitable for the analysis of compressible hyper-elastic material such as foam.

4.3.2 Neo-Hookean model

Neo-Hookean model is the simplest one among all the hyper-elastic material models since it contains only two parameters and hence it does not need any complex calculation. The strain energy function for incompressible Neo-Hookean model is

$$W = C_1(I_1 - 3) \tag{4.5}$$

where C_1 is material constant and I_1 is the first invariant of the right Cauchy-Green deformational tensor.

$$C_1 = \frac{\mu}{2} \tag{4.6}$$

$$I_1 = \lambda_1^2 + \lambda_2^2 + \lambda_3^2 \tag{4.7}$$

where μ is shear modulus and λ_i are the principal stretches.

This model consists of constant shear modulus, and it is recommended to use the model for the small strain under 20% as the model becomes inaccurate for materials under large strain deformation. However, due to its simplicity, Neo-Hookean model is used in a wide range of industry where the small strain can be satisfied in its application.

4.3.3 Arruda-Boyce model

Another commonly used method in prescribing the nonlinear stress-stress behavior is Arruda-Boyce model. The model named after Ellen Arruda and Mary Cunningham Boyce in 1993. The application of constitutive Arruda-Boyce model is mainly practiced in modelling of hyper-elastic materials like rubber and other polymeric substances.

The strain energy function for incompressible Arruda-Boyce model is

$$W = C_1 \sum_{i=1}^{5} \alpha_i \, \beta^{2i-2} \left(I_1^i - 3^i \right) \tag{4.8}$$

where
$$\beta := \frac{1}{\lambda_i^2} \tag{4.9}$$

$$\alpha_1 := \frac{1}{2} \qquad \alpha_2 := \frac{1}{20} \qquad \alpha_3 := \frac{11}{1050} \qquad \alpha_4 := \frac{19}{7000} \qquad \alpha_5 := \frac{519}{673750} \tag{4.10}$$

where C_1 is material constant, I_1 is the first invariant of the Cauchy-Green tensor and λ_i are the principal stretches.

Arruda-Boyce model becomes equivalent to the Neo-Hookean model in the case of infinite limiting network stretch condition. However, Arruda-Boyce model has higher accuracy rate than the Neo-Hookean model when dealing with high stretch situations.

4.3.4 Ogden model

The strain-energy function W of Ogden model can be represented either in terms of the principal invariants or the principal stretches (λ_1, λ_2, λ_3) as in equation (4.11). Rather than the strain invariant, the model with the terms of stretches as elongation ratio is widely applied in the strain energy model since it is an effective and practical function to describe a large deformational behavior of hyper-elastic materials such as rubber. This model expresses the strain energy as a function of

$$W = \sum_{k=1}^{N} \frac{\mu_k}{\alpha_k} \left(\lambda_1^{\alpha_k} + \lambda_2^{\alpha_k} + \lambda_3^{\alpha_k} - 3 \right) \tag{4.11}$$

where μ_k and α_k are shear modulus and material property value, respectively.

Since α_k itself is the material property value in Ogden model, it is possible to conduct the complex aspects of the strain energy function of rubber and can accurately express the nonlinearity in the high strain region. Although it is a serial model, the accuracy does not increase with the larger N value. In case of taking a larger N value, the unnecessary numerical calculation is likely to occur. Therefore, in this study, $N=3$ is used and the analysis is performed by the nominal stress F for uniaxial model to simulate 1D cord elements in equation (4.12) derived from equation (4.11) of Ogden model.

$$F = \sum_{k=1}^{N} \mu_k \left(\lambda^{\alpha_k - 1} - \lambda^{-1 - \frac{\alpha_k}{2}} \right) \tag{4.12}$$

4.4 Fundamental concept of hyper-elastic element analysis

In this study, the large displacement and large deformation analysis is performed using a nonlinear element force equation represented by the Ogden model. For this purpose, it is necessary to evaluate the usefulness of the Ogden model in the hyper-elastic element analysis by making a comparison with other strain concepts. The hyper-elastic element represented by rubber material

having Poisson's ratio close to 0.5 does not change in volume. In an ordinary elastic element, the relationship between the stress and strain can be assumed as linear expression as long as it is within the elastic range in which the material will deform during loading and can return to its original shape when unloading. In a hyper-elastic element, the amount of deformation in the elastic range is much larger than that of ordinary elastic element, and cannot be assumed as having a linear function. Therefore, it is necessary to develop a nonlinear element force equation that can prescribe closely to the hyper-elastic behavior. When analyzing the structures having hyper-elastic element, both the rigid body displacement and the amount of element deformation become comparatively large. Therefore, it is necessary to formulate the large displacement and large deformation analysis to prescribe the mechanical behavior of the structure exactly.

□ **Large displacement analysis**

Displacement represents the amount of movement, whereas the amount of movement of the element assumed to be rigid is called rigid body displacement. Even if the amount of strain generated in each element of existing structural system is small, the translational movement or rotational movement occurs significantly in the element. This causes large deformation in the entire structural system due to the rigid body displacement of composing elements, therefore the non-linear terms cannot be neglected throughout the analysis. In the tangent stiffness method used in this study, the rigid body displacement component is completely separated from the deformation behavior component in the nonlinear analysis. Therefore, the rigid body displacement can be accurately evaluated regardless of the amount of deformation.

□ **Large deformation analysis**

When the large deformation occurs, the element cannot be represented linearly no matter how small the element is subdivided. In a hyper-elastic element, large deformation is likely to occur since the cross-sectional area changes according to the elongation ratio although the volume does not change. The tangent stiffness method enables to perform the large deformation analysis by using the element behavior component described by the element force equation. Regardless of the degree of non-linearity of the element force equation, it is possible to obtain an equilibrium solution that matches the element behavior by adjusting the tangent stiffness equation in the iteration process.

4.5 Strain definition for hyper-elastic material by Ogden model

The constitutive equation for the hyper-elastic material is defined as a strain-energy function. Up to now, so many proposals for the hyper-elastic model have been published, but Ogden model may be used most often, because of its most practical reproducibility, even in the large strain areas both for compression and tension sides. This study also adopts three terms of Ogden function to compose the element force equation. In this study, the "rubber like" hyper-elastic material is adopted as an example to conduct the large deformation and large displacement analysis by the tangent stiffness method.
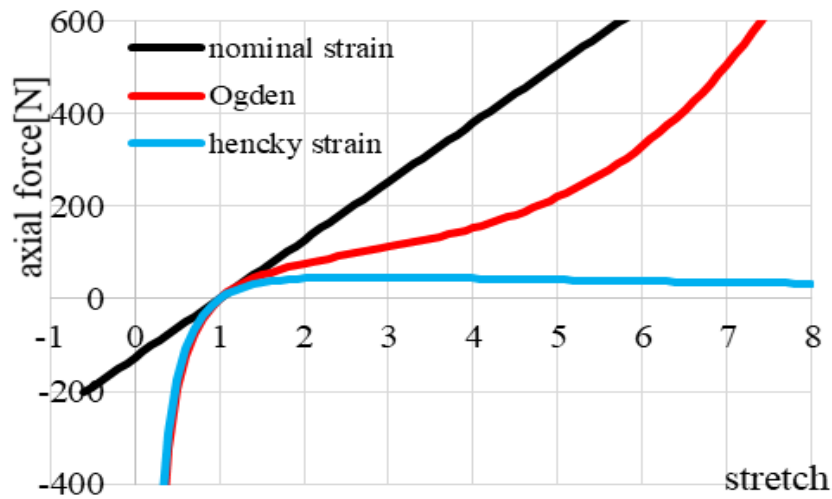
Figure 4.1 Axial force-stretch curve for each strain definition

Figure 4.1 is a comparison of the relation between the axial force and stretch in terms of nominal strain, Hencky strain and Ogden model under the uniaxial condition respectively. In case of nominal strain, when the stretch is around 1, it is possible to calculate the element force appropriately like the other strain definitions. However, the linear slope in the graph extends and penetrates the vertical axis that cannot be in reality to take the negative value of the element length. In Hencky strain definition, the hyper-elastic material having a certain degree of cross-sectional area tends to increase the rigidity when it is compressed. However, there is the deterioration by decreasing of cross-section in the tension side, showing the feature which is different from the realistic characteristic of the hyper-elastic material.

Apart from the previous strain definitions, the Ogden model shows the nonlinear curve in both sides as shown in figure 4.1. When the material such as rubber is greatly pulled out, the

material tends to behave the hardening in the high tensile strain region. Ogden model can capture the characteristic of stiffness hardening both in the compression and tension side. Therefore, the usefulness of the model in the high tensile strain region can be expected by the Ogden strain definition in the strong nonlinear analysis.

4.6 Development of element force equation for hyper-elastic and compression-free element

In the previous section, the usefulness of the Ogden model has been discussed, and so an element force equation is developed to support the hyper-elastic elements. The Ogden model is characterized by the element rigidity in both compression and tension side. However, when the compression-free element such as rubber cord is assumed, softening occurs in the compression side and the formation of slack is required. Therefore, only when the element is compressed, the element force equation should be performed by switching from formula by the Ogden model to another formula which can trace its relaxation.

Figure 4.2 shows the concept of switching the element force equations, where the Ogden model (indicated by gray curve in figure 4. 2) is used when the stretch λ is larger than the arbitrarily determined threshold λ_x, and when the stretch λ is smaller than λ_x, relaxation behavior will be evaluated by switching to the square root function (illustrated in red color) as shown in equation (4.13), which might be the simplest and easiest expression to simulate it. In this way, the natural behavior of rubber-like hyper-elastic material can be achieved without the requirement of complicated numerical calculations.
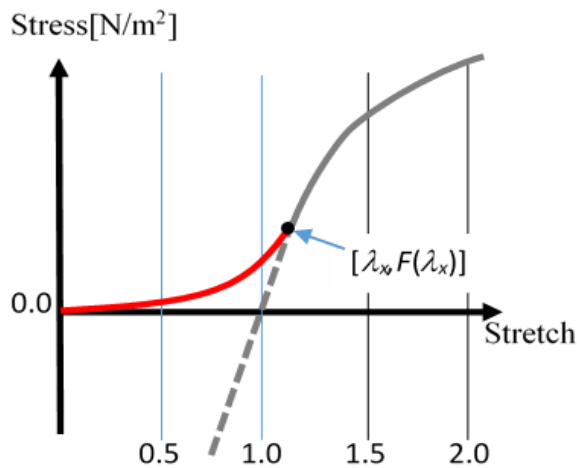

Figure 4.2 Interpolation function image

Of course, the threshold should have value of more than 1.0 which gives zero stress in each strain model including the tangent stiffness Ogden model.

$$F(\lambda) = -\sqrt{a\lambda + b} + c \tag{4.13}$$

The coefficients *a, b* and *c* in equation (4.13) are smoothly connected to the Ogden model by Lagrange interpolation.

4.7 Preparation of tangent matrixes

The tangent stiffness equation can be easily formulated by the first-order differentiation of the equilibrium equation between the nodal force vector of the general coordinate system and the element edge force vector in the element coordinate system. In other words, it can be said that the geometrical nonlinear analysis of any model is possible if the element force equation is changed for each analysis purpose. For example, in case of 1 dimensional element which connects two nodes, if the axial force of the elements is expressed as;

$$N = F(\lambda)A_0 \tag{4.14}$$

And this element force equation can control the element's own behavior. Here, *N, F, λ* and A_0 are the axial force, nominal stress, stretch, and primary area of cross-section of an element, respectively. In this case, the tangent stiffness equation for one elements becomes as following.

$$\delta \begin{bmatrix} \mathbf{B_i} \\ \mathbf{B_j} \end{bmatrix} = \left\{ \frac{N}{l} \begin{bmatrix} \mathbf{e\text{-}JJ^T} & \mathbf{JJ^T\text{-}e} \\ \mathbf{JJ^T\text{-}e} & \mathbf{e\text{-}JJ^T} \end{bmatrix} + \frac{\partial F}{\partial \lambda} \frac{A_0}{l_0} \begin{bmatrix} \mathbf{JJ^T} & \mathbf{-JJ^T} \\ \mathbf{-JJ^T} & \mathbf{JJ^T} \end{bmatrix} \right\} \delta \begin{bmatrix} \mathbf{d_i} \\ \mathbf{d_j} \end{bmatrix} \tag{4.15}$$

in which, *l* and l_0 are element length in current and initial state respectively. Therefore, we can define and use the element force equation of (4.15) depending on the material and the mechanical properties such as compression-free behavior.

4.8 Algorithm for nonlinear analysis of hyper-elastic element

In case of soft structures with large displacement and deformation, the scheme by using the exact tangent stiffness sometimes leads to diverge via the chaotic unbalanced situation far from the equilibrium solution. Therefore, an improved method is to obtain a convergent solution efficiently by combining the exact tangent stiffness iteration and a kind of modified Newton-Raphson method. That procedure is to switch the fixed tangent of nominal stress and the updated

one depending on the amount of unbalanced forces calculated in every iteration step. This realizes both of stability of calculation process and accuracy of solutions. Figure 4.3 demonstrates the flow chart of the proposed algorithm implemented for the analysis method in this study.
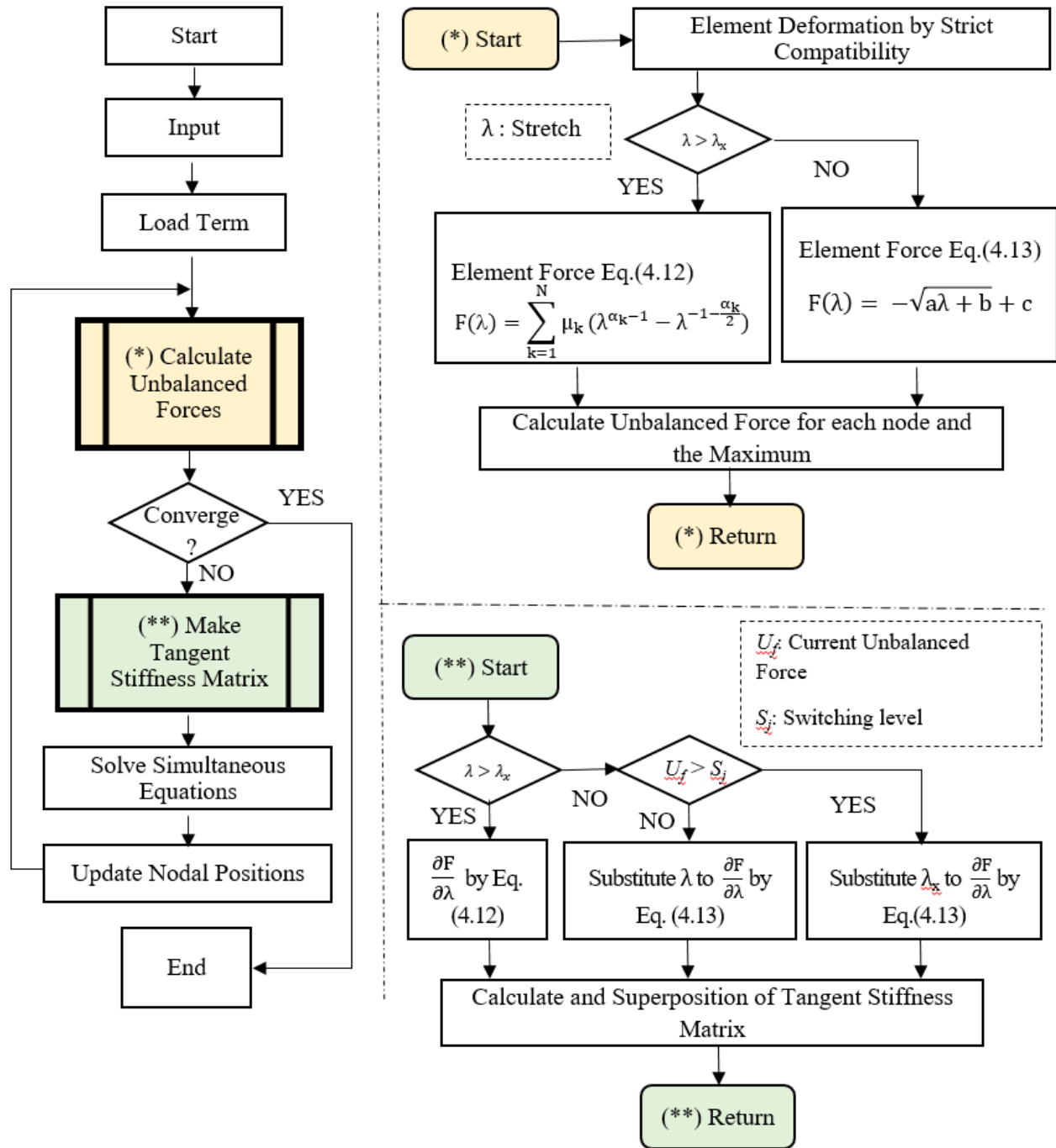

Figure 4.3 Flow chart of the proposed algorithm

In the nonlinear algorithm, the calculation procedure based on the tangent stiffness method is carried out iteratively. After establishing the required input data for the proposed model, the loading is assigned for each node of the structure. In the subroutine of calculating the unbalanced forces, the element deformation is found out by the application of strict compatibility which is the relation between nodal displacements and element deformation vector.

If the stretch λ is greater than the designated threshold λ_x, the element force is determined by equation (4.12) of Ogden function. In the case of λ being smaller than λ_x, the square root function of equation (4.13) is applied to calculate the unbalanced force. When the obtained unbalanced force is beyond the allowable limitation (adopting 1/10000 value of maximum of nodal forces), the iteration of the algorithm is started to make the convergence of the unbalanced force of each member.

In making the tangent stiffness matrix subroutine, the differential equation of Ogden function is used when λ is greater than λ_x. While the maximum unbalanced force U_f is greater than the switching level S_j designated arbitrarily, the fixed tangent of nominal stress F determined by the threshold λ_x without updating lets the unbalanced forces decrease steadily. By the way, even while $\partial F/\partial \lambda$ is fixed, the tangent stiffness is updated with the cosine vector and the length of elements. After the U_f converges to smaller than S_j, the tangent stiffness is updated to exact value calculating the current unbalanced state. This switching procedure realizes both the stability and the accuracy of the solution.

4.9 Numerical calculation

In this study, some numerical example models are assumed as net structures consisting of rubber string elements. Therefore, the examination for non-compressive property is required with appearance of relaxation. For the relaxation of fiber net structure, Inukai et al. [27] tried to apply the constitutive law using hyperbola asymptotic to two linear function. Also, Ijima et al. [28] applied the cable elements defined by hyperbolic function as conversion members of membrane elements. Sato et al. [29] examined the large displacement analysis of sagged net structures. However, the hyper-elastic material has strong nonlinearity itself and nominal stress of Ogden model is not expressed as a function of nominal strain but stretch. This study proposes a new and simple equation of square root function to express the behavior in compression area, which connects smoothly to Ogden function in tensile area.

4.9.1 Examination of threshold λ_x

Figure 4.4 shows the primary shapes of the analysis model of a square-shaped rubber net structure with each side of 12 m. The four vertices indicated as black square dots are fixed nodes and all the other nodes of green circular dots are free nodes. While giving vertical loads of w=0.01N (simulating very light self-weight) to all the free nodes, the fixed points are given compulsory displacements of 0.1m per step in the direction towards the center (arrows in figure 4.4) up to 50 steps. Using this calculation model, the difference in the transition of the solution will be examined depending on the presence or absence of relaxation process in the element force equation.

Figure 4.4 Analysis model of square-shaped rubber net structure

Figure 4.5 to figure 4.16 show the out coming shape formation in (a) bird's eye view, (b) side view and (c) plan view resulted, and elements with compressive strain with their stretches less than 1 are drawn in red lines. Figure 4.5 to figure 4.7 are from the analysis using only the element force equation of Ogden model without the square root function of equation (4.13). Without giving the relaxation process, the converged solution is formed in the dome-like shape. This shape has so many elements with compressive stress, and it may be in unstable equilibrium state with higher potential energy.

Moreover, the relaxation function is examined by designating the threshold λ_x at three values (1.01, 1.001 and 1.0001) in order to examine the proper value of threshold λ_x. The shear modulus and material property values for the Ogden model are adopted by the following values identified from the experimental results of Treloar [30] by Ishikawa et al. [31] as below.

$$\alpha_1 = 1.3, \ \alpha_2 = 5.0, \ \alpha_3 = -2.0$$

$$\mu_1 = 0.63, \quad \mu_2 = 0.0012, \quad \mu_3 = -0.01 \ \ [N/mm^2]$$
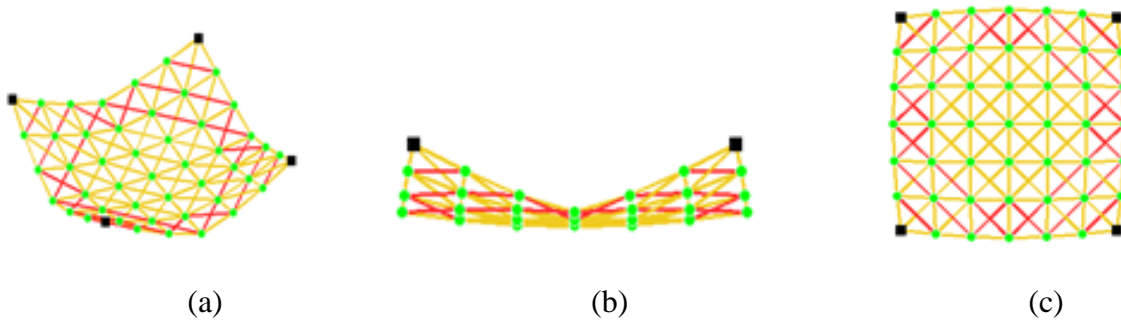
□ Without relaxation process

(a)   (b)   (c)

Figure 4.5 Without relaxation process (step 5)

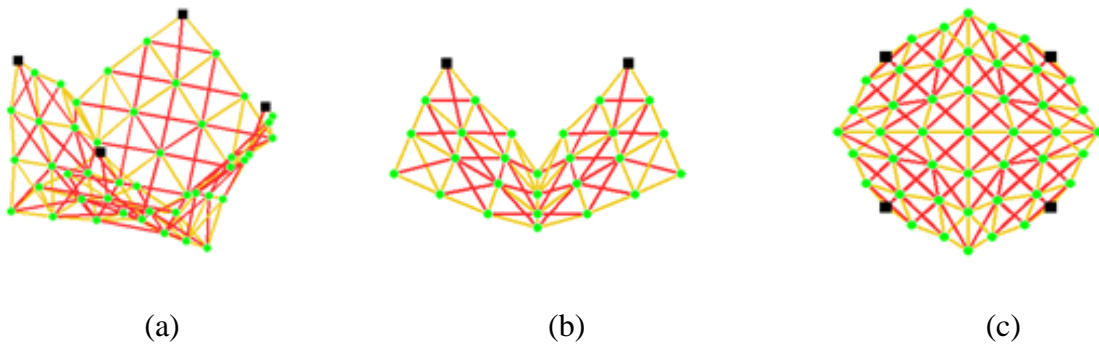(a)   (b)   (c)

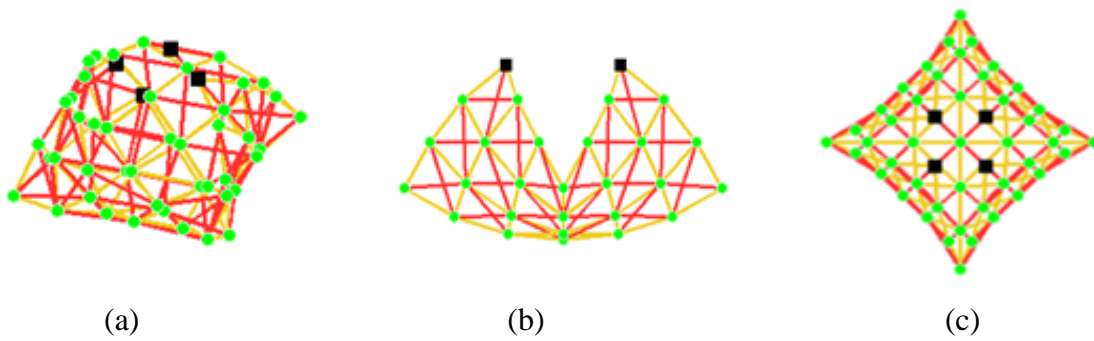Figure 4.6 Without relaxation process (step 25)

(a)   (b)   (c)
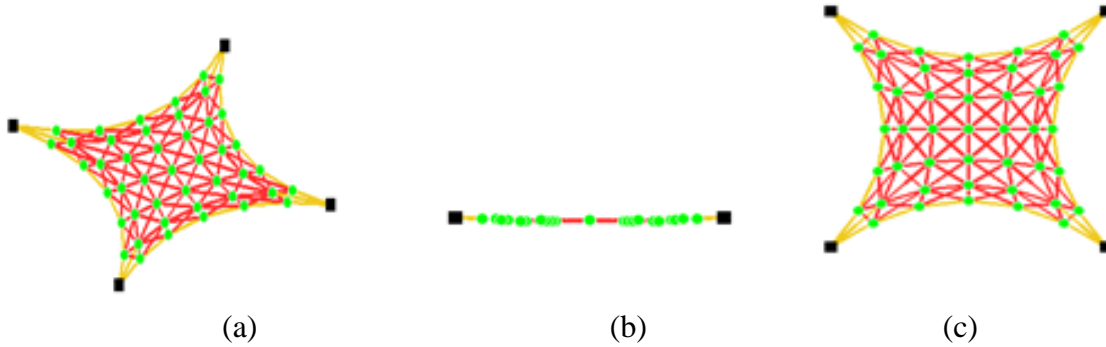
Figure 4.7 Without relaxation process (step 50)

(a)   (b)   (c)

Figure 4.8 With relaxation process at λ_x=1.01 (step 5)

(a)   (b)   (c)
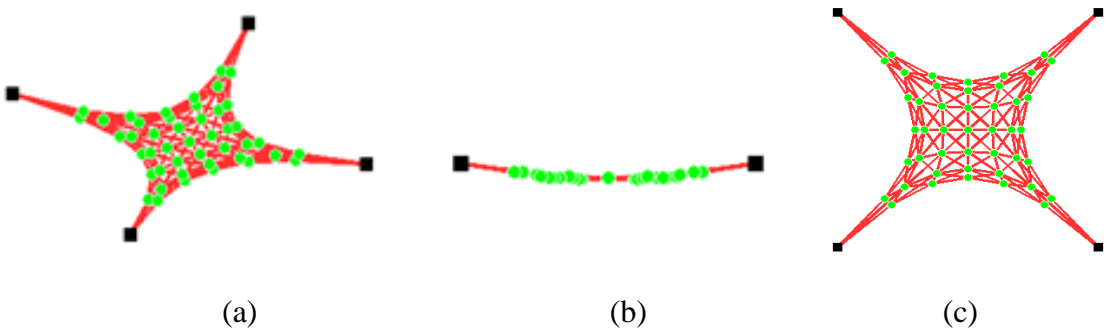
Figure 4.9 With relaxation process at λ_x=1.01 (step 25)
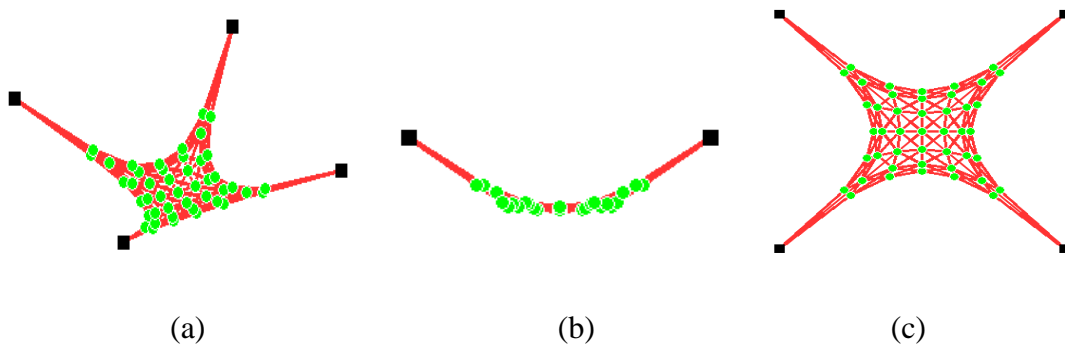

(a)   (b)   (c)

Figure 4.10 With relaxation process at λ_x=1.01 (step 50)

Figure 4.8 to figure 4.16 indicate the deformed state of net structure under the relaxation process at each λ_x respectively. When the model is treated with relaxation process, it converges in the form where the central point is lowered depending on the amount of λ_x. Furthermore, referring to figure 4.9, 4.10, 4.12, 4.13, most of the members have compressive strain, but some of them have very small tensile stress.

(a) (b) (c)
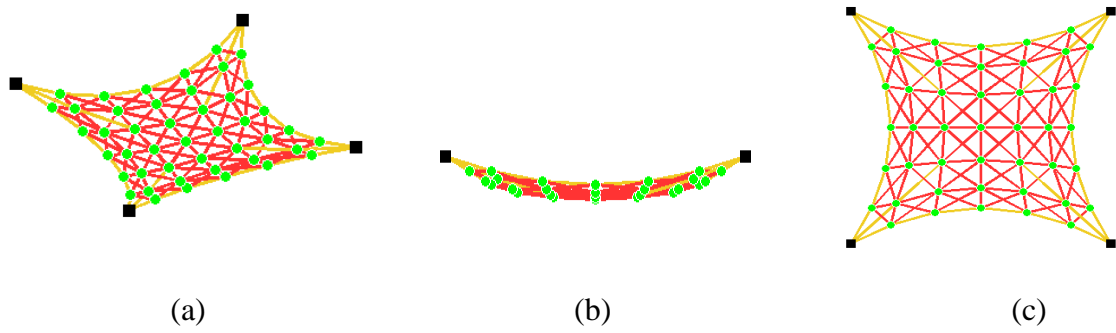
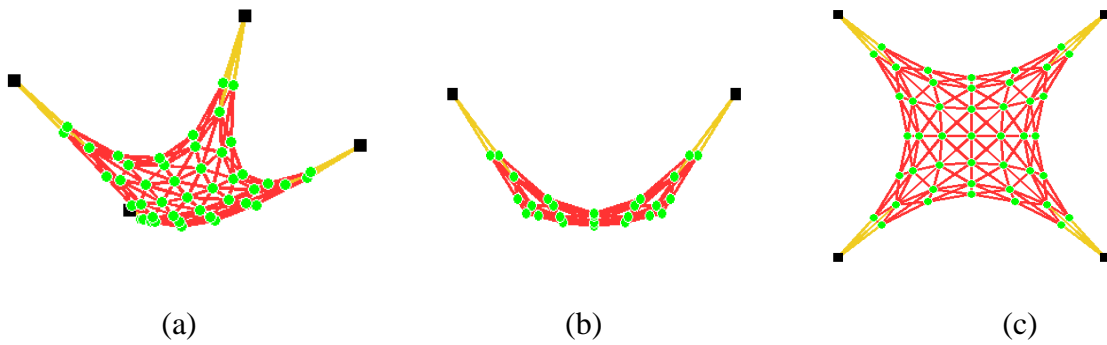Figure 4.11 With relaxation process at λ_x=1.001 (step 5)

(a) (b) (c)

Figure 4.12 With relaxation process at λ_x=1.001 (step 25)

(a) (b) (c)

Figure 4.13 With relaxation process at λ_x=1.001 (step 50)

71

(a)   (b)   (c)

Figure 4.14 With relaxation process at λ_x=1.0001 (step 5)

(a)   (b)   (c)

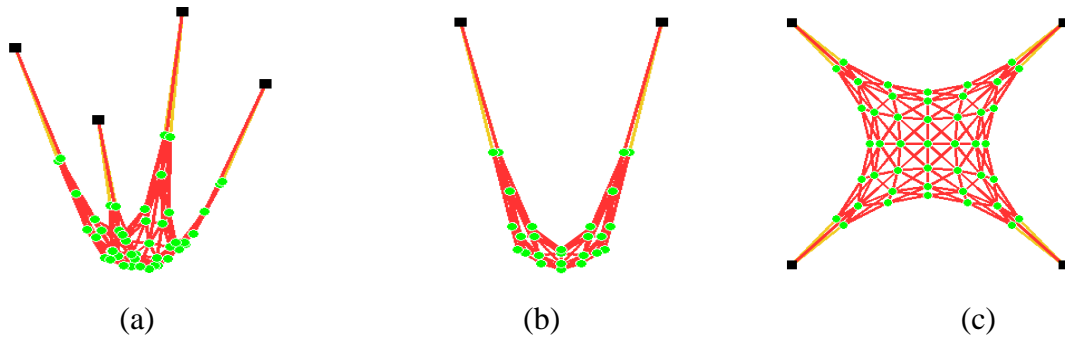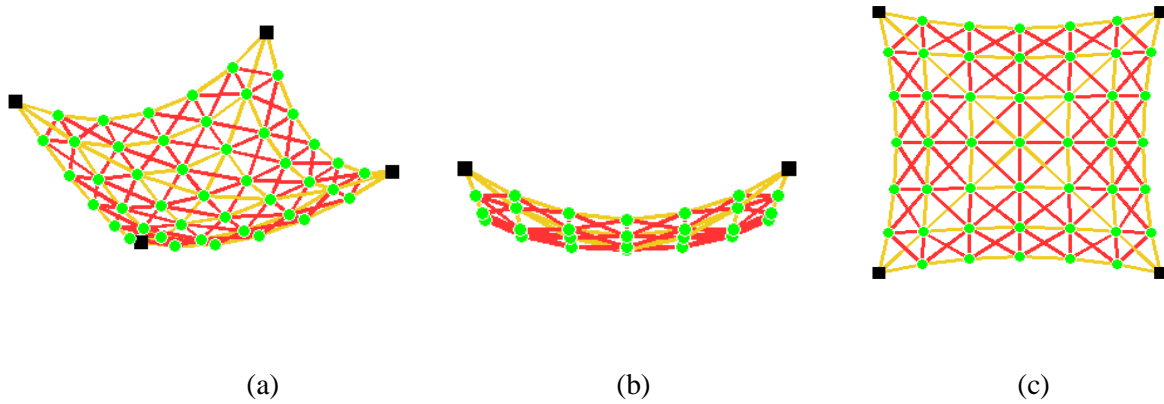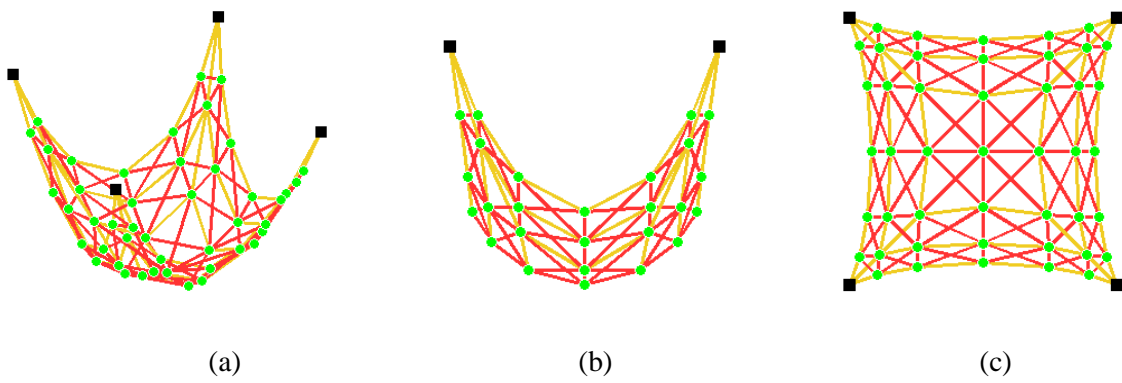Figure 4.15 With relaxation process at λ_x=1.0001 (step 25)

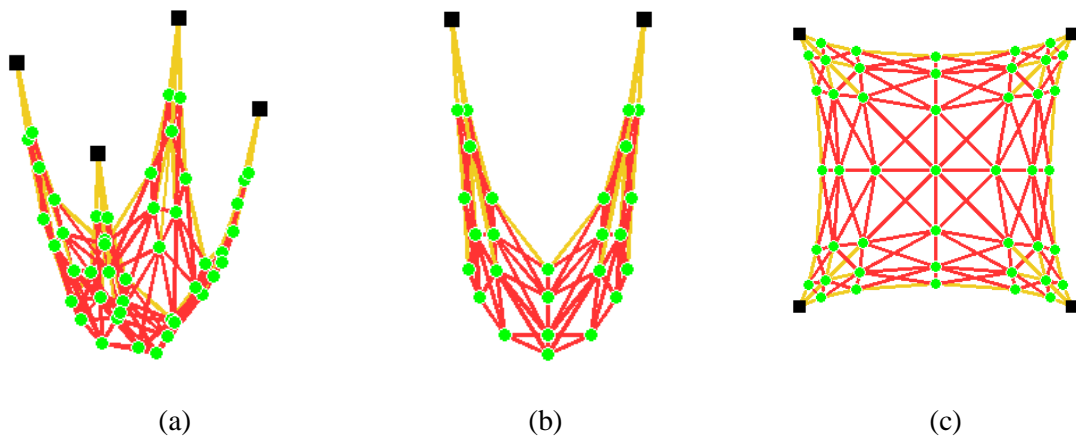(a)   (b)   (c)

Figure 4.16 With relaxation process at λ_x=1.0001 (step 50)

Figure 4.17 shows the relation between the amount of vertical displacement of central node and the amount of given compulsory displacement, corresponding to each threshold λ_x. According to this figure, only in case of without relaxation process, a dip in the curve is recognized, and this means the appearance of snap-through phenomenon.

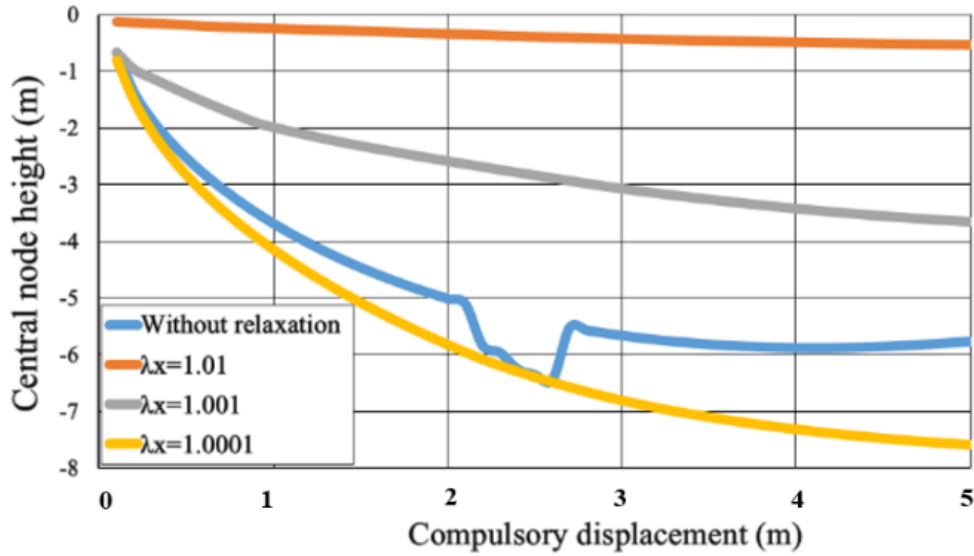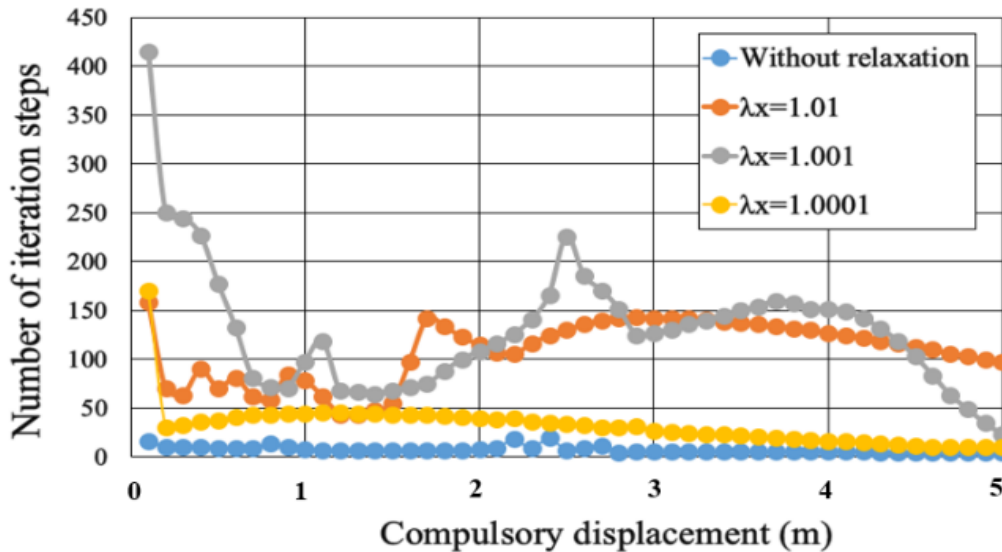Figure 4.17 The change in height of central node

Figure 4.18 Number of iterations for convergent process

When the relaxation process is adopted, it can be seen that when λ_x becomes closer to 1, the position of the central node tends to be lowered and the relaxation of the net structure can be expressed smoothly. Therefore, the relaxation characteristics can be performed effectively only by

switching between two different element force equations depending on the value of λ. In other words, tangent stiffness method can produce reliable solutions by appropriate selection of "the element force equation", even if the analysis is under tough and severe conditions of very strong nonlinear.

Figure 4.18 demonstrates the total number of iteration steps taken in each given increment amount of the compulsory displacement at the controlled nodes for each element force equation. According to this figure, the analysis without the treatment of relaxation process terminates the iteration process much quicker than the consideration of relaxation function. On the other hand, among the three designated thresholds, the relaxation function with the threshold λ_x=1.0001 takes fewer iteration steps to obtain the convergent solutions compared to the other two thresholds. Therefore, it can be assumed that the threshold λ_x closer to 1 can give a better performance with less time consuming in the analysis of large displacement and large deformation of the hyper-elastic material.

4.9.2 Uniaxial tensile test using rubber material

In order to identify the physical property values based on the measurement results, a uniaxial tensile test was conducted using the rubber material, having the length of 90 mm, the width of 15 mm and the cross-sectional area of 14.25 mm^2 shown in figure 4.19.

Firstly, the rubber band is placed on the hook, and the tip of measure tape is set at 0 cm and fixed it on the floor with rubber tape so that the measure tape cannot shift its position. One of the end of rubber band is attached to the hook and the other end is to the spring scale. The rubber band is pulled by increasing 5 cm each time under the applied tensile force and the length l of rubber band after deformation is recorded.

Figure 4.19 Sample of rubber band   Figure 4.20 Measurement of uniaxial tensile test

The above measurement procedure is repeated, but the previously used rubber band is replaced by the new rubber band of same type in order to increase the accuracy of measurement. The force F is obtained by multiplying the mass (measured at the time of current length l after each deformation) by the gravitational acceleration (g=9.80665). The cross sectional area A of rubber band is calculated from the width and thickness of cutting surface and the stress value σ is obtained by dividing the force F by the cross-sectional area A. The elongation ratio λ is calculated by dividing the elongated length l by the original length l_0. Then, the graph is prepared by plotting with horizontal axis having the values of elongation ratio (stretch) and vertical axis having the values of nominal tensile stress σ. Each test result is summarized for the curve fitting process and its derivation is presented in the following section.

4.9.3 Curve fitting process

For the analyses of finite element structures consisting of hyper-elastic material, the experimental data by Treloar is often used. However, that data is obtained from natural rubber and for practical use, some curve fitting process to determine the coefficients from measurements is required. Here, it is difficult for this process to identify the appropriate initial value. Up to now, many optimization methods have been proposed, but in this appendix, a simple method by Newton-Raphson iteration scheme is explained briefly.

Data of (λ_i, F_i), the stretch and the nominal stress at point i are obtained by the measurements, and $\tilde{F}_i$ is given by substitution of λ_i into equation (4.12) under uniaxial condition. The nonlinear least square method is provided with the purpose function of equation (4.16),

$$S = \sum_{i=1}^{n}(F_i - \tilde{F}_i)^2 \qquad (4.16)$$

When three terms of Ogden model are adopted, x in equation (4.17) consists of six coefficients should be determined. The algorithm for the Newton-Raphson method is to let X in equation (4.18) approach to zero.

$$\mathrm{x} = [\alpha_1, \alpha_2, \alpha_3, \mu_1, \mu_2, \mu_3] \qquad (4.17)$$

$$\mathrm{X} = [\frac{\partial S}{\partial \alpha_1}, \frac{\partial S}{\partial \alpha_2}, \frac{\partial S}{\partial \alpha_3}, \frac{\partial S}{\partial \mu_1}, \frac{\partial S}{\partial \mu_2}, \frac{\partial S}{\partial \mu_3}] \qquad (4.18)$$

Namely, the tangent equation becomes,

$$\delta X = \frac{\partial^2 S}{\partial x\, \partial x^T} \delta x \qquad (4.19)$$

and this is solved iteratively.

In this study, the ratio to be adjusted to the maximum measurement data of nominal stress is multiplied to the data of 6 coefficients determined form Treloar. This simple linear conversion produces the initial value of x, and the coefficients which form a curve enough close to measurements can be determined after several times of iteration just shown in figure 4.21.
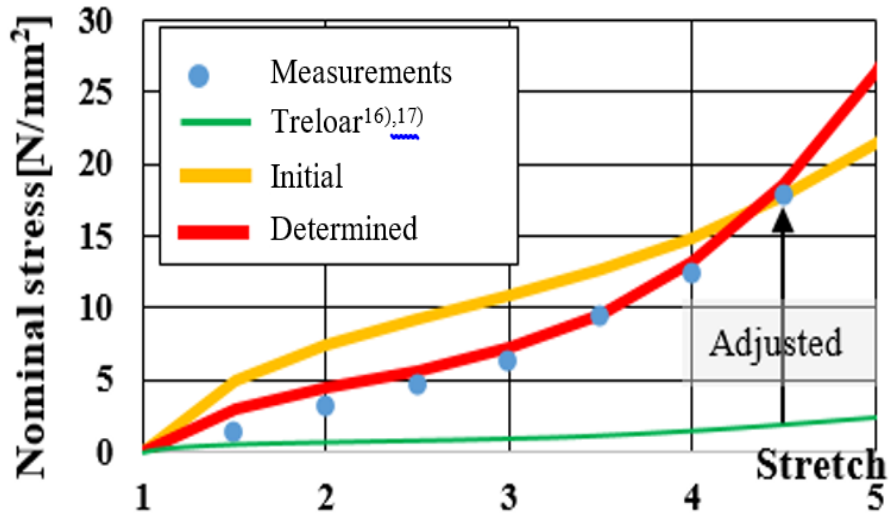

Figure 4.21 Curve fitting process

4.9.4 Examination of switching level S_j

In the extremely strong nonlinear analysis process, the condition where the unbalanced force is quite large and far from the true solution, it sometimes becomes difficult to apply the exact tangent stiffness directly because the direction of the tangent is quite far from the solution. Therefore, if the fixed tangent slope is designated, it makes the algorithm easier to get close to true solution. When the unbalanced force becomes smaller enough to expecting converge, switching to the exact tangent stiffness method is rational to obtain the solution faster. In this chapter, efficient switching level for the maximum unbalanced forces to switch the tangent is examined corresponding to the amount of vertical nodal force w. Figure 4.22 is the analysis model of the same rubber net structure as in the previous example. However, the middle point of one side is fixed likewise the four vertices. In this example, extremely large compulsory displacement is given only at this side fixed node with 2 m in both lateral directions towards center and 10 m in the

upward direction at once with the combination of *w*. The physical properties used in this analysis model are based on the experimental data and the threshold λ_x of 1.0001 is assigned for the relaxation function. Figure 4.23 illustrates (a) bird's eye view, (b) plan view, (c) side view 1 (d) side view 2 of the unsymmetrical shape deformation of the proposed analysis model in case of *w*=0.03N. The proposed rubber net structure is deformed unsymmetrically in a large scale where the relaxation of rubber strings is also achieved.
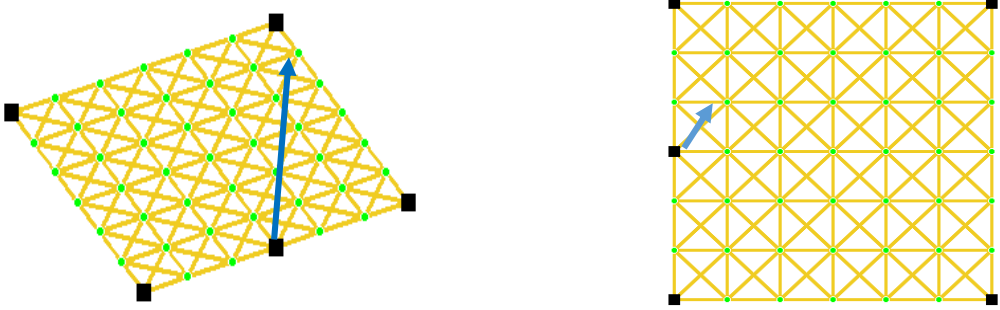

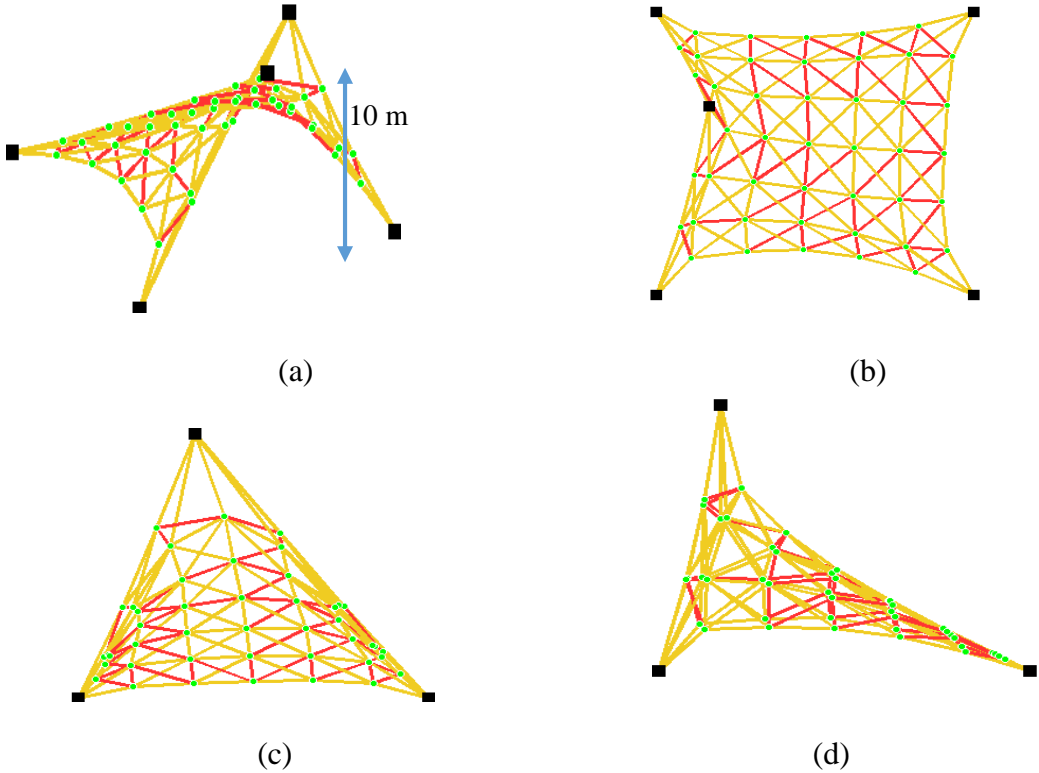Figure 4.22 Analysis model of square-shaped rubber net structure

(a)

(b)

(c)

(d)

Figure 4.23 Shape of solution with 10 m upward "one time" compulsory displacement

Moreover, for this example, a simple uniaxial tension test of rubber material is conducted and each physical property value is identified from the obtained stress value of hyper-elastic material, whereas experimental results of Treloar were used in the previous chapter. The derivation of the physical properties is described in the section of appendix. These physical properties are as below.

$$\alpha_1 = 0.88, \ \alpha_2 = 5.31, \ \alpha_3 = -1.01$$

$$\mu_1 = 7.15 \times 10^{-1}, \ \mu_2 = 2.05 \times 10^{-2}, \ \mu_3 = -9.10 \times 10^{-2}[\text{N/mm}^2]$$
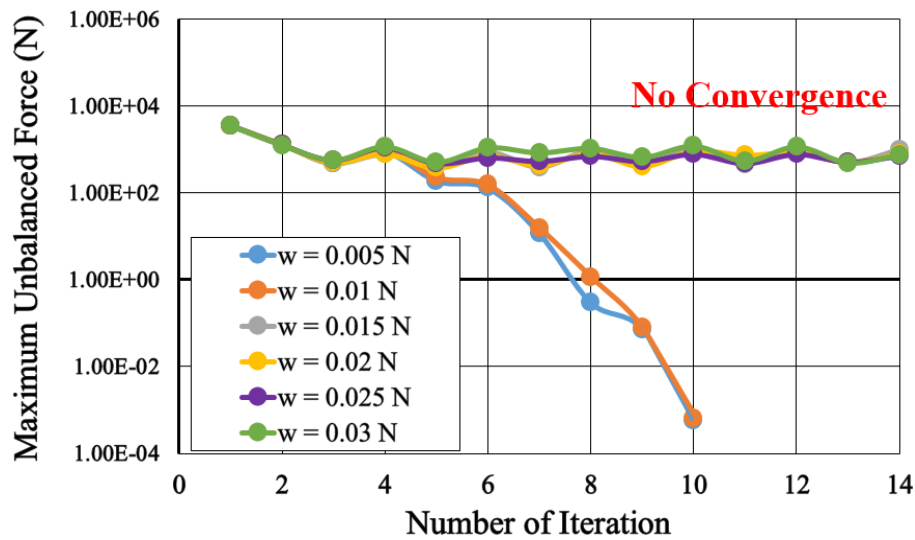
Figure 4.24 Convergence process without switching
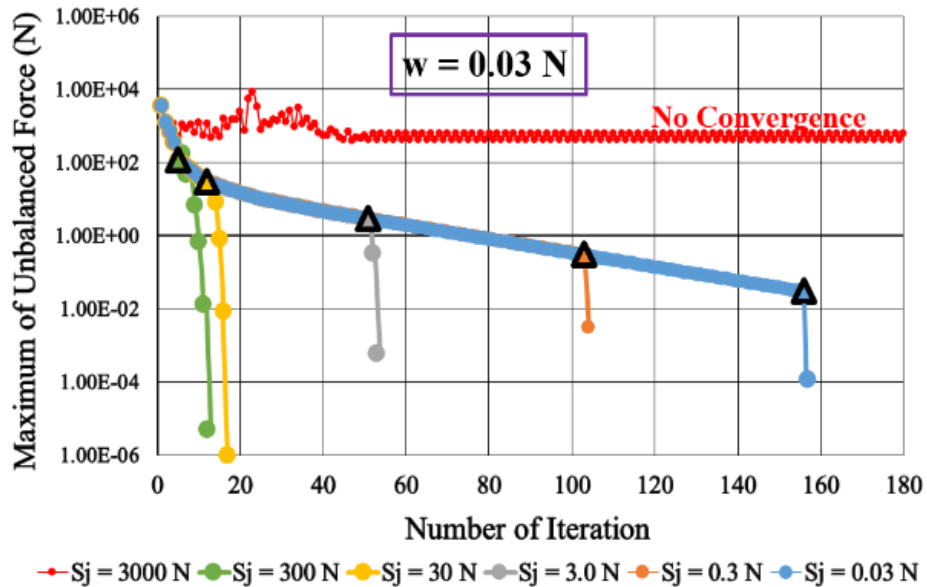
Figure 4.25 Convergence process for $w = 0.03$ N with switching

Aim of figure 4.24 is to verify the condition of self-weight w which requires the switching procedure of tangent by the comparison of convergent processes executed by "without" switching process. According to this, in case of less than w=0.01N, equilibrium solutions can be obtained without the switching, and it can be detected that the switching procedure is needed for the case w being bigger than 0.01N for this example model.

Figure 4.26 Convergence process for $w = 0.3$ N with switching

Figure 4.27 Convergence process for $w = 3.0$ N with switching

Next, the most efficient amount of S_j is examined when the switching is required. In figures 4.25, 4.26 and 4.27, the convergence processes with the switching procedure for w=0.03N (figure 4.23), w=0.3 N (figu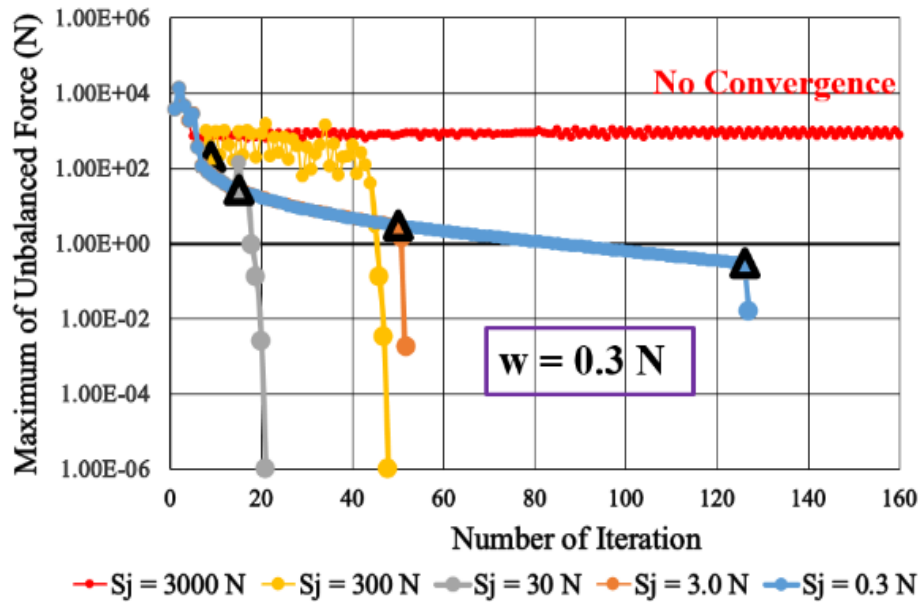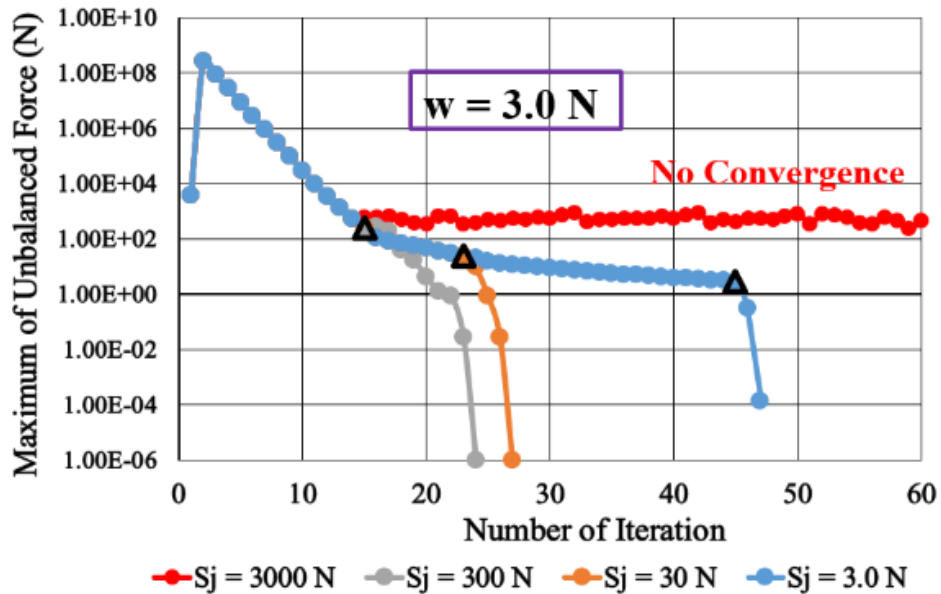re 4.26) and w=3.0N (figure 4.27) are shown. The black triangle in each figure indicates the switching level designated by S_j. During the process of the blue line (with dots), calculation is executed by fixed tangent, and its slope looks gentle. However after switching to the exact tangent with updating at each S_j, the unbalanced force converges suddenly and rapidly, except for not-converged case by "too large S_j settings" and for converged via vibration case of w=0.3 N with S_j =300 N. The setting of smaller amount S_j ensures convergence more, but it causes taking long time. It is ideal for S_j to be largest amount in the range of convergence.
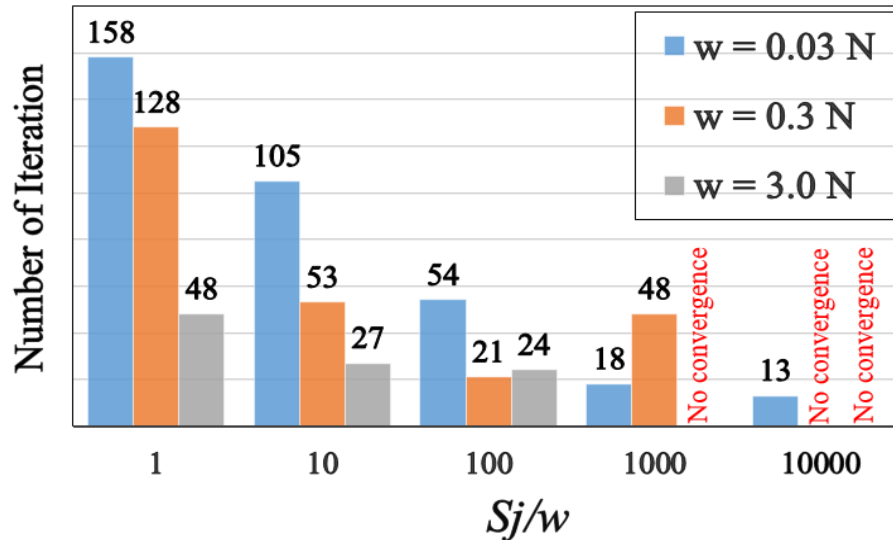
Figure 4.28 Comparison of switching performance at different w setting

Figure 4.28 shows the comparison of switching performance by the ratio of S_j/w. In this figure, it can be suggested that there is second order relationship between the number of iteration and the S_j/w. Therefore, it became evident that the rational calculation may be executed if the S_j/w has amount around 100.

4.10 Summary of chapter 4

From the first example model, it can be seen that the element force equation without relaxation results in the dome-like shape formation of the rubber net structure although it converges quickly. Among the three thresholds defined in the relaxation function, the threshold closer to 1.0 (λ_x = 1.0001) gives the slack rubber net structure with the smooth transition of large

deformational shape formation with the fewer iteration steps. In the second example model, the nonlinear analysis can also be conducted successfully by the application of the physical property values identified from the obtained stress value of uniaxial tension test. Moreover, the efficiency of switching tangent is verified and the appropriate switching level S_j is examined in order to improve the performance of convergence process of the unbalanced force. And there is a tendency to reduce the number of iteration steps with respect to the amount of designated S_j/w.

However, the obtained results are based on the proposed numerical example models and the coverage of the general statement has not been fully established yet. Nevertheless, the proposed method gives the high performance in conducting the large deformation and large displacement analysis with extremely strong nonlinearity such as hyper-elastic material structures by developing and incorporating the combined element force equations. Moreover, it contributes much information about the tendency of switching behavior of the computational algorithm and is expected to be applied as a base in more various aspects of future related studies.

List of Symbols

Symbol		Description
W	:	Strain energy function
B	:	Left Cauchy-Green deformation tensor
$\bar{I}_1, \bar{I}_2$	:	First and second invariant
C_1, C_2	:	Material constants
μ	:	Shear modulus
α	:	Material property value
λ_i	:	Principal stretch
λ_x	:	Arbitrarily determined stretch
λ	:	Obtained stretch in calculation
F	:	Nominal stress
a, b, c	:	Coefficients in square root function
N	:	Axial force
A_0	:	Primary cross-sectional area
l	:	Element length in current state
l_0	:	Element length in initial state
U_f	:	Current unbalanced force
S_j	:	Switching level
w	:	Self-weight load

References

[1] R. Rivlin, "Large Elastic Deformations of Isotropic Materials. I. Fundamental Concepts," *Journal of Mathematical, Physical and Engineering Sciences,* vol. 240, no. 822, pp. 459-490, January 1948.

[2] Q. Han, Z. Wang, C. Tang, L. Chen, C. Tsui and W. Law, "Hyper-elastic modeling and mechanical behavior investigation of porous poly-D-L-lactide/nano-hydroxyapatite scaffold material," *Journal of the Mechanical Behavior of Biomedical Materials,* vol. 71, pp. 262-270, July 2017.

[3] G. Saccomandi and L. Vergori, "Generalised Mooney–Rivlin models for brain tissue: A theoretical perspective," *International Journal of Non-linear Mechanics,* vol. 109, pp. 9-14, March 2019.

[4] S.Ramezani, R.Naghdabadi and S. Sohrabpour, "Constitutive equations for micropolar hyper-elastic materials," *International Journal of Solids and Structures,* vol. 46, no. 14-15, pp. 2765-2773, July 2009.

[5] Q. Zheng, "Theory of Representations for Tensor Functions—A Unified Invariant Approach to Constitutive Equations," *Journal of Applied Mechanics Reviews,* vol. 47, no. 11, pp. 545-587, November 1994.

[6] A. Damanpack, M. Bodaghi and W. Liao, "A robust hyper-elastic beam model under bi-axial normal-shear loadings," *International Journal of Non-linear Mechanics,* vol. 95, pp. 287-295, October 2017.

[7] J. Gwinner, "Non-linear elastic deformations," *Acta Applicandae Mathematica,* vol. 11, pp. 191-193, 1988.

[8] R. Rivlin, "Large Elastic Deformations of Isotropic Materials. II. Some Uniqueness Theorems for Pure, Homogeneous Deformation," *Journal of IASS,* vol. 240, no. 822, pp. 491-508, January 1948.

[9] R. Rivlin, "Stability of Pure Homogeneous Deformations of an Elastic Cube under Dead Loading," *QUARTERLY OF APPLIED MATHEMATICS,* pp. 398-404, October 1974.

[10] R. Ogden, "Local and global bifurcation phenomena in plane-strain finite elasticity," *International Journal of Solids and Structures,* vol. 21, no. 2, pp. 121-132, 1985.

[11] K. Lazopoulos and D. Bakogianni, "Singularities of homogeneous deformations of constrained hyper-elastic materials," *International Journal of Solids and Structures,* vol. 44, no. 11-12, pp. 3861-3874, June 2007.

[12] G. Uday and R. Bindu, "Computer simulation of hyper elastic re-treaded tire rubber with ABAQUS," *Materials Today: Proceedings,* vol. 43, no. 2, pp. 1992-2001, 2021.

[13] S. Kumar, B. Prasad and K. Kumar, "Effect of change of material model in Mooney Rivlin hyper-elastic material," *Materials Today: Proceedings,* vol. 26, no. 2, pp. 2511-2514, 2020.

[14] B. Fazekas and T. Goda, "New numerical stress solutions to calibrate hyper-visco-pseudo-elastic material models effectively," *Mateirals and Design,* vol. 194, p. 108861, September 2020.

[15] S. Peng, Y. Yang, J. Xiao and Y. Song, "Corneal hyper-viscoelastic model:," *Acta of Bioengineering and Biomechanics,* vol. 17, no. 2, pp. 73-84, 2015.

[16] H. Maedeh, R. Mohammad and G. Sevan, "Identification of hyper-viscoelastic material parameters of a soft member connected to another unidentified member by applying a dynamic load," *International Journal of Solids and Structures,* vol. 165, pp. 50-62, June 2019.

[17] C. Li and J. Lua, "A hyper-viscoelastic constitutive model for polyurea," *Materials Letters,* vol. 63, no. 11, pp. 877-880, April 2009.

[18] Y. Bai, C Liu, G. Huang, W. Li and S. Feng, "A Hyper-Viscoelastic Constitutive Model for Polyurea under Uniaxial Compressive Loading," *Journal of Polymers,* vol. 8, no. 4, 2016.

[19] D. Lin, D. Shreiber, E. Dimitriadis and F. Horkay, "Spherical indentation of soft matter beyond the Hertzian regime: numerical and experimental validation of hyperelastic models," *Biomech Model Mechanobiol,* vol. 8, no. 5, pp. 345-358, October 2009.

[20] E. Flores, S. Adhikari, M. Friswell and F. Scarpa, "Hyperelastic axial buckling of single wall carbon nanotubes," *Physica E: Low-dimensional Systems and Nanostructures,* vol. 44, no. 2, pp. 525-529, November 2011.

[21] M. Bodaghi, A. Damanpack, G. Hu and W. Liao, "Large deformations of soft metamaterials fabricated by 3D printing," *Materials and Design,* vol. 131, pp. 81-91, October 2017.

[22] A. Damanpack, M. Bodaghi and W. Liao, "Experimentally validated multi-scale modeling of 3D printed hyper-elastic lattices," *International Journal of Non-Linear Mechanics,* vol. 108, pp. 87-110, January 2019.

[23] T. Yamada, "Method of Nearby Problems for Large Deformation Analysis of Nearly Incompressible Hyperelasticity (in Japanese)," *Journal of JSCE, Ser A2, Applied Mechanics,* vol. 74, no. 2, pp. I_265-I_275, 2018.

[24] M. Tomioka, K. Ijima and H. Obiya, "Large deformation analysis of flexible membrane structures and the experiment," in *VII International Conference on Textile Compostes and Inflatable Structures, STRUCTURAL MEMBRANE 2015*, October, 2015.

[25] K. Kido, K. Ijima, H. Obiya and N. Kawasaki, "A method of replacing membrane structures by flexible cable elements and the large deformation analysis," in *roceeding of the International Association for Shell and Spatial Structres (IASS) Symposium 2010*, Shaghai, November, 2011.

[26] A. Ali, M. Hosseini and B. Sahari, "A Review of Constitutive Models for Rubber-Like Materials," *American Journal of Engineering and Applied Sciences,* vol. 3, no. 1, pp. 232-239, 2010.

[27] Y. Inukai, A. Kimura, F. Fuji and H. Noguchi , "Computatiional Techniques for Flexible and Incompressive Nets," *Journal of Structural Engiennering,* vol. 50, no. A, pp. 151-156, 2003.

[28] K. Ijima, H. Obiya and N. Kawasaki, "Large Displacement Analysis of Compression-free Membrane Structures Modeled by Elastic-catenary Cables," *Journal of Structural Engineering,* vol. 55, no. A, pp. 11-22, 2009.

[29] T. Sato, K. Ijima, H. Obiya and N. Kawasaki, "Large Displacement Analysis of Sagged Nets in Three-Dimensional Space," in *APCOM'07-EPMESC XI*, 2007.

[30] L. Treloar, "Stress-Strain Data for Vulcanized Rubber under Various Types of Deformation," *Transactions Faraday Society,* vol. 40, pp. 59-70, 1944.

[31] S. Ishikawa and T. Nagata, "Numerical Solution Methods for Elastomeric Damage Model," *Journal of the Society of Rubber Industry , Japan,* vol. 80, no. 2, pp. 41-45, 2007.

CHAPTER 5

Static Folding and Dynamic Deployment

5.1 Introduction

Tensegrity is one of the unique structures which possesses highly geometrical nonlinearity and can undergo large deformation under the proper treatment of external loading or compulsory displacement. Due to its high degree of transformational property, tensegrity is actively involved in the foldable and deployable structures such as in the fields of mechanical and aerospace applications.

For the folding and the deployment process of tensegrity, it is preferable to utilize flexible mechanism with self-equilibrium forces since the tensegrity structure can be stable without additional restraint [1]. Generally, strut-based actuation is found to be difficult to achieve if the internal forces are substantial. Moreover, when the strut-actuation is applied in deployment process, the structure may have no stiffness until it reaches the full stage of deployment [131]. On the other hand, the investigation of the cable-based actuation can be found in many literatures related to the active and deployable structures. Pinaud et al. modeled a small-scaled tensegrity boom and investigated the asymmetrical configurations under the deployment by controlling the tendon [3]. The application of the cable-control mechanism is also found in the vibrational damping of tensegrity structure [4] and the shape control of tensegrity prism [5]. Bouderbala and Motro processed the folding strategy of the octahedron tensegrity and showed that the strut-controlling is more complicated than the cable-controlling [6].

The ordinary nonlinear differential equations were applied in the literatures of Sultan and Skelton to develop a dynamic model during the deployment process of tensegrity structure [7]. Sultan made some investigations for the deployment phenomenon of tensegrities with the introduction of exploiting the infinitesimal mechanism by nonlinear dynamic equations [8]. Shu Yang and Sultan proposed an energy-based approach to deploy the foldable tensegrity-membrane structure and determine the equilibrium system [9].

Recently, tensegrity is actively applied not only in the dynamic analyses but also in the earthquake-proof structures. Fraternali and Santos developed a mechanical model in which the super-elastic tensegrity braces are reinforced as seismic-resistant structure [10]. Masic and Skelton

conducted the dynamic control performance and optimized the prestress of a tensegrity structure by using the linearized dynamic model [11]. Kanchanasaratool and Williamson introduced a dynamic model for a general class of tensegrity structures with an approach of a nonlinear constrained particle method [12] . With an experimental study, Chan et al. performed an active vibration control of a triple-layered tensegrity structure in which the active damping is controlled by the force and acceleration feedback [13]. Later, Ali and Smith proposed vibration control system for a full-scale active tensegrity structure by modifying the self-stress which influences the dynamic behavior [14], [15].

Since tensegrity is composed of struts in the network of cables, it is highly flexible in the shape transition or shape deformation. This property is useful when the structure is kept in a compact form and let it deploy when necessary. Therefore, this chapter will discuss the folding process of a tensegrity structure and thereafter, bringing the folded tensegrity back to its original configuration. The process of folding is carried out by three steps: giving constraints to designated points, calculating the proper amount of forced displacement or compulsory displacement and applying it on the control points of the structural model. Since the folding procedure is implemented by the static analysis, the shape transition of equilibrium solution is governed by the balanced equation between the nodal force vector (in general coordinate) and element edge force vector (in local coordinate).

After obtaining the perfectly folded tensegrity, it will undergo the deployment process. The constrained nodes are released again, and the launch load is applied to initiate vibration in the folded tensegrity model. The introduction of launch load causes the oscillatory mechanism during deploying and it will be examined by the dynamic analysis. The simulation of dynamic deployment will be approached by the time integration method which will evaluates the dynamic response of a structure under a given loading that varies over a specified time function. The effect of vibration caused by the kinematic energy will be reduced by the damping coefficients. Rayleigh damping model will be applied in order to design the appropriate amount of damping coefficients. The mode decomposition is achieved by the Eigen value analysis to calculate the required mechanical values of Rayleigh model. In this study, the static folding and dynamic deployment will be explained by the consistent algorithm in which the same proposed tensegrity model is used in order to demonstrate the whole tensegrity simulation, including the form-finding process.
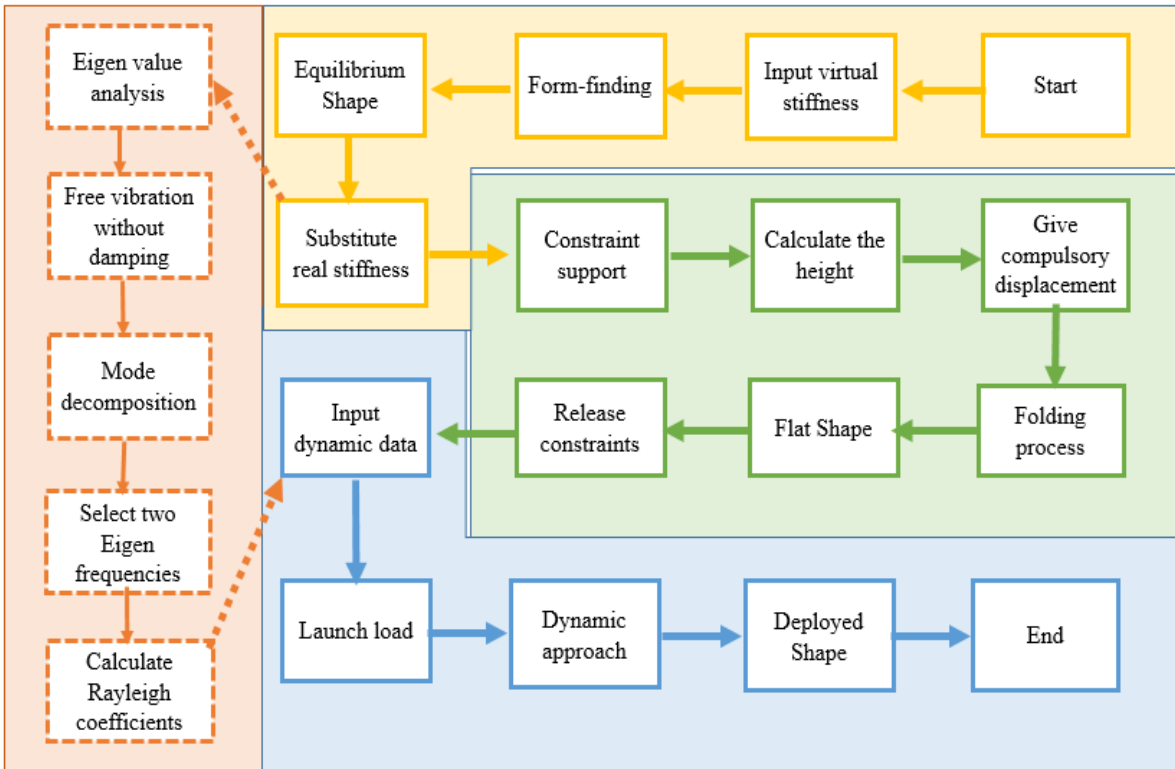
87

5.2 Consistent algorithm

Figure 5.1 Consistent algorithm

The proposed consistent algorithm includes four main parts. The first part illustrated in yellow color is form-finding process using the virtual elements of measure potential. After the equilibrium shape is determined, each member is substituted by the real elements such as aluminum for strut and rubber material for the cable. In the second part shaded in orange color, the self-equilibrated tensegrity having the real stiffness undergoes the free vibration simulation. The Eigen value analysis is carried out and its displacement modes are examined to calculate the damping coefficients. The third part shown in green color is folding process in which the proposed model is perfectly folded by the compulsory displacement. The folded tensegrity retains its original configuration by the deployment process as shown in the final part of blue color. This is accompanied by the dynamic simulation in which the tensegrity structure makes its full-scale deployment and the reduction of kinematic energy in its oscillatory mechanism is achieved by giving the appropriate amount of damping.

5.3 Finding an equilibrium configuration

Starting from the unbalanced form of two-layered pentagonal tensegrity structure (the same model of Chapter 3), the shape analysis is carried out by the power function of measure potential $N = C (l - l_0)^n$ in which the coefficients for strut members are designated as ($C_s = 2 \times 10^9$, $n_s = 1$, $l_{0s} = 7.0$) and the coefficients for cable members are assigned as ($C_c = 0.8$, $n_c = 5$, $l_{0c} = 0$). The coefficients used in the form-finding are user-defined and therefore, can be assumed as virtual.

The connectivity of members and the designated support condition are selected appropriately and the rotational conversion of members are calculated properly so that the obtained equilibrium solution figure 5.2(b) will be almost the same as the primary unbalanced form figure 5.2(a). The resulted tensegrity is three-dimensional configuration in self-equilibrated and stable condition in which the brown color refers to the compression force carried by the strut and the red color illustrates the tensile force suffered in the cables.

However, the shape formation derived by the form-finding keeps its equilibrium state by the tension or compression element forces provided by the virtual stiffness. Therefore, by using the Newton-Raphson method, the actual non-stressed length of each member is re-calculated depending on the amount of element edge forces which governs the shape formation of equilibrium solution.

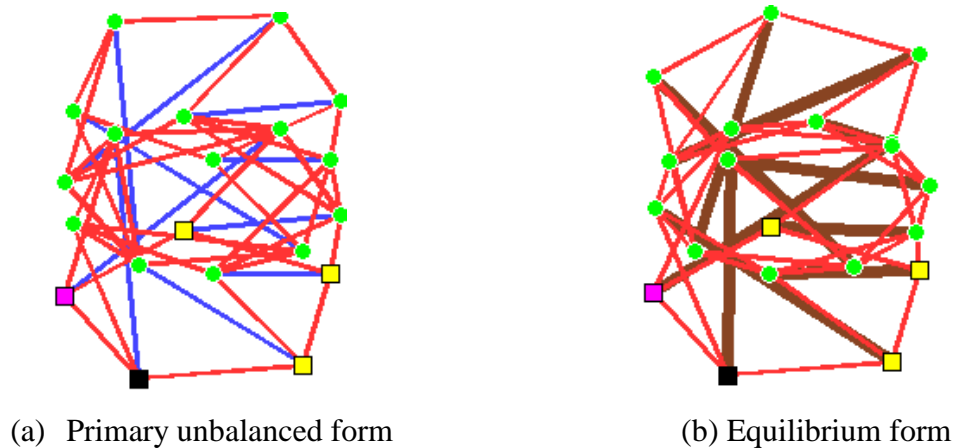(a) Primary unbalanced form   (b) Equilibrium form

Figure 5.2 Finding equilibrium solution by shape analysis

After the derivation of actual non-stressed length, each and every member of the whole tensegrity structure is substituted by the real material stiffness. Since one of the unique

characteristics of tensegrity is "being lightweight", the main supporting stiffer elements (strut) are designed to have material stiffness of aluminum with Young's modulus of 68 GPa and cross-sectional area of 0.01 m^2. Meanwhile, the cable member is substituted by the rubber elements having cross-sectional area of 0.003 m^2 whose mechanical values are characterized by the experimental result of uniaxial test using the Ogden model (the detail procedure has been discussed in the previous chapter).

5.4 Fundamental concept of dynamic analysis

In the static analysis, the consideration of equilibrium equation is based on the stiffness matrix between the nodal force vector and the displacement vector. Meanwhile, when the structure is in the oscillatory system, the equation of motion is considered to prescribe its dynamic behavior. In general, the equation of motion can be expressed as;

$$\mathbf{M\ddot{u} + C\dot{u} + K\Delta u = B} \tag{5.1}$$

Where, $\mathbf{M}$: mass matrix $\mathbf{\ddot{u}}$: acceleration

$\mathbf{C}$: damping matrix $\mathbf{\dot{u}}$: velocity

$\mathbf{K}$: stiffness matrix $\mathbf{\Delta u}$: displacement

$\mathbf{B}$: External force vector

In the case of free vibration without damping, only the mass matrix and stiffness matrix are considered in calculation since the damping matrix will become zero. Therefore, free vibrational movement of the structure can be fully observed and decomposed into mode displacement by means of Eigen value analysis. The stiffness matrix has been prepared in the previous analysis and is adjusted according to dynamic analysis. The derivation of mass matrix, Eigen value analysis and damping coefficients will be presented in the following sections.

5.5 Derivation of mass matrix for truss element

In general, there are two ways to form the mass matrix of a structure. One is direct mass lumping which produces diagonal lumped mass matrix in which the cross coupling is ignored and the size of total mass elements is directly proportional to the total number of freedom of nodes. And the other is variation mass lumping which construct the consistent mass matrix. Recently,

template mass lumping is introduced which gives a generalized formulation for both of the previous methods. Consistent mass matrix has fully-distributed entries whereas lumped mass matrix is composed of only diagonal entries. Since the strut member of tensegrity is considered as truss element, the consistent mass matrix can be derived as follow.

Assume that the displacement distribution in the element by the polynomial interpolation function using the node displacement as in figure 5.3.
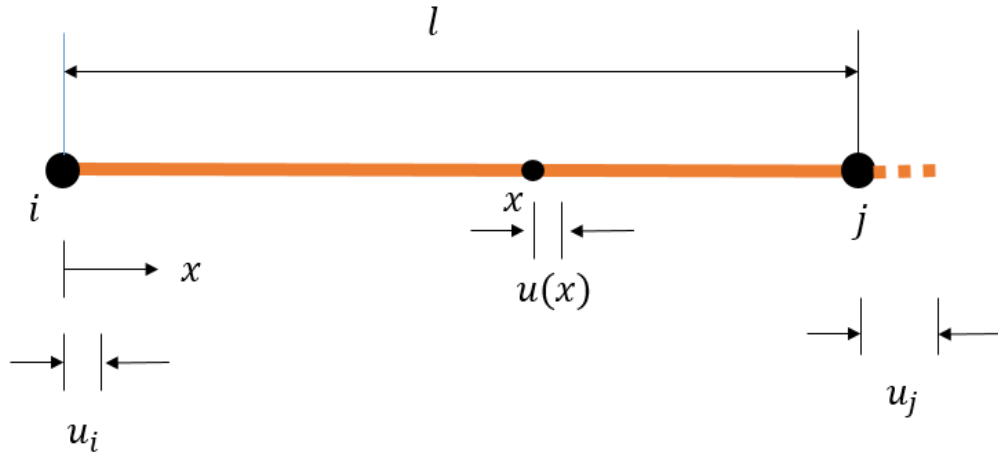

Figure 5.3 Displacement distribution in truss element

The displacement u at point x in the element can be derived by using the relation of nodal displacement $[\mathbf{d}]^{\mathrm{T}} = [u_i, u_j]^{\mathrm{T}}$ as below.

$$u(x) = \left(1 - \frac{x}{l}\right) u_i + \frac{x}{l} u_j = \begin{bmatrix} 1 - \frac{x}{l} & \frac{x}{l} \end{bmatrix} \begin{bmatrix} u_i \\ u_j \end{bmatrix} = \mathbf{s}^{\mathrm{T}} \mathbf{d}^{\mathrm{T}} \tag{5.2}$$

The kinematic energy T can be obtained from the displacement distribution represented by the nodal displacement as in equation (5.3).

$$T = \frac{1}{2} \int_0^l \dot{\mathbf{u}}(\mathbf{x}) \rho \dot{\mathbf{u}}(\mathbf{x}) \, dx \tag{5.3}$$

$$= \begin{bmatrix} \dot{u}_i & \dot{u}_j \end{bmatrix} \frac{\rho l}{6} \begin{bmatrix} 2 & 1 \\ 1 & 2 \end{bmatrix} \begin{bmatrix} u_i \\ u_j \end{bmatrix}$$

Here, A is the cross-sectional area defined by the following equation.

$$A = \iint dydz \tag{5.4}$$

Therefore, the element mass matrix of one truss element is given by the following equation.

$$\mathbf{m_e} = \frac{\rho l}{6}\begin{bmatrix} 2 & 1 \\ 1 & 2 \end{bmatrix} \tag{5.5}$$

where γ is the specific gravity, g is the gravitational acceleration and l is the length of element. Since the element's mass matrix is formed in local coordinate, it is then generalized into global coordinate system by transformation matrix.

5.6 Eigen value analysis

5.6.1 Fundamental concept of Eigen value analysis

The Eigen value analysis is the method which finds out the vibrational characteristics of the structure, including the Eigen frequencies and Eigen modes. In the Eigen value analysis, there is no input load since it needs only the vibrational characteristic to conduct the analysis. Therefore, the amount of the whole displacement cannot be checked although the Eigen displacement modes can be seen as a result of analysis. The relative position of the nodes can be evaluated to represent the displacement. However, the amount of displacement that the structure is moved out cannot be described. Since the excessive amount of damping can affect in Eigen frequency, the Eigen mode and Eigen frequency are normally specified without consideration of attenuation in the ordinary Eigen value analysis.

5.6.2 Introduction of fundamental equations

In this section, some of the basic equations for Eigen value analysis will be introduced and the result of Eigen value analysis will be used in the conversion to a mode coordinate system.

In the Eigen value analysis, a free vibration state with no damping and no given load is assumed for the basic equation of dynamic analysis. This can be expressed in the following equation.

$$\mathbf{M\ddot{u} + Ku = 0} \tag{5.6}$$

Since the solution **x** is a simple harmonic vibration, it can be set as follow.

$$\mathbf{u} = \mathbf{\phi}e^{i\omega t} \tag{5.7}$$

where, $\mathbf{\phi}$:   Overall displacement vector

i :   Imaginary unit

ω :   Circular frequency

t :   Time

Consequently, the first and second derivative of u can be derived as below.

$$\dot{\mathbf{u}} = i\omega\mathbf{\phi}e^{i\omega t} \tag{5.8}$$

$$\ddot{\mathbf{u}} = -\omega^2\mathbf{\phi}e^{i\omega t} \tag{5.9}$$

Substituting equation (5.8) and (5.9) into equation (5.6),

$$-\omega^2\mathbf{\phi}e^{i\omega t}.\mathbf{M} + \mathbf{\phi}e^{i\omega t}.\mathbf{K} = 0 \tag{5.10}$$

After simplifying,

$$[\omega^2.\mathbf{M} - \mathbf{K}]\mathbf{\phi} = 0 \tag{5.11}$$

Here, ω^2 is the Eigen value and $\mathbf{\phi}$ is the Eigen vector, and Eigen value analysis is to find these values that are related to the number of degree of freedom. If the mass matrix **M** or stiffness matrix **K** has $n \times n$ entries, then there will be n Eigen values and Eigen vectors, respectively.

5.6.3 Eigen value analysis by Jacobi method

When the coordinate values (x, y) and ($\bar{x}$, $\bar{y}$) in the global Cartesian coordinate system represent the same point in relation between (x, y) and ($\bar{x}$, $\bar{y}$) can be expressed in equation (5.12).

$$\begin{bmatrix} \bar{x} \\ \bar{y} \end{bmatrix} = \begin{bmatrix} cos\theta & -sin\theta \\ sin\theta & cos\theta \end{bmatrix} \begin{bmatrix} x \\ y \end{bmatrix} \tag{5.12}$$

Here, the coordinate system ($\bar{x}$, $\bar{y}$) is obtained by rotating the coordinate system of (x, y) by the angle θ.

The conversion matrix of equation (5.12) is called an orthogonal matrix, and therefore the rotational matrix $\mathbf{R}$ can be expressed as in equation (5.13) and (5.14).

$$\mathbf{R^T} = \mathbf{R^{-1}} = \begin{bmatrix} cos\theta & sin\theta \\ -sin\theta & cos\theta \end{bmatrix} \tag{5.13}$$

$$\mathbf{R} = \begin{bmatrix} cos\theta & -sin\theta \\ sin\theta & cos\theta \end{bmatrix} \tag{5.14}$$

in which $\theta = \dfrac{\pi}{4}$ in general.

The above calculation will be performed for all the non-diagonal entries. When the non-diagonal term that has become zero once makes the other non-diagonal terms zero, it becomes non-zero in turn. However, the value of $sin\theta$ and $cos\theta$ will be less than 1 by multiplying the conversion matrix for multiple times, making the non-diagonal terms approach to zero gradually.

By multiplying the conversion matrix $\mathbf{R^T}, \mathbf{R}$ to before and after of square matrix for n number of times, the non-diagonal terms will become less than the permissible value and it can be expressed as follow.

$$\mathbf{R_n^T} . \mathbf{R_{n-1}^T} \ldots \mathbf{R_2^T} . \mathbf{R_1^T} . \mathbf{M^{-1}K} . \mathbf{R_1} . \mathbf{R_2} \ldots \mathbf{R_{n-1}} . \mathbf{R_n} = \mathbf{I\Lambda} \tag{5.15}$$

where, $\mathbf{I}$ is the unit matrix with size of $(n \times n)$ and $\mathbf{\Lambda}$ is a diagonal matrix in which its diagonal entries are the Eigen values.

Equation (5.16) can be derived by multiplying $\mathbf{R_n} . \mathbf{R_{n-1}} \ldots \mathbf{R_2} . \mathbf{R_1}$ in front of equation (5.15) for both sides.

$$\mathbf{M^{-1}K} . \mathbf{R_1} . \mathbf{R_2} \ldots \mathbf{R_{n-1}} . \mathbf{R_n} = \mathbf{R_1} . \mathbf{R_2} \ldots \mathbf{R_{n-1}} . \mathbf{R_n} . \mathbf{\Lambda} \tag{5.16}$$

If the series of rotational matrix is described as below,

$$\mathbf{R_1} . \mathbf{R_2} \ldots \mathbf{R_{n-1}} . \mathbf{R_n} = \mathbf{X} \tag{5.17}$$

In a normal Eigen value analysis, $\mathbf{X}$ can be defined as the matrix composed of Eigen vectors and $\mathbf{\Lambda}$ is the matrix composed of Eigen values, and can be expressed as in equation (5.18) and (5.19).

$$\mathbf{X} = [\mathbf{x_1}, \quad \mathbf{x_2}, \ldots, \mathbf{x_n}] \tag{5.18}$$

$$\Lambda = \begin{bmatrix} \lambda_1 & \cdots & \cdots & 0 \\ \vdots & \lambda_2 & & \vdots \\ \vdots & & \ddots & \vdots \\ 0 & \cdots & \cdots & \lambda_n \end{bmatrix} \qquad (5.19)$$

Using equation (5.18) and equation (5.19), the calculation of Eigen value analysis for the target matrix $\mathbf{M^{-1}K}$ using Jacobi method can be expressed as in equation (5.20).

$$\mathbf{M^{-1}K.X = X.\Lambda} = [\lambda_1\, \mathbf{x_1}, \lambda_2\, \mathbf{x_2}, \dots , \lambda_n \mathbf{x_n}] \qquad (5.20)$$

5.7 Preparation for damping matrix

5.7.1 Damping coefficient and damping ratio

Damping coefficient is the property of material that reduces or prevents the oscillation of the structure. If a structure has relatively high damping coefficient, its energy absorption property will reduce the undesired response to some extent when the structure undergoes a vibration or shock. In dynamic loading conditions, the damping materials play an important role such as in shock absorption, noise reduction, vibration control in structural and mechanical engineering.

Damping ratio is a dimensionless measure to describe the dissipation of oscillation in a system when a disturbance force or loading is given. The oscillatory behavior can be observed when a system is disturbed from its static equilibrium condition. The damping ratio (ζ) can be described by a mathematical expression in which the actual damping of material (c_0) is relative to critical damping (c_c).

$$\zeta = \frac{c_0}{c_c} \qquad (5.21)$$

5.7.2 Derivation of Rayleigh damping coefficients

The mechanism of damping coefficient derivation may be complicated compared to the stiffness and mass matrixes, and many theories to construct the damping matrix are proposed. Rayleigh damping model is one of the commonly used methods since it is a linear combination of mass and stiffness matrixes. Damping matrix in the dynamic equation can be expressed by two terms, named Rayleigh damping coefficients. These can be determined by the orthogonality of damping matrix for a mode shape. With the appropriate treatment of Rayleigh damping coefficients, the result of dynamic analysis of multi-degree of freedom system can be taken as the

same as the experimental data. Rayleigh coefficients can be computed from damping matrix $\mathbf{C}$ of following equation.

$$\mathbf{C} = \alpha\mathbf{M} + \beta\mathbf{K} \tag{5.22}$$

where α is proportional to mass matrix $\mathbf{M}$ and β is proportional to stiffness matrix $\mathbf{K}$.

When the structure is in free vibration without external force, the critical damping (c_c) can be formulated as $c_c = 2\sqrt{mk}$ from the relation of natural frequency $\omega_0 = c_c/2m$. Assuming that the actual damping (c_0) can have any value, then the damping ratio ζ can be rewritten as follow.

$$\zeta = \frac{c_0}{c_c} = \frac{1}{2\sqrt{mk}}(\alpha\mathbf{m} + \beta\mathbf{k}) = \frac{1}{2}\left(\sqrt{\frac{\mathbf{m}}{\mathbf{k}}}.\alpha + \sqrt{\frac{\mathbf{k}}{\mathbf{m}}}.\beta\right) \tag{5.23}$$

And when the equation (5.23) is expressed in term of frequency ω.

$$\zeta = \frac{1}{2}\left(\frac{\alpha}{\omega}\right) + \beta\omega \tag{5.24}$$

In the case of underdamped where vibration is occurred, the damping ratio is in the range of $0 \leq \zeta < 1$.

To calculate the Rayleigh coefficients, two reference vibration modes and two Eigen frequencies are specified from the total n-degree of freedom in the order of i and j, as in equation (5.25) and (5.26).

$$\zeta_i = \frac{1}{2}\left(\frac{\alpha}{\omega_i}\right) + \beta\omega_i \tag{5.25}$$

$$\zeta_j = \frac{1}{2}\left(\frac{\alpha}{\omega_j}\right) + \beta\omega_j \tag{5.26}$$

Solving the above equations, α and β can be collected as below.

$$\alpha = \frac{2\omega_i\omega_j.(\zeta_i.\omega_j - \zeta_j.\omega_i)}{\omega_j^2 - \omega_i^2} \tag{5.27}$$

$$\beta = \frac{2.(\zeta_j.\omega_j - \zeta_i.\omega_i)}{\omega_j^2 - \omega_i^2} \tag{5.28}$$

If the two damping ratios are assumed to have the same value, then α and β can be simplified as;

$$\alpha = \frac{2\omega_i\omega_j\zeta}{\omega_i+\omega_j} \tag{5.29}$$

$$\beta = \frac{2\zeta}{\omega_i+\omega_j} \tag{5.30}$$

5.7.3 Mode decomposition

When a structure is in oscillation under damping, the damping matrix is needed to be considered in the equation of motion. However, the amount of damping is quite difficult to measure in practical compared to that of mass or stiffness of the structure. On the other hand, it is possible to characterize the damping effect either based on the experience of user-defined values or by applying the appropriate formularization in the dynamic theory. This can be achieved by determining the appropriate amount of Rayleigh damping coefficients. In order to calculate Rayleigh coefficients, the required Eigen frequencies can be obtained by analyzing mode decomposition of the structural displacement. Eigen values for each mode can be derived by the Eigen value analysis from free vibration system before determining the damping effect.

The equilibrium model shown in figure 5.2 (b) undergo the free vibration for given time lap of 3 seconds and its total energy is conserved until around 0.7 second as in figure 5.4. In the tensegrity system, one free node has 3-degree-of-freedom, and the proposed model has total 20 nodes. However, the base nodes of model are given by 8 constraints so that total 52-degree-of-freedom will be obtained in the free vibration mechanism. Total 52 Eigen values and corresponding Eigen vectors are obtained by Jacobi method as in table 5.1. Investigating the mode displacement pattern of figure 5.5, the 3rd and 20th modes are selected as two Eigen frequencies to calculate the Rayleigh coefficients since these two modes demonstrate the relatively significant displacement among the total mode patterns. Meanwhile, the damping ratio is assigned to have the same value of 0.2 and the corresponding α and β can be calculated by equation (5.29) and (5.30).
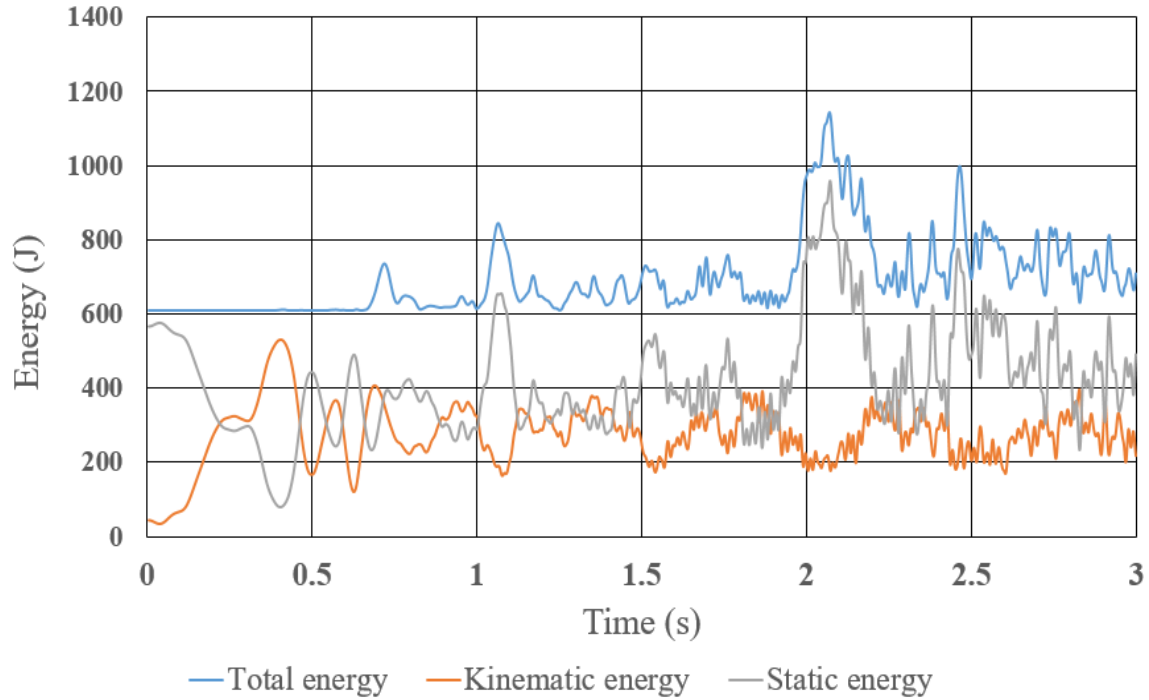
Figure 5.4 Energy distribution by free vibration

Table 5.1 Result of Eigen value analysis

| Mode	Eigenvalue	Mode	Eigenvalue	Mode	Eigenvalue	Mode	Eigenvalue
1	1.24E+01	14	1.97E+03	27	1.17E+04	40	5.17E+04
2	1.26E+01	15	1.99E+03	28	1.22E+04	41	5.23E+04
3	1.82E+01	16	2.14E+03	29	1.31E+04	42	5.25E+04
4	5.08E+01	17	2.79E+03	30	1.52E+04	43	8.20E+08
5	1.22E+02	18	4.13E+03	31	1.85E+04	44	8.37E+08
6	1.61E+02	19	4.81E+03	32	1.99E+04	45	1.50E+09
7	2.10E+02	20	5.32E+03	33	2.06E+04	46	1.50E+09
8	2.15E+02	21	6.44E+03	34	2.27E+04	47	1.50E+09
9	3.26E+02	22	6.55E+03	35	2.32E+04	48	1.68E+09
10	5.40E+02	23	6.62E+03	36	3.72E+04	49	1.68E+09
11	6.86E+02	24	7.85E+03	37	4.01E+04	50	1.68E+09
12	1.00E+03	25	8.88E+03	38	4.94E+04	51	1.68E+09
13	1.60E+03	26	1.00E+04	39	5.06E+04	52	1.68E+09
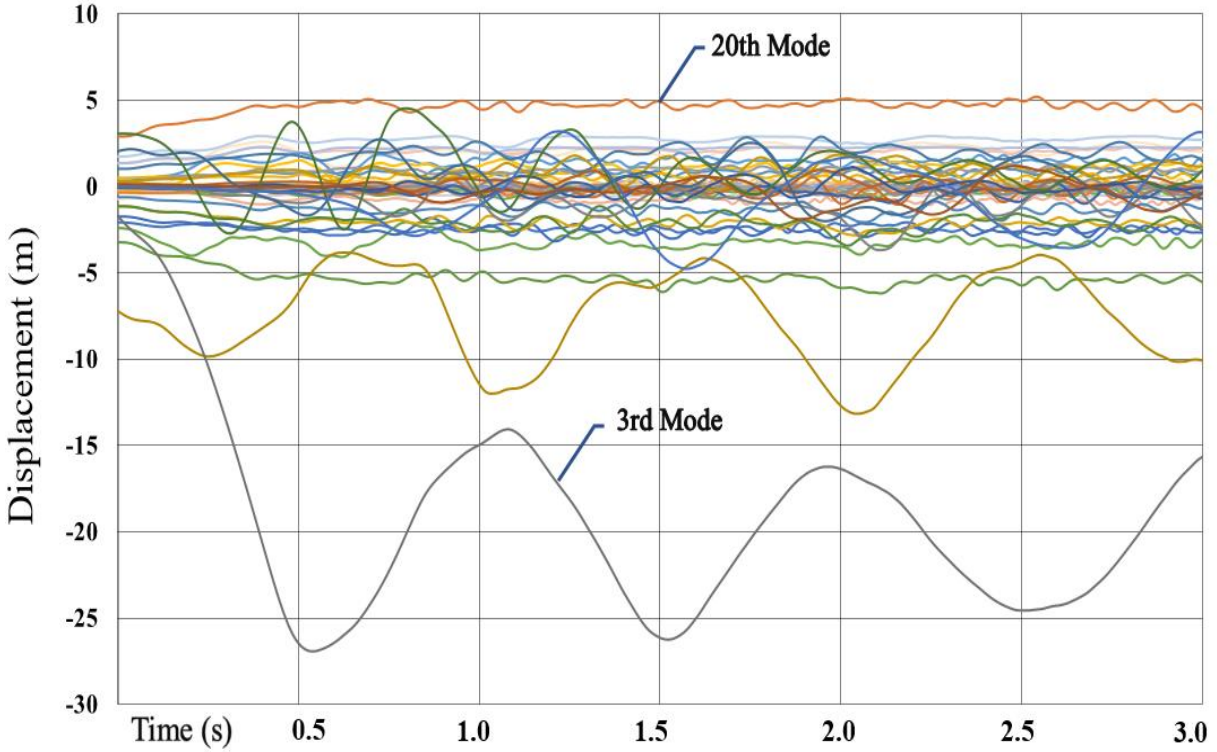
Figure 5.5 Result of mode decomposition

5.8 Folding process with compulsory displacement

The equilibrium solution of figure 5.2 (b) is taken as a base model for the folding process. And, all the free nodes (green color) in the middle and top layer of tensegrity model are given as constrained points (yellow color) as in figure 5.6.
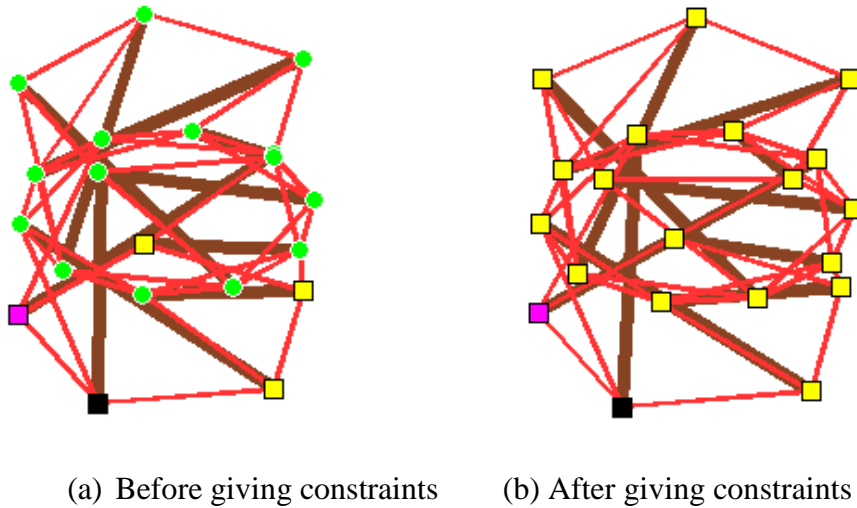

(a) Before giving constraints   (b) After giving constraints
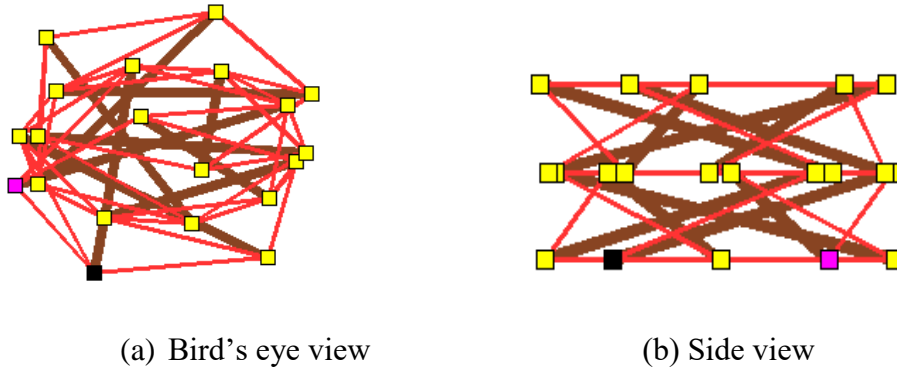
Figure 5.6 Assignment of constrained nodes

(a) Bird's eye view   (b) Side view

Figure 5.7 Folding tensegrity model at step 3

(a) Bird's eye view   (b) Side view
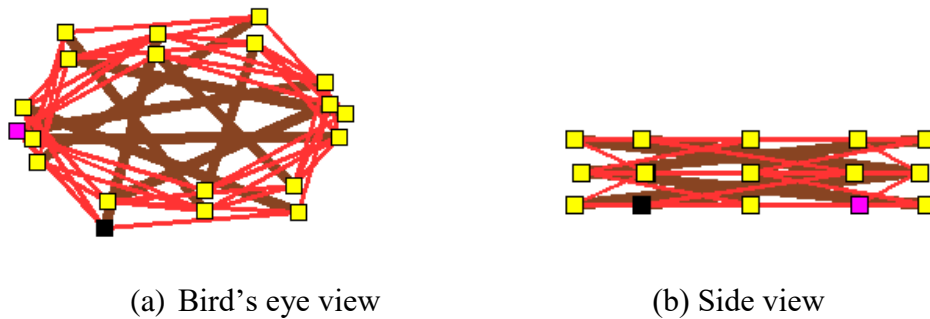
Figure 5.8 Folding tensegrity model at step 7

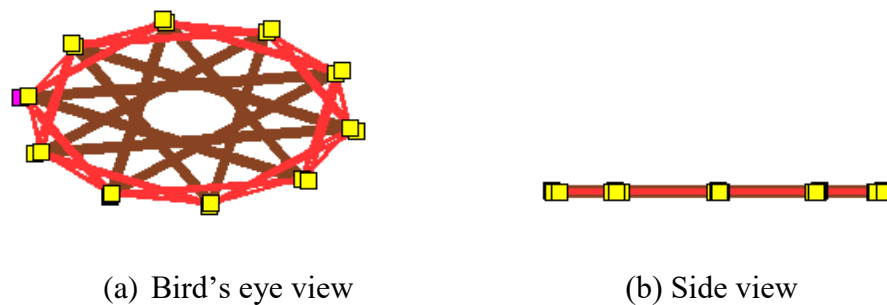(a) Bird's eye view   (b) Side view

Figure 5.9 Folding tensegrity model at step 10

The height of equilibrium model is checked and the number of steps for folding is designated to determine the appropriate displacement to be given. The lowest nodes are the base points so that no compulsory displacement is needed. For the topmost nodes, the full amount of compulsory displacement is given and for the layer-connecting middle nodes, half amount of designated displacement is enough to proceed the folding process. In this way, the process of

folding the tensegrity model is successfully achieved in all cases of strut and cable material combination without the requirement of any complicated calculation. The resulted solution is a perfectly folded two-dimensional equilibrium configuration. Figure 5.7 to 5.9 show the illustrations of (a) bird's eye view and (b) side view of folding model gradually at step 3, step 7 and the final step 10.

5.9 Deployment by dynamic approach

After the folding process of tensegrity by the compulsory displacement, the given constrained nodes will be released as in figure 5.10. Deploying into its original self-equilibrium configuration will be established by the performance of dynamic approach. In this time, the damping effect will be taken into account in which the value of Rayleigh coefficients and other required dynamic data are specified as shown in table 5.2.
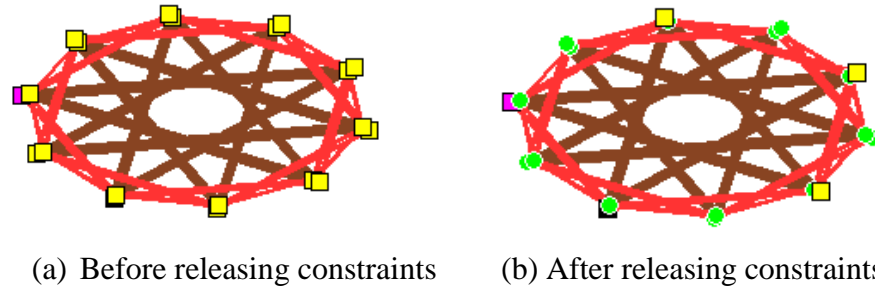

| (a) Before releasing constraints | (b) After releasing constraints |

Figure 5.10 Releasing constrained nodes

Table 5.2 Specification of dynamic data

▪ **Member**	❖ **Damping coefficients**	➢ **Time specification**
▪ Strut >> Aluminum Specific gravity = 2.7	❖ Attenuation to mass α=1.612	➢ Time increment Δt=0.001 sec
▪ Cable >> Rubber Specific gravity = 1	❖ Attenuation to stiffness β=0.0052	➢ Time limitation t=8 sec

5.9.1 Procedure of dynamic analysis

In the final part of consistent algorithm, the deployment of folded tensegrity will be performed by dynamic analysis. Figure 5.11 demonstrates the general flow of dynamic procedure adopted in this study. The specified launch load is applied to all the free nodes of middle and top layer of folded tensegrity in order to initiate the vibration. In this process, the free nodes of tensegrity model will undergo the oscillatory mechanism in which the multi-degree-of-freedom will be realized in this system.

Since the deployment process of proposed tensegrity will be implemented by the dynamic analysis involving large displacement, the performance of the nonlinear dynamic calculations is based on time integration method. The time integration method evaluates the dynamic response of a structure under a given loading that may vary over a specified time function. Time integration method is a behavioral study of a structure in which the amplitude or acceleration of the structure is calculated for each time increment. This practice may require more calculation time, but produce the precise and accurate results.

Let the acceleration, velocity and displacement under the loading of $\mathbf{P_i}$ at the current time t_i as $\mathbf{\ddot{u}_i}$, $\mathbf{\dot{u}_i}$ and $\mathbf{u_i}$, respectively which are "known values", then equation of motion at current state can be rewritten in the scalar form as equation (5.31).

$$\mathbf{m\ddot{u}_i + c\,\dot{u}_i + ku_i = P_i} \tag{5.31}$$

Then, the change in structural response after the time increment Δt can be expressed as follow.

$$\mathbf{m\ddot{u}_{i+1} + c\,\dot{u}_{i+1} + ku_{i+1} = P_{i+1}} \tag{5.32}$$

The "unknown values" of mechanical values at consecutive time step t_{i+1} can be obtained by several numerical methods. In this study, Newmark β method is adopted which is one of the most efficient methods in the time integration algorithm. This implicit method calculates the mechanical quantities of next time step based on the current condition and the resulted solutions will be renewed into the consecutive step. This iteration process will be repeated over the specified time function and terminated when the time increment reaches the limited time interval, and output the mechanical quantities. The numerical derivation of Newmark β method will be presented in the next section.
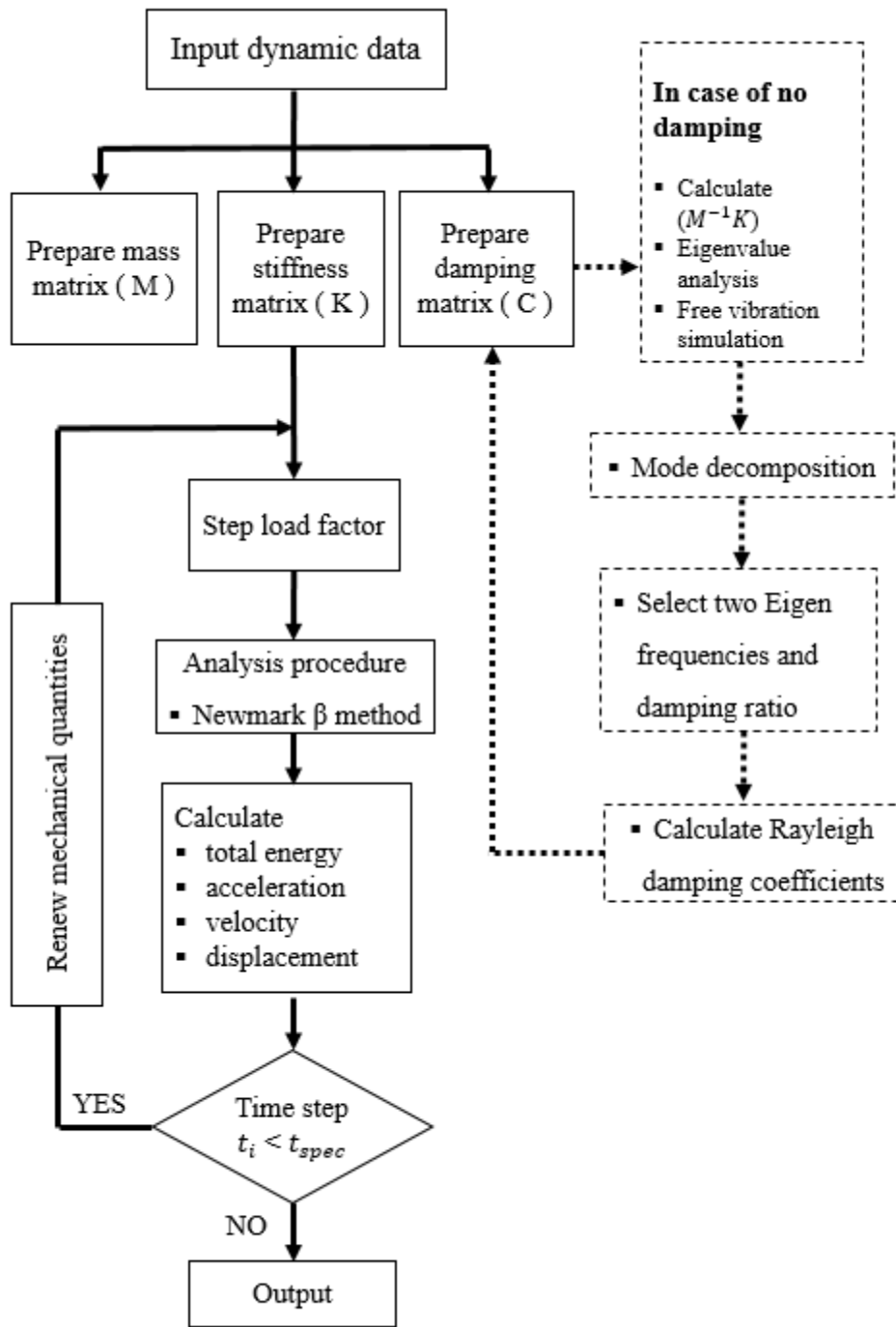
Figure 5.11 Flow chart of dynamic procedure

5.9.2 Newmark $\beta = 1/4$ method

In nonlinear function of structural design, the dynamic performance must be modified accordingly. A solution of the equation of motion for a multi-degree-of-freedom system is usually impossible if the amplitude of nonlinear oscillatory system varies arbitrarily with time function. Such problems can be solved by numerical time-stepping methods for integration of differential equations.

Newmark β method, introduced by N.M. Newmark in 1959 for structural dynamics, is based on the following equations.

$$\dot{u}_{i+1} = \dot{u}_i + (1-\gamma)\Delta t.\ddot{u}_i + \gamma\Delta t.\ddot{u}_{i+1} \tag{5.33}$$

$$u_{i+1} = u_i + \Delta t.\dot{u}_i + \left(\frac{1}{2}-\beta\right)\Delta t^2.\ddot{u}_i + \beta\Delta t^2.\ddot{u}_{i+1} \tag{5.34}$$

The parameters γ and β define the rate of change in acceleration over a time increment which governs the stability and accuracy of the method.

In the average constant acceleration approach, the setting of $\gamma = 1/2$ and $\beta = 1/4$ is used to determine the dynamic response of nonlinear structure.

The conceptual model of Newmark $\beta = 1/4$ method is as in figure 5.12.
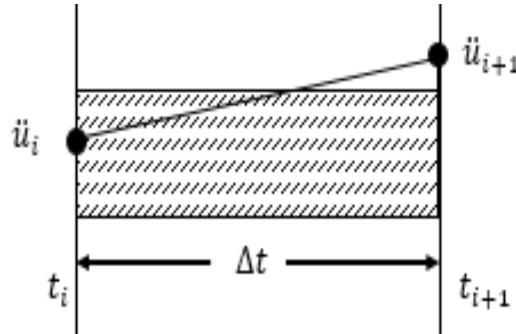

Figure 5.12 Concept of Newmark $\beta = 1/4$ method

Here, the acceleration is assumed to be constant during the time increment and therefore, the average value between two accelerations at time t_i and t_{i+1} is calculated as below.

$$\ddot{u} = \frac{1}{2}(\ddot{u}_i + \ddot{u}_{i+1}) \tag{5.35}$$

Consequently, the related velocity and displacement of next time step can be derived by the following differential equations.

$$\dot{u}_{i+1} = \dot{u}_i + \frac{1}{2}(\ddot{u}_i + \ddot{u}_{i+1}).\Delta t \tag{5.36}$$

$$u_{i+1} = u_i + \dot{u}_i t + \frac{1}{4}(\ddot{u}_i + \ddot{u}_{i+1}).\Delta t^2 \tag{5.37}$$

Defining $\Delta u = u_{i+1} - u_i$ and $u_{i+1} = u_i + \Delta u$, then equation of velocity can be expressed as,

$$\dot{u}_{i+1} = \frac{2}{\Delta t}.\Delta u - \dot{u}_i \tag{5.38}$$

Accordingly, the equation of acceleration can be derived from the following relation.

$$\ddot{u}_{i+1} = (\dot{u}_{i+1} - \dot{u}_i).\frac{2}{\Delta t} - \ddot{u}_i \tag{5.39}$$

Substituting equation (5.38) into equation (5.39),

$$\ddot{u}_{i+1} = \left(\frac{2}{\Delta t}.\Delta u - \dot{u}_i - \dot{u}_i\right).\frac{2}{\Delta t} - \ddot{u}_i \tag{5.40}$$

After simplifying into simplex form, the equation of acceleration can be expressed as,

$$\ddot{u}_{i+1} = \frac{4}{\Delta t^2}.\Delta u - \frac{4}{\Delta t}.\dot{u}_i - \ddot{u}_i \tag{5.41}$$

Substituting equation (5.41) into equation of motion (5.32), the increment of displacement Δu can be calculated from the "known values".

$$\left(\frac{4}{\Delta t^2}.m + \frac{2}{\Delta t}.c + k\right).\Delta u = P_{i+1} + m\left(\frac{2}{\Delta t}.\dot{u}_i + \ddot{u}_i\right) + c\dot{u}_i \tag{5.42}$$

Comparing with stiffness equation ($K.\Delta u = B$), the right side of equation (5.42) can be put as load factor part while the product complement of Δu can be put as stiffness factor part which follows the concept of the tangent stiffness method.

5.9.3 Stages of deploying tensegrity model

The followings are the illustrations of deployment process of proposed tensegrity model. The model is in a large deformation and tends to retain its original configuration within the first 3 seconds. After the oscillatory mechanism is gradually slow down due to the damping effect, the stably full scale deployment is achieved within the specified time limit of 8 seconds. The grey color in the models indicates the compression strain where relaxation occurs in cable members.
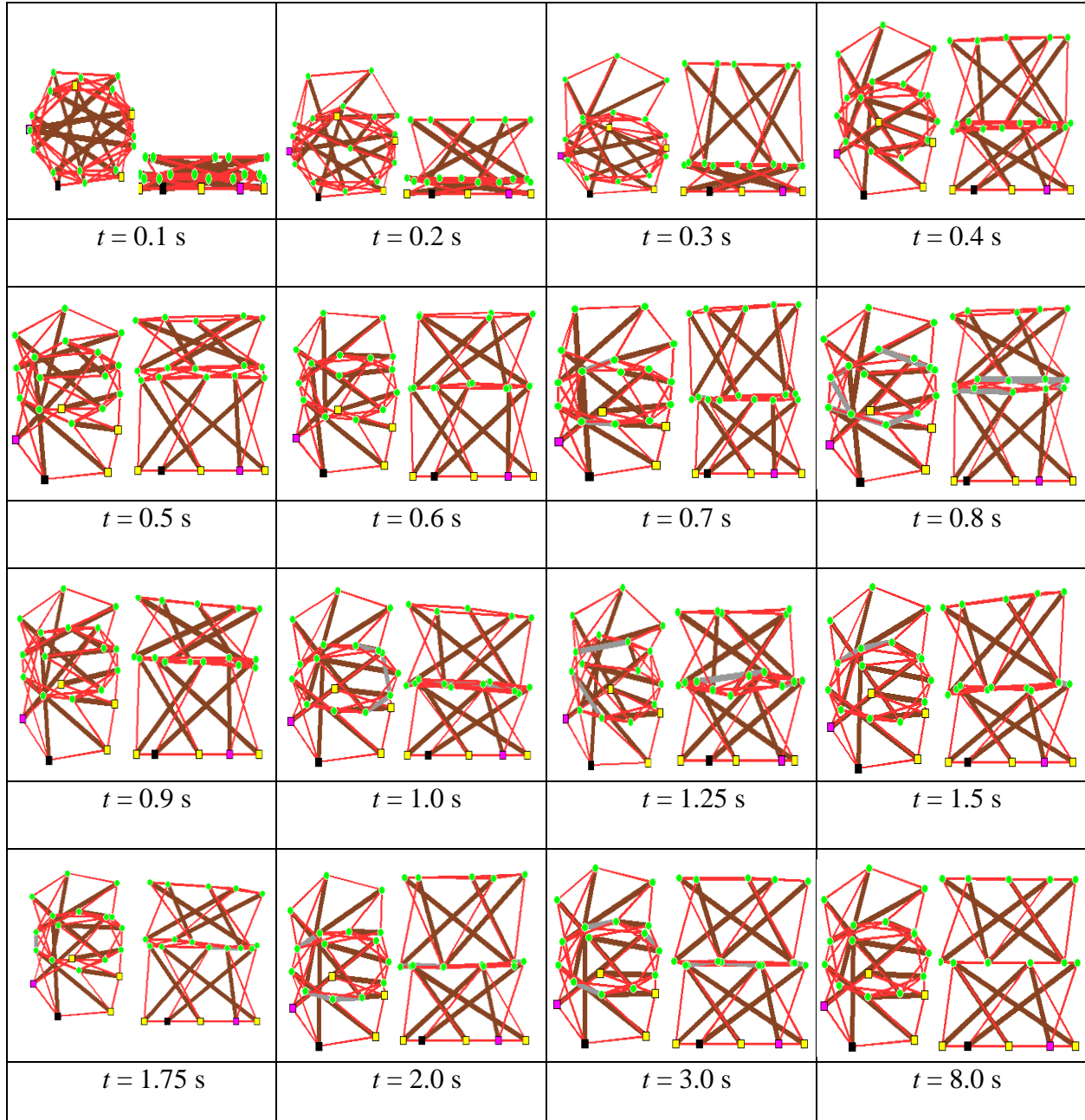

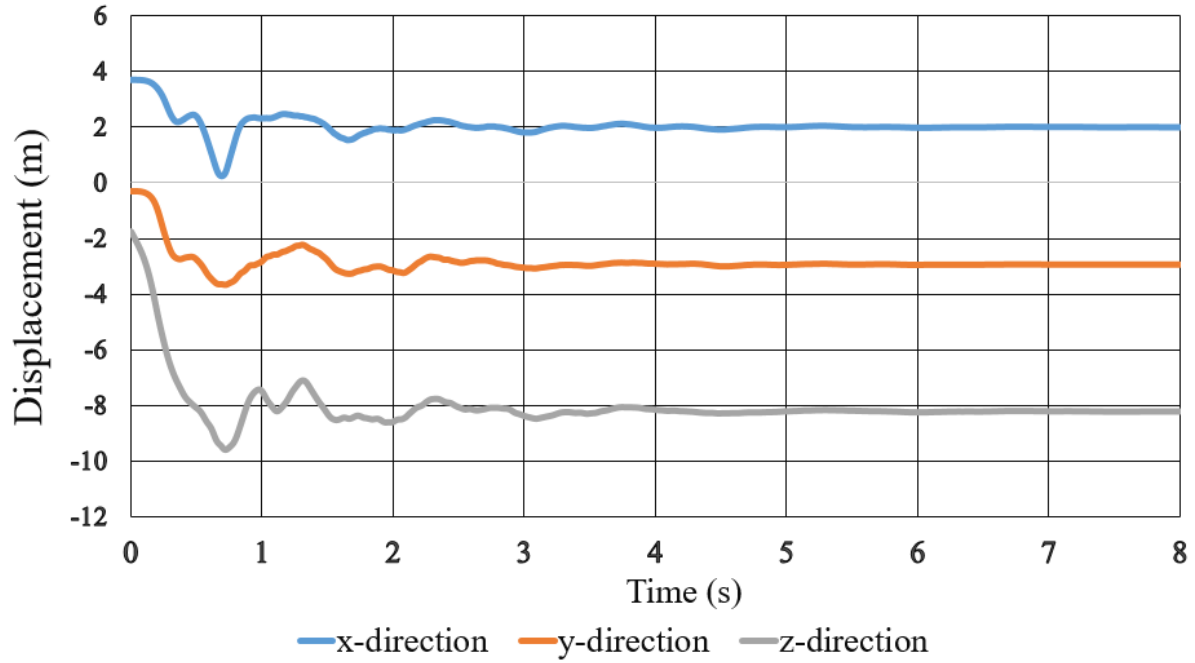Figure 5.13 Stages of tensegrity deployment
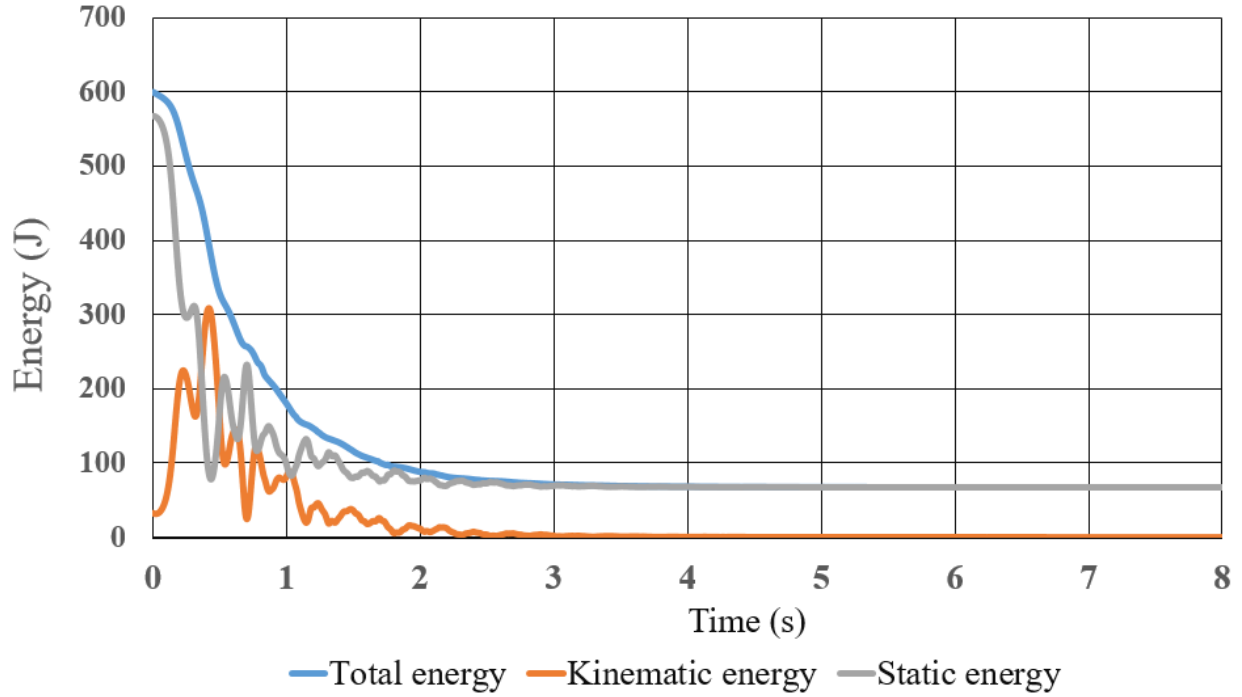
Figure 5.14 Displacement of top node

Figure 5.15 Energy distribution under damping effect

Figure 5.14 shows the displacement of one top node of proposed model and figure 5.15 presents the energy distribution of the whole structure. From these graphs, it can be seen that the structure oscillates greatly with high amount of energy within the first 3 seconds of deployment process. However, the treatment of proper damping makes the structure gradually stable and the kinematic energy is getting closer to zero within 3~6 seconds and keeps its stability until the specified time limitation. In this way, the folded tensegrity model makes its full deployment entirely and the simulation of dynamic analysis is successfully accomplished by selecting appropriate mode displacement and corresponding damping coefficient.

5.10 Summary of chapter 5

In this study, a simple tensegrity structure is proposed as a numerical model to conduct a series of structural analyses. In the consistent algorithm, form-finding analysis produces the equilibrium configuration by means of element's measure potential, and each member of the model is transformed into real element. The combination of aluminum struts and rubber cables makes the lightweight structure and allows the tensegrity model to perform large deformation analysis. Static folding of tensegrity is simply achieved by the application of compulsory displacement, producing a perfectly folded tensegrity without the need of complicated calculation process. The deployment process is simulated by the dynamic analysis with the appropriate amount of damping coefficient which allow the model to make a stable full-scale deployment. Therefore, the proposed algorithm gives a reliable solution for both static and dynamic problems in geometrical nonlinear analysis.

List of Symbols

Symbol		Description
N	:	Axial force
C_s	:	Coefficient of stiffness for strut
C_c	:	Coefficient of stiffness for cable
n_s	:	Multiplier for strut
n_c	:	Multiplier for cable
l_{0s}	:	Non-stressed length for strut
l_{0c}	:	Non-stressed length for cable
$\mathbf{M}$	:	Mass matrix
$\mathbf{C}$	:	Damping matrix
$\mathbf{K}$	:	Stiffness matrix
$\ddot{\mathbf{u}}$	:	Acceleration
$\dot{\mathbf{u}}$	:	Velocity
$\Delta\mathbf{u}$	:	Displacement
Δt	:	Time increment
$\mathbf{B}$	:	External force vector
$\mathbf{P}$	:	Loading
ζ	:	Damping ratio
c_0	:	Actual damping
c_c	:	Critical damping
α, β	:	Rayleigh coefficients
ω_0	:	Natural frequency
ω_i, ω_j	:	Eigen frequencies
$\mathbf{m_e}$	:	Lumped sum matrix for one element
T	:	Kinematic energy
ρ	:	Density

References

[1] S. Ali and R. Motro, "FOLDABLE / UNFOLDABLE CURVED TENSEGRITY SYSTEMS," *JOURNAL OF THE INTERNATIONAL ASSOCIATION FOR SHELL AND SPATIAL STRUCTURES: J. IASS,* vol. 48, no. 3, pp. 153-160, December 2007.

[2] Nizar Bel Hadj Ali; Landolf Rhode-Barbarigos; Ian F.C. Smith, "Analysis of clustered tensegrity structures using a modified dynamic relaxation algorithm," *International Journal of Solids and Structures,* vol. 48, no. 5, pp. 637-647, 2011.

[3] J. Pinaud, S. Solari and R. Skelton, "Deployment of a class 2 tensegrity boom," *Proceedings of the SPIE,* vol. 5390, pp. 155-162, July 2004.

[4] S. Djouadi, R. Motro, J.C. Pons and B. Crosnier, "Active Control of Tensegrity Systems," *Journal of Aerospace Engineering ,* vol. 11, no. 2, April 1998.

[5] A. Wroldsen, M. Oliveira and R. Skelton, "Modelling and control of non-minimal non-linear realisations of tensegrity systems," *International Journal of Control,* vol. 82, no. 3, pp. 389-407, 2009.

[6] M. Bouderbala and R. Motro, "Folding Tensegrity Systems," in *IUTAM-IASS Symposium on Deployable Structures: Theory and Applications*.

[7] C. Sultan and R. Skelton, "Deployment of tensegrity structures," *International Journal of Solids and Structures,* vol. 40, no. 18, pp. 4637-4657, September 2003.

[8] C. Sultan, "Tensegrity deployment using infinitesimal mechanisms," *International Journal of Solids and Structures,* vol. 51, no. 21-22, pp. 3653-3668, October 2014.

[9] Shu Yang, Cornel Sultan , "Deployment of foldable tensegrity-membrane systems via transition between tensegrity configurations and tensegrity-membrane configurations," *International Journal of Solids and Structures,* vol. 160, pp. 103-119, March 2019.

[10] F. Fraternali and F. Santos, "Mechanical modeling of superelastic tensegrity braces for earthquake-proof structures," *Extreme Mechanics Letters,* vol. 33, p. 100578, November 2019.

[11] M. Masic and R. Skelton, "Selection of prestress for optimal dynamic/control performance of tensegrity structures," *International Journal of Solids and Structures,* vol. 43, no. 7-8, pp. 2110-2125, 2006.

[12] N. Kanchanasaratool and D. Williamson, "Modelling and control of class NSP tensegrity structures," *International Journal of Control ,* vol. 75, pp. 123-139, 2002.

[13] W. Chan, D. Arbelaez, F. Bossens, R. Skleton, "Active vibration control of a three-stage tensegrity structure," in *In: SPIE 11th Annual International Symposium on Smart Structures and Materials*, San Diego, California, USA., 2004.

[14] N. Ali and I. Smith, "Dynamic behavior and vibration control of a tensegrity structure," *International Journal of Solids and Structures,* vol. 47, no. 9, p. 12851296, 2010.

[15] Z. Kan, H. Peng, B. Chen and W. Zhong, "Nonlinear dynamic and deployment analysis of clustered tensegrity structures using a positional formulation FEM," *Composite Structures,* vol. 187, pp. 241-258, March 2018.

CHAPTER 6

Discussion and Conclusion

In this study, tensegrity simulation with a versatile procedure in which the proposed tensegrity model can undergo a series of structural analyses, valid for both static and dynamic. In the algorithm, the purpose of each analysis is achieved by introducing the corresponding element force equation that describes the element behavior in the element stiffness component of stiffness matrixes. Since a large deformation is associated with tensegrity, the geometrical nonlinearity should be considered in the form-finding of tensegrity structures. Then nonlinear analysis based on the tangent stiffness method allows the author to describe the element behavior freely, even real or virtual elements. Therefore, form-finding process is implemented by the measure potentials. The virtual potential functions have the parameters of element measurement and its differential functions as the element force equations which prescribe the element behavior. In this study, power function is proposed for form-finding analysis and the influence of each coefficient on the shape formation is evaluated by numerical model of double-layered pentagonal tensegrity. In the virtual function, the variation of the multiplier and non-stressed length ratio plays a governing role than stiffness function, and various shape formation can be achieved by the appropriate selection of each coefficient. Moreover, the element force equation is modified to introduce the concept of multiple non-stressed length function whose potential function has multiple stoppage points. In this way, wide diversity of tensegrity form-finding is achieved even under the same connectivity of one structural model.

In the part of large deformation and large displacement analysis, the mechanical behavior of hyper-elastic material is studied and is applied in the substitution of real stiffness of tensegrity structure in the later section. It is expected to achieve the element's behavior in which the sag should occur with compression of deformation and also the hardening should be simulated in the higher tension area. A new algorithm with the application of relaxation process is proposed. In order to explore the features of shape deformation of hyper-elastic material to a full extent, the rubber net structure is used as a numerical model. Although the Hencky strain and nominal strain definitions cannot describe the behavior of the real hyper-elastic material properly, the Ogden model can be characterized by the element rigidity in both compression and tension sides. However, in the assumption of the compression-free elements such as rubber cord, softening occurs in the

compression side and formation of slack is required. Therefore, a simple equation of square root function is proposed to express the softening behavior in compression area, which connects smoothly to Ogden function in tensile area. Moreover, a rational computational procedure is implemented to switch between the modified Newton-Raphson method and the iteration of strict tangent stiffness equation. This realizes both the stability of iterated calculation process and the accuracy of output solutions.

As the final part of the study, a consistent algorithm is developed based on the knowledge of numerical results of the previous chapters. This algorithm enables to analyze the tensegrity structure both statically and dynamically with strong geometrical nonlinearity of structure. This chapter mainly highlights the involvement of dynamic analysis in the process of deployment of folded tensegrity model. The tangent stiffness method gives the adjustment to use the appropriate element force equation and corresponding material stiffness matrix depending on the theme of analysis. The static analysis includes finding equilibrium shape formation and simulation of folding process by the forced displacement. Before making the deployment of tensegrity, the structure is simulated by a free vibration and the decomposition of mode displacement is characterized by the Eigen value analysis. The Rayleigh coefficients are then calculated to apply the damping effect in the dynamic deployment. The appropriate selection of damping amount in Newmark β method makes the oscillation of the structure slow down gradually and the kinematic energy dissipation is successfully achieved. In this way, the proposed algorithm is valid for both static and dynamic analyses with a great performance.

All in all, this dissertation is aimed to be a reference for the future related studies of geometrical nonlinear problems for all structural system, including tensegrity.